AD-A189 725   FUNDAMENTAL STUDIES ON HIGH TEMPERATURE DEFORMATION                1/2
              RECRYSTALLIZATION AND.. (U) MARYLAND UNIV COLLEGE PARK
              DEPT OF CHEMICAL AND NUCLEAR ENGIN..  S ANKEM ET AL.
UNCLASSIFIED  JAN 88 AFOSR-TR-88-0055 AFOSR-85-0367       F/G 11/6.1    NL
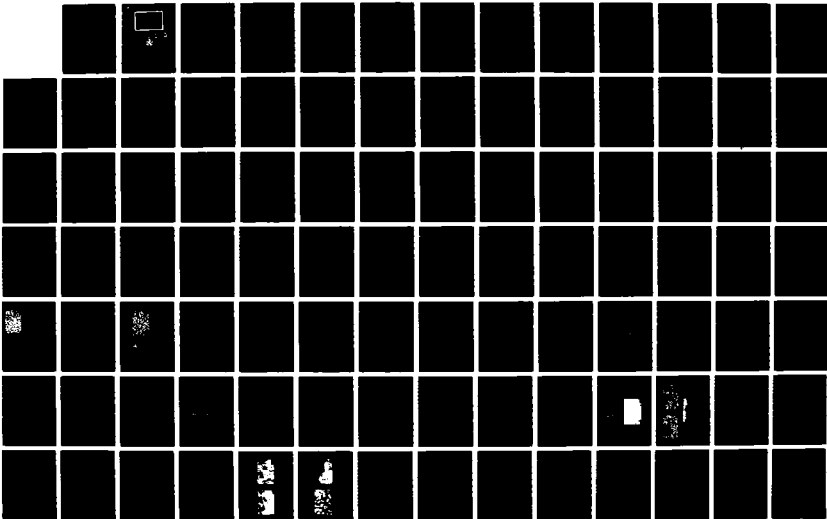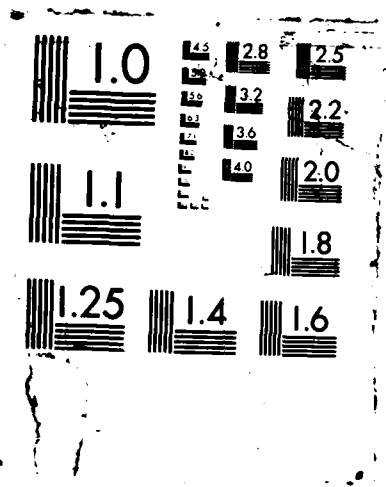
AD-A189 725

## INTERIM TECHNICAL REPORT

SUBMITTED TO
Dr. ALAN H.ROSENSTEIN
AIR FORCE OFFICE OF SCIENTIFIC RESEARCH
ELECTRONIC AND SOLID STATE SCIENCES
BOLLING AIR FORCE BASE
WASHINGTON, DC 20332

FOR THE PERIOD
DECEMBER 1, 1986 - NOVEMBER 30, 1987

DTIC
ELECTED
FEB 2 5 1988
S H D

Technical Information Division

AIR FORCE OFFICE OF SCIENTIFIC RESEARCH (AFSC)

Department of
Chemical and Nuclear Engineering

# Engineering Materials Program

College of Engineering
University of Maryland
College Park

88 2 24 130

# INTERIM TECHNICAL REPORT

SUBMITTED TO
Dr. ALAN H. ROSENSTEIN
AIR FORCE OFFICE OF SCIENTIFIC RESEARCH
ELECTRONIC AND SOLID STATE SCIENCES
BOLLING AIR FORCE BASE
WASHINGTON, DC 20332

FOR THE PERIOD
DECEMBER 1, 1986 - NOVEMBER 30, 1987

## FUNDAMENTAL STUDIES ON HIGH TEMPERATURE DEFORMATION RECRYSTALLIZATION , AND GRAIN GROWTH OF TWO - PHASE MATERIALS

BY
S. ANKEM, G. GREWAL, AND M.N. VIJAYSHANKAR

AFOSR - 85 - 0367

DTIC

FEB 2 5 1988

H

JANUARY 1988

# REPORT DOCUMENTATION PAGE

| 1a. REPORT SECURITY CLASSIFICATION | 1b. RESTRICTIVE MARKINGS |
|---|---|
| Unclassified | |

| 2a. SECURITY CLASSIFICATION AUTHORITY | 3. DISTRIBUTION / AVAILABILITY OF REPORT |
|---|---|
| | Approved for public release, distribution unlimited |
| 2b. DECLASSIFICATION / DOWNGRADING SCHEDULE | Approved for public release," |

| 4. PERFORMING ORGANIZATION REPORT NUMBER(S) | 5. MONITORING ORGANIZATION REPORT NUMBER(S) |
|---|---|
| | AFOSR·TR· 88-0065 |

| 6a. NAME OF PERFORMING ORGANIZATION | 6b. OFFICE SYMBOL (If applicable) | 7a. NAME OF MONITORING ORGANIZATION |
|---|---|---|
| University of Maryland | | AFOSR/NE |

| 6c. ADDRESS (City, State, and ZIP Code) | 7b. ADDRESS (City, State, and ZIP Code) |
|---|---|
| Dept. of Chemical & Nuclear Engineering University of Maryland College Park, Md. 20742-2111 | Bldg. U10, Bolling Air Force Base Washington, D.C. 20332-6448 |

| 8a. NAME OF FUNDING/SPONSORING ORGANIZATION | 8b. OFFICE SYMBOL (If applicable) | 9. PROCUREMENT INSTRUMENT IDENTIFICATION NUMBER |
|---|---|---|
| AFOSR/NE | | AFOSR - 85 - 0367A |

| 8c. ADDRESS (City, State, and ZIP Code) | 10. SOURCE OF FUNDING NUMBERS | | | |
|---|---|---|---|---|
| | PROGRAM ELEMENT NO. | PROJECT NO. | TASK NO. | WORK U ACCESSIC |
| Same 7b | 61102F | 2306 | A1 | |

11. TITLE (Include Security Classification)
Fundamental Studies on High Temperature Deformation, Recrystallization and Grain Growth of Two-Phase Materials.

12. PERSONAL AUTHOR(S)
S. Ankem, G. Grewal and M.N. Vijayshankar

| 13a. TYPE OF REPORT | 13b. TIME COVERED | 14. DATE OF REPORT (Year, Month, Day) | 15 PAGE COUNT |
|---|---|---|---|
| Interim | FROM 12/01/86 TO 11/30/87 | February 4, 1988 | 130 |

16. SUPPLEMENTARY NOTATION

| 17 | COSATI CODES | | 18 SUBJECT TERMS (Continue on reverse if necessary and identify by block number) |
|---|---|---|---|
| FIELD | GROUP | SUB-GROUP | |
| | | | |

19 ABSTRACT (Continue on reverse if necessary and identify by block number)

During this period, work was concentrated on two areas: (1) Particle coarsening kinetics and (2) High temperature deformation studies. Isothermal particle growth studies were carried out on several Ti-Mn and Ti-V alloys at 973 K, 1023 K and 1073 K. It was found that, at any given temperature, the particle growth behavior could be expressed in terms of simple relationships between volume percent of phases and time. The growth of alpha and beta phases was attributed to a two way diffusion mechanism of the solute and solvent. Considerations of bulk diffusion alone did not explain the particle coarsening kinetics and hence the alternate mechanism of a mixed grain boundary plus bulk diffusion was proposed. Studies of the particle growth kinetics at different temperatures indicated that the temperature dependency of the particle sizes of the alpha and beta phase, at any given volume fraction, could be expressed in a simple Arrhenius type relationship. The studies seem to suggest that as the temperature of annealing is increased, there is a gradual change in mechanism from a predominently grain boundary diffusion at 973 K to predominently bulk diffusion at 1073 K.

| 20. DISTRIBUTION / AVAILABILITY OF ABSTRACT | 21 ABSTRACT SECURITY CLASSIFICATION |
|---|---|
| ☐ UNCLASSIFIED/UNLIMITED  ☐ SAME AS RPT  ☐ DTIC USERS | UC |

| 22a. NAME OF RESPONSIBLE INDIVIDUAL | 22b TELEPHONE (Include Area Code) | 22c OFFICE SYMBOL |
|---|---|---|
| | (202) 767-4933 | NE |

DD FORM 1473, 84 MAR — 83 APR edition may be used until exhausted — All other editions are obsolete

The high temperature deformation behavior at 973 K was found to be similar to that at 923 K for the six Ti-Mn alloys tested. Strain softening was observed in beta as well as in the alpha-beta alloys. The magnitude of flow stress drop (softening) increased with increasing beta volume percent as well as with an increase in the strain rate for a given beta volume percent. The high temperature (973 K and 923 K at a strain rate of $1.1 \times 10^{-4}$/Sec) flow stresses of Alloy 4, which has nearly equal volume percents of alpha and beta, were significantly lower than those expected by the Law of mixture rule. This was attributed to a change in the deformation mechanism from slip in the alpha and beta single phase alloys to predominently interface sliding in the alpha-beta alloys. This suggestion needs to be confirmed. It was further interesting to note that the flow stresses of Alloy 4 actually decreased with a decrease in temperture from 973 K to 923 K. This appears to be associated with a refinement in the size of the alpha and beta phases resulting in increased interface sliding activity. Experiments are under way to confirm this suggestion. The results to date indicate that the high temperature strength of alpha-beta alloys need not decrease with increase in temperature and depends on the volume percents and size of the constituent phases.

# TABLE OF CONTENTS

Page

# 1. INTRODUCTION

Two-phase materials are technologically important because optimum properties can be obtained by a proper combination of the two phases. Among these materials, two phase Titanium alloys are of particular interest for high temperature aerospace applications. However, there is a lack of understanding in the areas of high temperature deformation, recrystallization and grain-growth behavior of two-phase alloys in terms of the properties of the component phases. Such an understanding is essential to develop new titanium alloys with greater high temperature strength and stability for high temperature applications.

The lack of understanding is due to the complex deformation behavior of these two-phase materials. Whenever a material comprising two or more phases is subjected to stress, the component phases deform differently and this results in inhomogeneous strain and stress distributions. In addition, ' interaction stresses ' develop as a result of interactions between the deforming phases. For these reasons, the deformation behavior of two-phase materials cannot be explained by the simple ' law of mixture rule '. This is due to the fact that the law of mixture rule always assumes either constant stress or constant strain and as mentioned before, this never happens in reality.

It is known that recrystallization is a nucleation and growth process and this process is promoted by increased cold work and high temperature. Therefore, the recrystallization process in single phase materials is somewhat straightforward. However, in two-phase alloys, where both the phases can deform, the

1

recrystallization behavior is not easy to understand. In these materials, the softer phase deforms more than the harder phase and therefore it can be argued that the recrystallization process is much faster in the softer phase than in the harder phase. However, the recrystallization process is also temperature dependent which implies that diffusion plays an important role. Therefore, if the diffusivity is higher in the harder phase, then it is difficult to predict which phase recrystallizes faster. This is particularly true in the case of some of the alpha-beta Titanium alloys where the beta phase is harder but its diffusivities are higher than that of the alpha phase. To further complicate this matter, the nature and magnitude of strain inhomogenity depends also on the volume percent of the phases. To date, there is no model or mechanism which explains the recrystallization of two-ductile phase alloys in terms of the volume percent of the phases, strain inhomogenities, and diffusivities of the component phases.

For many single phase materials, iso-thermal grain growth data can be represented by the empirical equation of the form

$$D = Kt^n$$

Where D is the mean grain diameter, t is the time, K is a constant of proportionality and n is the grain growth exponent. It is also known that impurity atoms in solid solution and impurities in the form of inclusions and second phase particles retard grain growth. Furthermore, in two-phase materials, size and volume fraction of the second phase is also known to effect the grain growth characteristics. However, there is no significant information as

2

to the empirical relationships which can predict grain growth behavior in two-phase materials. Recently, Anken and Margolin derived empirical relationships for grain growth of two-phase alloys in terms of the volume fractions of phases. Their derivations are based on the experimental results on alpha-beta titanium alloys. They found that under identical conditions, alpha-phase retards grain growth of the beta-phase much more effectively than vice-versa. Reasons were suggested for this behavior, but never proven. In addition, no atomistic or any other physical model was suggested for the grain growth of two-phase materials.

The aim of this program is to systematically study the high temperature deformation, recrystallization and grain growth behavior of two-phase materials. While this study will be focussed on two-phase materials where both the phases can deform, it is expected that the information and mechanisms to be developed can be applied to any two-phase material system. It is hoped that the outcome of this study will be useful in improving processing (forging, rolling, superplastic forming, etc.) methods, obtaining optimal microstructures for improved mechanical properties and increasing the high temperature capability of two-phase materials. Such a fundamental knowledge will be of great help in developing new titanium alloys for high temperature applications.

3

# 2. OBJECTIVES OF THE PROGRAM

1. Determine the high temperature (923 - 1023 K) deformation behavior of two-phase Titanium-Manganese and Titanium-Vanadium alloys. The factors to be varied include volume percent and nature of second phase (strength, diffusivity), temperature and strain rate.

2. Determine the high temperature deformation mechanisms in the two-phase titanium alloys: Slip, interface sliding, etc.

3. Study the recrystallization behavior of these two-phase titanium alloys by taking into account the inhomogeneous strain distributions and diffusivity differences between the component phases.

4. Study *the particle coarsening* and grain growth mechanisms and develop grain-growth relationships for two-phase alloys in terms of the volume fraction of phases, diffusivities, temperature, etc.

5. Theoretically Predict the stress-strain curves and stress and strain distributions in various two-phase materials.

6. Based on this information, propose models for high temperature deformation, recrystallization and grain growth of two-phase materials.

## 3. RESEARCH PROGRESS

In this report, research progress made during the second period of the program, December 1, 1986 - November 30, 1987, is presented. During this period work was concentrated on two areas

(A)  Particle Coarsening Studies

(B)  High Temperature Deformation Studies

The results of these studies are presented in separate sections and each section is entirely self contained in all respects.

# (A)  PARTICLE COARSENING STUDIES

## (a) ISOTHERMAL PARTICLE GROWTH IN
## TWO PHASE TITANIUM ALLOYS

**G. Grewal\* and S. Ankem \*\***

Isothermal particle growth studies were carried out on several Ti-Mn and Ti-V alloys consisting of varying amounts of $\alpha$ and $\beta$ phases at $973^0$ K. It was found that the particle growth kinetics of the $\alpha$ and the $\beta$ phases, in titanium alloys, could be represented by simple equations in terms of time and volume percents of the phases. The growth process is presented as a two-way diffusion process where the solvent and the solute atoms move in opposite directions resulting in conversion of $\alpha$ to $\beta$ and $\beta$ to $\alpha$ leading to the growth of the particles. The LSW theory , which considers only solute diffusion for growth of particles, is slightly modified to incorporate the diffusion of solute and solvent into the growth equation. The observation of the growth kinetics indicated that under identical conditions the growth of $\alpha$ particles in a $\beta$ matrix was faster than the growth of $\beta$ in an $\alpha$ matrix. Furthermore , for identical conditions, the growth kinetics of Ti-Mn are faster than those of the Ti-V alloys. While the faster kinetics are consistent with higher bulk interdiffusivities, the magnitude of the differences could not be explained on the bulk diffusivities alone. This was attributed to a mixed mode diffusion mechanism consisting of bulk diffusion as well as grain boundary diffusion controlling the growth process at $973^0$ K. Details of the investigation and various growth models of $\alpha$–$\beta$ Titanium alloys are presented.

\* G. Grewal is a graduate student and \*\* S. Ankem is an Assistant Professor, Department of Chemical Engineering, University of Maryland, College Park, Maryland 20742

# I. INTRODUCTION

For many single phase materials, isothermal grain growth data can be represented by equations of the form —

$$D = K\,t^n \text{------------------------}( 1 )$$

where D is the mean grain diameter, $t$ is the time, $K$ is the constant of proportionality and $n$ is the grain growth exponent. It is also known that impurity atoms in solid solution and impurities in the form of inclusions or second phase particles retard grain growth. Though it is known that the size and the volume fractions of the second phase affects the growth in two phase alloys (1 - 5 ), up until recently there was no significant empirical information available on the growth relationships in these alloys (6). Ankem and Margolin (6) derived empirical relationships for grain growth of the two - phase alloys in terms of the volume fractions of the phases. Their derivations, which are based on experimental work on two - phase α-β Titanium alloys, showed that under identical conditions, α retards grain growth of β phase much more effectively than vice - versa. Though reasons based on diffusivity considerations were given, they were not proven. Their study was limited to grain growth. They did not consider the particle coarsening kinetics. It is necessary to understand the particle coarsening kinetics to rationalize the grain growth kinetics since particles at the grain boundaries control the growth of grains.

To date, various two phase systems have been investigated in the literature to understand the particle coarsening kinetics. The two phase systems which have been theoretically investigated are the typical ostwaldian type of systems. A typical ostwaldian system is a two - phase system constituting a solute lean matrix dispersed with solute rich particles. A statistical dispersion of particles in a matrix is thermodynamically unstable due to the excess free energy associated with their interfacial surface area and thus the system tends to decrease this free energy by the process of particle coarsening. The solubility or the dissolution of these particles depends on their radii of curvature and is described by the Gibbs - Thompson relation (2).

$$C_r = C_\infty (1 + 2\ \gamma V_m / R\,T\,r)\text{----------------}( 2 )$$

where:

$C_r$ = Concentration in matrix of solute near a particle of size $r$

$C_\infty$ = Equilibrium solute concentration in matrix.

$\gamma$ = Surface free energy

$V_m$ = Molar volume

$R,T$ = Gas constant and temperature respectively

The fundamental theory of particle coarsening in a supersaturated solid solution decomposing by diffusion has been developed by Lifshitz and Slyosov (7) and independently

by Wagner (8), and is referred to as the LSW theory. The basic growth mechanism of the LSW theory is assumed to be a long range concentration gradient driven diffusion of solute through the matrix, between the second phase particles. The concentration gradients are created locally in the matrix near the particle matrix boundaries as a result of the dependence of the equilibrium solute concentration, $C(r)$ on the radius of the particles. The LSW theory was derived for the limiting case of the second phase tending to zero (7, 9) and is thus generally not valid for finite volume fractions of the second phase.

To bring real, finite second phase volume fraction systems into the framework of the LSW theory, modifications were made by Ardell (9). This modified LSW theory, known as the MLSW theory predicts that while the basic $t^{1/3}$ kinetics of the LSW theory are maintained, the coarsening rate increases with increasing volume fraction. This result is valid at even very small volume fraction of the second phase (9).

The Ardellian modification is based on the assumption that the diffusion of the solute to a growing particle will depend on a distance characteristic of the spatial distribution of particles in the matrix. In addition, the assumption of steady state diffusion under conditions of spherical symmetry are assumed (9). A somewhat different approach than that used by Ardell (9) was used by Davies, et al., (10) to incorporate the effect of finite volume fraction second phases into the framework of LSW theory. The rationale of the Davies (10) modification is the observation that the Ardellian approach predicts a strong volume fraction dependent growth kinetics which are generally not experimentally observed. The central idea of the Davies approach is that of "*encounters*" between growing particles. A growing particle encounters another growing particle, and a strong diffusion interaction results as a consequence of which the particles spontaneously coalesce to become a single particle. This theory, as modified by Davies, et al. is referred to as the LSEM theory (10). A more recent work by Brailsford, et al. (11) developed a theory of particle coarsening, which assumes that the growth rate of particles of one size class is a function of the entire size distribution and the existing concentration gradients around the particles. The growth rate predicted by this theory is more sensitive to volume fraction of the second phase than the theory proposed by Davies but is less sensitive to the theory proposed by Ardell.

Apart from the above theories, various models have been developed to explain the shape of the particle size distributions curves observed in real finite volume Ostwaldian type of systems. These models essentially use different geometrical approaches to obtain expressions for the radius of the influence sphere. The expression for the influence sphere is then substituted into the standard LSW theoretical formulation and the kinetic expression is evaluated by solving the resulting equation. An excellent paper which develops six such models is that of Tsumuraya, et al. (12). The particle coarseing theories reviewed above do not consider the diffusion of the Solvent. Furthermore, diffusion through the particles is assumed not to occur. In addition, the starting point of the LSW theory assumes a spherically symmetrical concentration gradient around a growing or shrinking particle and diffusion of solute occurs to the particle under steady state conditions (9).

In the two phase alloys, such as $\alpha-\beta$ titanium alloys, the geometry and distribution of the phases is complex and hence the conditions of spherical symmetrical symmetry cannot

8

be made. Furthermore, neither of the two phases can be considered as solute rich or solute lean and thus for the growth process to occur the diffusion of the solute as well the solvent have to be considered. In addition, as the volume percent of the *second phase* becomes considerable, the growth process occurs by the diffusion of the solute and the solvent through both the phases. This is in marked contrast to particle coarsening where diffusion is not allowed to occur through the second phase dispersoids.

The aim of this study was to systematically study the effect of volume percents of phases, temperature and diffusivity of the alloying elements on the particle growth kinetics of $\alpha - \beta$ titanium alloys. It is hoped that such an understanding will be helpfull for optimizing the microstructure of $\alpha - \beta$ titanium alloys through thermo-mechanical treatments and in developing new titanium alloys with increased microstructural stability for high temperature applications.

## II. EXPERIMENTAL

### A. MATERIALS

For this study six *Ti-Mn* and six *Ti-V* were used. The alloys were melted as 13.6 kg (30 - lb) ingots at RMI company. The aim alloy compositions are indicated in Figures 1 and 2 respectively. The actual chemistries of the ingots are given in Tables 1 and 2. Note that the actual chemical compositions of the ingots are close to the aim compositions in most of the cases. All of the Ingots were processed to 1.74 cm diameter by forging and rolling . The final step ( rolling ) was carried out in the $\alpha - \beta$ field at $973°K$ and a 60 % reduction in area was given for all the alloys . This work was found to be sufficient to recrystallize all of the alloys within 6 hours at $973°K$.

### B. HEAT TREATMENT

The heat treatments were carried for 25, 50, 100, 200 and 400 hours at $973°K$, followed by water quenching. The treatments were carried out in vacuum encapsulated quartz tubes. The specimen were sealed, in batches of twelve, at a pressure better than or equal to $10^{-5}$ torr

### C. OPTICAL METALLOGRAPHY

Standard polishing and etching techniques were used. The *Ti-Mn* alloys were etched with *A*- etch for 10 seconds, followed by etching with *R*- etch for about 10 seconds. This two - step etching was found to be beneficial for $\alpha - \beta$ microstructures. The compositions of *A*- etch and *R*- etch are given below:

*A*- etch:  25 ml *HF 50%*

25 ml *HNO₃* conc

50 ml Glycerine

9

*R*- etch:    18.5 gm (17 ml) Benzalkonium
              Chloride (50%)
              35 ml Ethanol

The *Ti-V* alloys were etched with the following etchant for 6 to 10 seconds.

4 ml *HNO₃* conc.

2 ml *HF* 50%

Bal. $H_2O$

The particle sizes and the volume fractions of the phases were measured by the linear intercept method ( 13 ).

## III. RESULTS

The volume percents of alpha, for the α - β *Ti-Mn* alloy system, varied from 10% for alloy no.# 5 to 79% for alloy no.# 2. The volume percents of alpha for the α - β *Ti-V* alloy system varied from 7% for alloy no.# 11 to 70% for alloy no.# 7. It is pertinent to note that though the volume fractions of the alloys studied are different, the chemical compositions of the alpha and the beta phases is the same in all the alloys in each of the two systems studied, since all of them were heat treated at the same temperature, see Figs. 1 and 2. The chemical composition of the phases, in the two system studied is shown by the ends of the tie lines drawn for 973°K, in Figs. 1 and 2 respectively.

The heat treatments resulted in equiaxed α + β microstructures of *Ti-Mn* and *Ti-V* alloys. For example the microstructures , of the α–β Ti-Mn alloys, heat treated for 200 hours at 973°K are shown in Fig. 3. Fig. 4 ( a ) shows the time evolution of a *Ti-Mn* alloy. In Fig. 4(b) a comparison of particle sizes is made between a *Ti-Mn* and a *Ti-V* alloy of same volume fractions of the α and the β phases. As expected, the α and the β sizes increased as a function of time. The particle sizes of the α and β phases plotted as a function of time for alloys 2, 3, 4 and 5 of the *Ti-Mn* system and for alloys 7, 8, 9, 10 and 11 of the *Ti-V* system are shown in Figs 5 to 8

It was found that in the *Ti-Mn* system, particle growth of the α and β phases could be expressed by equations of the form

$$D_\alpha^{\alpha-\beta} = K_\alpha^{\alpha-\beta} t^n \text{---------------------(3)}$$

$$D_\beta^{\alpha-\beta} = K_\beta^{\alpha-\beta} t^n \text{---------------------(4)}$$

where $D_\alpha^{\alpha-\beta}$, $D_\beta^{\alpha-\beta}$ are particle sizes of the α and the β phases respectively in microns, *t* is the time in hours, and *n* is the growth exponent. $K_\alpha^{\alpha-\beta}$, $K_\beta^{\alpha-\beta}$ are growth parameters

10

for the $\alpha$, and the $\beta$ phases respectively.

The growth exponent $n$ gave a constant value of approximately .28 for the Ti-Mn alloys studied. It was furthermore found that the growth parameters $K_\alpha^{\alpha-\beta}$, and $K_\beta^{\alpha-\beta}$ depended on the volume percents of the respective phases. It was found that the growth parameters could be represented by equations of the form.

$$K_\beta^{\alpha-\beta} \; = \; K_\beta \; / \; V_\alpha^{m\alpha} \text{------------------(5)}$$

$$K_\alpha^{\alpha-\beta} \; = \; K_\alpha \; / \; V_\beta^{m\beta} \text{------------------(6)}$$

where $K_\beta$, $K_\alpha$ are constants of the $\beta$ and the $\alpha$ phases respectively. $V_\alpha$, $V_\beta$ are volume percents and $m_\alpha$ and $m_\beta$ are known as the retardation exponents as per the terminology introduced by Ankem and Margolin (6). Plots of $K_\alpha^{\alpha-\beta}$ versus $V_\beta$ and $K_\beta^{\alpha-\beta}$ versus $V_\alpha$ are shown in Fig. 9(a). The numerical form of the equations (5), and (6) obtained for the Ti-Mn system are:

$$K_\beta^{\alpha-\beta} \; = \; 105 \; / \; V_\alpha^{1.146} \text{------------------(7)}$$

$$K_\alpha^{\alpha-\beta} \; = \; 23 \; / \; V_\beta^{.738} \text{------------------(8)}$$

It was found that equations identical to (3), (4), (5) and (6) could be written for the Ti-V system, with only the constants having different values. The growth exponent $n$ gave an approximately constant value of .24 for all the Ti-V alloys studied. Plots of $K_\alpha^{\alpha-\beta}$ versus $V_\beta$ and $K_\beta^{\alpha-\beta}$ versus $V_\alpha$ are shown in Fig. 10(a). The numerical form of equations (5) and (6) for Ti-V system is given below

$$K_\beta^{\alpha-\beta} \; = \; 89 \; / \; V_\alpha^{1.120} \text{------------------(9)}$$

$$K_\alpha^{\alpha-\beta} \; = \; 22 \; / \; V_\beta^{.757} \text{------------------(10)}$$

## IV. DISCUSSION

Comparison of equations (7) and (8), which correspond to the Ti-Mn system, show two differences. The first difference pertains to the numerators $K_\beta$ and $K_\alpha$ respectively in

11

equations (7) and (8). The $K_\beta$ value is larger than the $K_\alpha$ value by a factor of almost 4.5. The second difference is in the exponents $m_\alpha$ and $m_\beta$. We note that $m_\alpha$ is larger than the value of $m_\beta$. The isothermal growth parameters $K_\beta{}^{\alpha-\beta}$ and $K_\alpha{}^{\alpha-\beta}$, in equations (7) and (8) respectively, are scaled measures of the sizes of the $\beta$ and the $\alpha$ phases respectively. For values of $V_\alpha$ greater than about 50%, the isothermal growth parameter $K_\beta{}^{\alpha-\beta}$, in equation (7), is a measure of the size of particulate $\beta$ in an $\alpha$ matrix. Similarly for values of $V_\beta$ greater than about 50% the isothermal growth parameter $K_\alpha{}^{\alpha-\beta}$ in equation (8) is an measure of the size of particulate $\alpha$ in a beta matrix.

Thus the values of $K_\beta{}^{\alpha-\beta}$, and $K_\alpha{}^{\alpha-\beta}$ in the right hand side of Fig. 9(a) are a measure of particulate $\beta$ and $\alpha$, respectively. The values of $K_\beta{}^{\alpha-\beta}$ and $K_\alpha{}^{\alpha-\beta}$ on the left hand side of Fig 9(a) correspond to the mean spacing of the matrix. The corresponding sizes of matrix phases and the particulate phase of each of the alloys studied in the *Ti-Mn* system have been indicated by dashed arrows in Fig. 9(b). From Fig. 9(a) or 9(b) one infers that for any given volume percent of the matrix phase the particle size of the $\alpha$ phase is larger than the particle size of the $\beta$ phase. The ratio $K_\alpha{}^{\alpha-\beta}/K_\beta{}^{\alpha-\beta}$ has a maximum value of 1.43 for the limiting case of $V_\alpha = V_\beta = 100\%$. Furthermore, as the volume percent of the matrix phase is continuously reduced, the ratio $K_\alpha{}^{\alpha-\beta}/K_\beta{}^{\alpha-\beta}$ decreases and becomes unity at $V_\alpha = V_\beta = 42\%$

Analysis of the *Ti-V* system shows a trend similar to the *Ti-Mn* system. Thus, an examination of equations (9) and (10) show that $K_\beta$ is larger than $K_\alpha$, and the value of $M_a$ is larger than the value of $M_\beta$. The right half of Fig. 10(a), which represents the isothermal growth parameters of particulate $\beta$ and $\alpha$, shows that for any given volume percent of the matrix phase, the particle size of the $\alpha$ phase is larger than the particulate size of the $\beta$ phase. The corresponding sizes of the matrix and the particulate phase for each of the *Ti-V* alloys studied are indicated by dashed lines in Fig. 10(b). The ratio $K_\alpha{}^{\alpha-\beta}/K_\beta{}^{\alpha-\beta}$ of the Isothermal growth parameters for particulate $\alpha$ to particulate $\beta$ respectively, attains its maximum value of 1.31 for the limiting case of $V_\alpha = V_\beta = 100\%$. Furthermore, as the volume percents of the matrix phase is continously reduced, the ratio $K_\alpha{}^{\alpha-\beta}/K_\beta{}^{\alpha-\beta}$ decreases and becomes unity at $V_\alpha = V_\beta = 47\%$.

## A. RATIONALE FOR THE GROWTH PROCESS OCCURING IN TWO PHASE ALLOYS

A two phase alloy, with a fine dispersion of the two phases is thermodynamically unstable due to its large interfacial area. To reduce the excess free energy associated with the interphase interfaces, the two phase system tends toward a state where the surface area is minimized. The process occurs by an exchange of fluxes of the constituent components

between nearest neighbor interfaces. Thus the interfaces move by the process of conversion of one phase to the other. Thus in an $\alpha - \beta$ two phase system, regions of $\alpha$ phase convert to $\beta$ and regions of $\beta$ convert to $\alpha$ and the interfaces move. Since the volume fractions of the two constituent phases remains invariant with time, the rate of conversion of $\alpha$ to $\beta$ and vice versa for the whole system is zero. The mutual exchange of fluxes between the $\alpha$-$\beta$ interfaces can only occur by the process of long range diffusion. Depending on whether the diffusion process predominantly occurs in the $\alpha$, the $\beta$ or in both the $\alpha$ and the $\beta$ Phases, three distinct classes of the coarsening processes can be identified. These three classes, together with the characteristics of the type of alloys which belong to them are discussed in detail below. The *Ti-Mn* alloy system has been used as the model system for the sake of the exposition.

## CLASS 1: DIFFUSION PROCESSES OCCURING PREDOMINANTLY THROUGH THE $\beta$ PHASE.

The diffusion processes, resulting in the conversion of phases at the interfaces, will predominate in the $\beta$ phase when the total bulk volume fraction of the $\alpha$ phase is small. Thus the two phase alloy microstructures belonging to class 1 are those which contain small volume fractions of $\alpha$ distributed in $\beta$ matrix.

Fig. 11(a) shows a small volume fraction of $\alpha$ particles distributed in a matrix of $\beta$. The $\alpha$ particles are mostly distributed at beta boundaries. To bring out the details of the atomistic process resulting as a consequence of flux exchange between interfaces, we consider a two particle system in Fig. 11(b).

From Figs. 1 and 2 we note from the tie lines at $973°K$ in the two systems that the $\beta$ phase is solute rich and the $\alpha$ phase is solute lean. If one assumes that the growth of particle $C$ at the expense of particle $A$ does not involve the creation of a vacancy concentration higher than the already present equilibrium vacancy concentration, then the growth process will involve the following steps.

(1)     Atoms of *Ti* in the shrinking $\alpha$ particle $A$, jump across the $\alpha - \beta$ boundary and diffuse to the $\beta$ regions near the growing $\alpha$ particle $C$.

(2)     Atoms of *Mn* in the beta matrix near the growing particle $C$ diffuse towards $\alpha$ particle $A$ and jump across the $\alpha - \beta$ boundary of particle $A$.

(3)     Atoms of newly formed $\alpha$ near the interface of particle $C$ jump across the $\alpha$-$\beta$ interface into particle $C$.

As a consequence of these series of events $\alpha$ particle $A$ shrinks with a part of it transforming to $\beta$ and the $\alpha$ particle $C$ grows by a part of the $\beta$ matrix adjacent to it transforming to $\alpha$. The diffusion process thus involves the following fluxes—

$$( I ) \quad Mn_C{}^{\beta} \to A \quad ( II ) \quad Ti_A{}^{\beta} \to C$$

The subscripts in (I) and (II) above indicate the source of flux, the arrow points towards the sink, and the superscript indicates the medium in which the diffusion occurs. The flow process has been shown schematically in Fig. 11(c). A schematic showing the transformed regions is shown in Fig. 17(d). Finally, Fig. 17(e) shows the net result of the diffusional exchange process.

Using simple conservation of mass and flux balancing, it can be shown that the $N_{Ti}{}^{\alpha \to \beta}$, the number of moles of atoms of $Ti$ per unit volume moving out of the shrinking $\alpha$ particle $A$ (where regions of $\alpha$ are transforming to $\beta$) is given by

$$N_{Ti}{}^{\alpha \to \beta} = \Omega ( X_{Ti}{}^{\alpha} - X_{Ti}{}^{\beta} ) \text{------------}( 11 )$$

where:

$\Omega$ : molar atomic density. It is assumed $\alpha$ and $\beta$ have same number of atoms per unit volume.

$X_{Ti}{}^{\alpha}$ : mole fraction of $Ti$ in $\alpha$ phase

$X_{Ti}{}^{\beta}$ : mole fraction of $Ti$ in $\beta$ phase

obviously $N_{Ti}{}^{\beta \to \alpha}$ the number of moles atoms of $Ti$ per unit volume moving into the growing particle $C$ is also given by equation (11). It can be similarly shown, that $N_{Mn}{}^{\beta \to \alpha}$, the number $Mn$ atoms per unit volume moving out from the $\beta$ region near the growing $\alpha$ particle $C$ is given by

$$N_{Mn}{}^{\beta \to \alpha} = \Omega ( X_{Mn}{}^{\beta} - X_{Mn}{}^{\alpha} ) \text{------------}( 12 )$$

where :

$X_{Mn}{}^{\beta}$ : mole fraction of Mn in $\beta$ phase

$X_{Mn}{}^{\alpha}$ : mole fraction of Mn in $\alpha$ phase

obviously $N_{Mn}{}^{\alpha \to \beta}$, the number of atoms of $Mn$ per unit volume moving into the shrinking particle $A$ is also given by equation (12). From (11) and (12) one can note that

$$N_{Mn}{}^{\beta \to \alpha} = N_{Ti}{}^{\alpha \to \beta} \text{------------}( 13 )$$

or in other words conversion of $\alpha$ to $\beta$ occurs by the process of replacing a given number of *Ti* atoms by an equal number of *Mn* atoms. Similarily for the conversion of $\beta$ to $\alpha$, a given numbers of *Mn* atoms are replaced by an equal number of *Ti* atoms. It is thus apparent that the growth process occuring by mutual nearest neighbors interparticle flux exchange will preserve the volume fractions of the $\alpha$ and the $\beta$ phases.

## CLASS 2 : DIFFUSION PROCESSES OCCURING PREDOMINANTLY THROUGH THE $\alpha$ PHASE.

The diffusion processes, resulting in the conversion of phases at the interfaces, will predominate in the $\alpha$ phase when the bulk volume fraction of the $\beta$ phase is small. Thus the two phase alloy microstructure belonging to class 2 are those which contain small volume percents of $\beta$ distributed in a matrix of $\alpha$.

Fig. 12(a) shows a small volume fraction of $\beta$ particles distributed in a matrix of $\alpha$. The $\beta$ particles are mostly distributed at $\alpha$ boundaries. To bring out the details of the atomistic process resulting as a consequence of flux exchange between interfaces, we consider a two particle system in Fig. 12(b). In a manner similar to the previous case discussed (Class 1), the mutual growing and shrinking process will involve the following steps.

(1) *Mn* atoms from the smaller $\beta$ particle *A* jump across the $\alpha$ - $\beta$ interface and diffuse to $\alpha$ matrix regions adjacent to the growing $\beta$ particle *C*.

(2) *Ti* from the $\alpha$ matrix regions near the growing $\beta$ particle *C* diffuse to the shrinking particle *A* and jump across the $\alpha$ - $\beta$ interface.

(3) Atoms of newly formed $\beta$ near the interface of particle *C* jump across the $\alpha$ - $\beta$ interface into particle *C*.

As a consequence of this occurrence, the $\beta$ particle *A* shrinks with a part of it transforming to $\alpha$ and the $\beta$ particle *C* growing by a part of the $\alpha$ matrix adjacent to it transforming to $\beta$. The diffusion process thus involves the following fluxes.

$$( \text{I} ) \qquad Mn_A{}^{\alpha} \rightarrow C \qquad ( \text{II} ) \quad Ti_C{}^{\alpha} \rightarrow A$$

The notation used above has the same meaning as in Class 1. It may be noted that the direction of fluxes of the two constituent species in class (II) is in a direction opposite to their respective flux directions in the class 1 case discussed before.

The flow process has been shown schematically in Fig. 12(c). A diagram showing the transformed regions is shown in Fig. 12(d). Finally, Fig. 12(e) shows the net result of the diffusional exchange process.

$N_{Ti}{}^{\alpha \rightarrow \beta}$, the number of atoms of *Ti* per unit volume and $N_{Mn}{}^{\beta \rightarrow \alpha}$, the number

of atoms of Mn per unit volume required for $\alpha \rightarrow \beta$ and $\beta \rightarrow \alpha$ conversions are given by equations ( 11 ) and ( 12 ) respectively .

## CLASS 3: DIFFUSION PROCESSES OCCURING THROUGH THE $\alpha$ AS WELL AS THE $\beta$ PHASES

The type of alloys in which the class (3) diffusion process will operate are those in which neither of two phases can be considered as small. Thus alloys with nearly equal volume percents of the $\alpha$ and the $\beta$ phases fall into this category. In such an alloy, motion of the $\alpha$ - $\beta$ interfaces will result by diffusion through $\alpha$ and $\beta$. Thus the atomistic processes described in Class (1) and Class (2) will occur simultaneously. A typical microstructure in which the Class (3) diffusion process occurs has been shown schematically in Fig. 13.

The particle growth mechanisms discussed above assume a mechanism of bulk diffusion for the transport of the component species between particles. An alternate mechanism of transport is grain boundary diffusion. Thus for Class 1 microstructures grain boundary diffusion will occur predominantly via the $\beta$ – $\beta$ boundaries. In Class 2, the diffusive paths will be the $\alpha$ – $\alpha$ boundaries, while in class 3 the predominant paths will be the $\alpha$ – $\alpha$ and the $\beta$ - $\beta$ boundaries. This alternate mechanism has been schematically shown in Fig. 14.

## B. THE DRIVING FORCE FOR GROWTH

Consider a schematic of a typical two phase network in a two phase alloy, as shown in Fig. 15(a). The network comprises of $\alpha$ – $\alpha$ grain boundaries, $\beta$ - $\beta$ grain boundaries, and $\alpha$ – $\beta$ interphase interfaces. It is worthwhile to note that, in general, the network will tend towards a state where the total area comprising of the $\alpha$ – $\alpha$, $\beta$ – $\beta$, and the $\alpha$ – $\beta$ boundaries is minimized. But since the problem being addressed in this study is the time evolution of the mean particle size, we will be primarily concerned with the $\alpha$ – $\beta$ interfaces.

From thermodynamic consideration it is known that only 3 boundaries can intersect at a point. Thus in Fig. 15(a) each node can have only three vertices. . From Fig. 15(b) it can be seen that any terminating node, of any given interphase interface, is also a terminating node for a grain boundary (can be $\alpha$ – $\alpha$ or $\beta$ – $\beta$) and another $\alpha$ – $\beta$ interphase interface .Fig. 15(c) is an exploded view of two nearest neighbor $\alpha$ – $\beta$ interfaces $AB$, and $ED$. The interfaces exchange flux with each other through the Beta matrix. The new position of the interfaces after a time $\Delta t$ is shown by dashed lines. It is assumed that the boundary moves parallel to itself and that the nodes of the interface track on adjacent grain boundaries as shown in Fig. 15(c). Making a first order approximation that the only changes occuring in the geometry of network is the displacement of interfaces, $AB$ and $CD$, an expression for the driving force for flux exchange is presented below.

In Fig. 15(c) let the Interface $AB$ Convert $dV_1$ volume of $\alpha$ to $\beta$ and let the interface $ED$ convert $dV_2$ volume of $\beta$ to $\alpha$ , by interacting with each other through the process of diffusional exchange of $Ti$ and $Mn$ through the $\beta$ matrix. If this occurs in a time, $dt$, then invariance of

16

volume fractions demands

$$d V_1 \quad + \quad d V_2 \quad = \quad 0$$

or $\quad ( d V_1 \quad + \quad d V_2 ) / d t = 0$

from above we obtain

$$dV_1 / d t = - d V_2 / d t \text{————————————}( 14 )$$

In two dimensions we replace volumes by areas and areas are replaced by linear dimensions. Thus equation (14) becomes

$$d A_1 / d t = - d A_2 / d t \text{————————————}( 15 )$$

where $A_1$ and $A_2$ are the respective areas associated with interfaces $AB$ and $ED$. If $b_1$ and $b_2$ are the instantaneous lengths of interfaces $AB$, and $ED$ respectively, and $v_1$ and $v_2$ are the respective velocities of interfaces $AB$ and $ED$, then from (15) we obtain

$$v_1 \, b_1 = - v_2 \, b_2 \text{————————————————} ( 16 )$$

Now the condition of spontaneous growth is

$$d( b_1 + b_2 ) / d t \leqslant 0$$

$$\Rightarrow \quad d b_1 / d t + d b_2 / d t \leqslant 0$$

If $l_1$ and $l_2$ are the instantaneous distances of interfaces $AB$, and $ED$ respectively from their initial position at $t = 0$ then the above equation becomes

$$d b_1 / d l_1 . ( d l_1 / d t ) + d b_2 / d l_2 . ( d l_2 / d t ) \leqslant 0$$

$$\Rightarrow \quad d b_1 / d l_1 . v_1 + d b_2 / d l_2 . v_2 \leqslant 0 \text{——————}( 17 )$$

Plugging values of $v_2$ from equation (16) into equation (17) we obtain

$$d b_1 / d l_1 . v_1 - v_1 . ( b_1 / b_2 ) . d b_2 / d l_2 \leqslant 0$$

$$\Rightarrow \quad v_1 ( b_2 . d b_1 / d l_1 - b_1 . d b_2 / d l_2 ) \leqslant 0$$

If $v_1$ defined positive in the above equation above, the condition of net reduction in surfaces

17

becomes

$$b_2 \cdot (db_1 / dl_1) - b_1 \cdot (db_2 / dl_2) \leqslant 0 \text{----------------}(18)$$

Now, the net change of free energy per unit movement of interface, $AB$ is the driving force, $F$, for growth, or

$$F = - dG / dl_1 = - dG / dt \cdot dt / dl_1 \text{----------------}(19)$$

$$\Rightarrow \quad F = - dG / dt \cdot dt / dl_1 = - \gamma (.d(b_1 + b_2)) / dt / (dl_1 / dt)$$

$$= - \gamma \cdot v_1 \cdot (db_1 / dl_1 - b_1 / b_2 \cdot (db_2 / dl_2)) / v_1$$

$$\Rightarrow \quad F = - \gamma (db_1 / dl_1 - b_1 / b_2 \cdot (db_2 / dl_2)) \text{----------------}(20)$$

The above expression gives the driving force for the diffusional exchange between any two "nearest neighbor" interacting interfaces.

The driving force results in the flow of constituent species between the two interfaces which result in a net decrease in the surface area. For diffusion to occur through the bulk, the expected inter-particle concentration profiles for the growth of $\beta$ particles in $\alpha$ matrix and for $\alpha$ particles in $\beta$ matrix are shown in Figs. 16(a) and 16(b) respectively. The concentartion gradients arize by a probable modulation of concentration of the respective components in the matrix about their mean value. A constant concentration gradient has been shown in Figs. 16(a), and 16(b), though in reality this is not going to be the case.

## C. IDENTIFICATION OF THE RATE CONTROLLING STEP
There are two distinct dynamical processes involved in the particle growth of two phase titanium alloys. These are.

(I) Migration of atoms across the "source" and "sink" interfaces.

(II) Long range diffusion of solute and solvent atoms between interfaces.

The question that arises at this stage is as to which of the above two processes is the rate controlling step in the coarsening of particles in $\alpha-\beta$ alloys. We will consider the possibility of an interface control first.

18

## (I) INTERFACE CONTROL

It is known that for certain type of coherent or semi-coherent interphase interfaces the boundary mobilities are extremely low. Since the velocity of an interphase is proportional to the interface mobility there is the possibility of a certain measure of interface control to exist (15). In the $\alpha$–$\beta$ Titanium alloys studied in the present work, the particle phase is located at either triple junctions or at the grain boundaries. For particles located at triple junctions it has been shown (17) that on the average only one interphase out of three is a coherent or a semi coherent boundary. For particles located at grain boundaries it is known (16) that generally either both the interfaces are incoherent or one interface is incoherent and the other is coherent. Thus, as a lower bound, 50% of interfaces will be incoherent interfaces. A typical $\alpha$–$\beta$ titanium microstructure with coherent and incoherent interfaces is shown in Fig. 17. Since on an average 50% of the interfaces are incoherent interfaces it is reasonable to assume that the kinetics of the coarsening process is not interface controlled. This is also confirmed by looking at the right side of Figs. 9(b) and 10(b). From these figures it can be seen that, for any given volume fraction of the matrix phase, the particle size of $\alpha$ in $\beta$ matrix is larger than vice-versa. However if the kinetics were to be interface controlled, then the size of $\alpha$ particles would have been equal to the particle size of the $\beta$ phase. Another pointer against the possibility of interface control existing comes from particle coarsening theories. These theories predict that if the slowest step in the coarsening process is the transfer of atoms across the interfaces (22) then the mean particle size evolves as the square root of time, $t$ ($\overline{D} \propto$ $t^{.5}$). Since the actual observed exponents are far less than .5, it is reasonable to conclude that the particle coarsening process is not interface controlled. However it is important to note that in the widmanstatten $\alpha$ and $\beta$ structures there is the possibility that the process may be interface controlled, but these structures are not considered in this paper.

Having thus discounted the possibility of the kinetics being interface controlled, we move on to the process of long range diffusion.

## (II) LONG RANGE DIFFUSION

Long range diffusion processes can occur by either of the following three (or in combinations) mechanisms.

(a) dislocation (pipe) diffusion
(b) bulk diffusion
(c) grain boundary diffusion

## (a) DISLOCATION (PIPE) DIFFUSION

It is known that the contribution of diffusion through dislocation becomes significant below .5 $T_m$ (16). The apparent diffusion coefficient Dapp is approximately related to the diffusivities of lattice and pipe by the following expression —

19

$$Dapp = D_l + g\, D_P$$

where $D_l$ = Diffusivity of lattice

$g$ = a geometrical factor (cross section area of pipe per unit area of matrix)

$D_p$ = Diffusivity through dislocation "pipes". Because the activation energy for pipe diffusion is much smaller than bulk diffusion (16), at sufficiently low temperatures, the term $g\, D_p$ becomes so large that

$$Dapp \approx g\, D_p \text{----------------------------------------------------------(21)}$$

in such a case the kinetics is said to be controlled by pipe diffusion. In the $\alpha$–$\beta$ Titanium alloys investigated in this study, it has been shown (17) that the $\beta$ phase has a extremely low dislocation density in comparison to the $\alpha$ phase. Thus if the kinetics were purely controlled by Pipe diffusion then the sizes of $\beta$ particles in $\alpha$ matrix would have been larger then the size of $\alpha$ particles in $\beta$ matrix. But the results of Figs. 9(b) and 10(b) show an exactly reverse trend. The possibility of dislocation control existing is thus remote.

## (b) BULK DIFFUSION

In a binary alloy where diffusion occurs by a substitutional mechanism, the conservation of lattice sites requires

$$J_A + J_B + J_V = 0 \text{----------------------------------------------------(22)}$$

where $J_A$ = flux of component $A$

$J_B$ = flux of component $B$

$J_V$ = flux of Vacancies

Than from (22), above, and ficks first law we have

$$J_V = (D_A - D_B) . \delta C_A / \delta X \text{--------------------------------(23)}$$

from equation (23) we get

$$\delta J_V / \delta X = \delta((D_A - D_B) . \delta C_A / \delta X) / \delta X = \delta C_V / \delta t$$

or in other words a flux gradient of a component will lead to the generation or consumption of vacancies. If an equilibrium concentration of vacancies is to be maintained, then a mechanism of vacancy consumption (or production) must operate in the alloy. Under such conditions the ficks first law for diffusion in substitutional binary alloys can be written as (16)

$$J_A = \tilde{D}\, \delta N_A / \delta X$$

$$\text{------------------------------------(24)}$$

and $\quad J_B = \tilde{D} \, \delta N_B / \delta X$

where $\tilde{D}$ is interdiffusion coefficient, and is defined as

$$\tilde{D} = D_A X_B + D_B X_A \text{------------------------------------} (25)$$

where $D_A, D_B$ = are respective intrinsic diffusivities of components $A$ and $B$

$\qquad X_A . X_B$ = are respective mole fractions of components $A$ and $B$.

In the limiting cases of $\alpha$ particles distributed in a $\beta$ matrix (class 1 microstructure) and $\beta$ particles distributes in an $\alpha$ matrix (class 2 microstructures), the kinetics of the growth process controlled by bulk diffusion should be explainable in the framework of the LSW theory. Since the LSW theory primarily concerns itself with the diffusion of a single species (the solute), minor modifications have to be made to apply it to the present situation of a two way interdiffusion process. These modifications are considered below for class 1 and class 2 microstructures. Again the Ti-Mn system has been used for the discussion.

Consider a class 1 microstructure of $\alpha$ particles distributed in a matrix of $\beta$. The molar free energy plots of $\alpha$, and $\beta$ phases as a function of mole fractions of $Ti$, $X_{Ti}$ is shown in Fig. 18(a). Invoking the thermodynamic conditions of equilibrium it can be shown that

$$X_{Ti}^{\beta *} = X_{Ti}^{\beta} . ( exp ( 2 . \gamma^{\alpha - \beta} . \Omega_{Ti}^{\alpha} / R . T . r ) ) \text{------------} (26)$$

where

$X_{Ti}^{\beta *}$ = equilibrium concentration of $Ti$ in matrix, near an $\alpha$ particle of radius $r$

$X_{Ti}^{\beta}$ = equilibrium concentration of $Ti$ in matrix in the absence of interfaces.

$\gamma^{\alpha - \beta}$ = $\alpha$–$\beta$ interface energy

$\Omega_{Ti}^{\alpha}$ = partial molar volume of $Ti$ in $\alpha$ phase

$R, T$ = gas constant, and temperature respectively

$r$ = radius of $\alpha$ particle

The concentration gradient at the particle matrix interface is given (following LSW theory) by

$$dC / dR ( R = r ) = C' . C_r / r \text{-----------------------------------} (27)$$

where $C'$ is the concentration at a very large distance from the particle - matrix interface and $C_r$ is the concentration in matrix near a particle of radius r. Writing equation (27) in terms of

21

mole fractions instead of concentrations, we obtain

$$dC_{Ti}/dr = \Omega^\beta (X_{Ti}^{\beta'} - X_{Ti}^{\beta*})/r \quad \text{-------------------}(28)$$

where $\Omega^\beta$ is the number of atoms per unit volume in the $\beta$ phase. The rate of growth of a particle of radius $r$ can now be obtained as per LSW theory as

$$dr/dt = -(\tilde{D}^\beta . U . \Omega^\beta . ((X_{Ti}^{\beta'} - X^\beta_{Ti}) + (X_{Ti}^\beta - X_{Ti}^{\beta*})))/r \text{-----}(29)$$

The terms in equation (29) are defined later. On plugging in the value of $X_{Ti}^\beta - X_{Ti}^{\beta*}$ from equation (26) into equation (29), we obtain

$$dr/dt = -(\tilde{D}^\beta . U . \Omega^\beta . ((X_{Ti}^{\beta'} - X_{Ti}^\beta) - 2 . X_{Ti}^\beta . \gamma^{\alpha-\beta} . \Omega_{Ti}^\alpha /R.T.r))/r$$
$$\text{-----------------}(30)$$

The solution of equation (30), following the approach of LSW theory results in the kinetic expression

$$\bar{r}^3 - \bar{r}_0^3 = (6 . \gamma^{\alpha-\beta} . \Omega^\beta . \Omega_{Ti}^\alpha . U . \tilde{D}^\beta . X_{Ti}^\beta /R.T) / t \text{---------}(31)$$

where
$\bar{r}$ = mean particle radius of $\alpha$ at time, $t$
$\bar{r}_0$ = mean initial particle radius

$\Omega^\beta$ = no. of atoms per unit volume in $\beta$ phase

$\Omega_{Ti}^\alpha$ = partial molar volume of $Ti$ in $\alpha$ phase.

$\tilde{D}^\beta$ = interdiffusion coefficient in $\beta$ phase.

$1/U$ = no. of moles of $Ti$ or $Mn$ atoms per unit volume for $\alpha \rightarrow \beta$ and $\beta \rightarrow \alpha$ transformation.

$X_{Ti}^\beta$ = equilibrium mole fraction of $Ti$ in $\beta$ matrix in the absence of interfaces.
$t$ = time

The molar free energy plot of $\beta$ particles in an $\alpha$ matrix (class 2 microstructures) as a function of mole fraction of $Mn$, $X_{Mn}$ is shown in Fig. 18(b). In a manner equivalent to that for class 1 microstructures it can be shown that for class 2 microstructures the kinetic expression is

$$\bar{r}^3 - \bar{r}_0^3 = (6 . \gamma^{\alpha-\beta} . \Omega^\alpha . \Omega_{Mn}^\beta . U . \tilde{D}^\alpha . X_{Mn}^\alpha /R.T) t \text{--------}(32)$$

where

22

$\Omega^\alpha$ = no. of atoms per unit volume in $\alpha$ phase.

$\Omega_{Mn}^\beta$ = partial molar volume of $Mn$ in $\beta$ phase.

$\tilde{D}^\alpha$ = interdiffusion coefficient in $\alpha$ phase

$X_{Mn}^\alpha$ = equilibrium concentration of $Mn$ in $\alpha$ matrix and other terms are, as already explained in equation(31). From equations (31) and (32), we expect for the $Ti$ - $Mn$ system (for class 1 and class 2 microstructures).

$$( D_\beta^{\alpha-\beta} / D_\alpha^{\alpha-\beta} )^3{}_{Ti\text{-}Mn} = ( \Omega^\alpha . \Omega_{Mn}^\beta . \tilde{D}^\alpha . X_{Mn}^\alpha ) / . ( \Omega^\beta . \Omega_{Ti}^\alpha . \tilde{D}^\beta X_{Ti}^\beta )$$

$$\text{----------------( 33 )}$$

where $D_\beta^{\alpha-\beta}$, $D_\alpha^{\alpha-\beta}$ are particle sizes of the $\beta$ and the $\alpha$ phases, respectively. $\tilde{D}^\alpha$, $\tilde{D}^\beta$ are the respective interdiffusion coefficients in the $\alpha$ and $\beta$ phases. A similar expression should hold for the $Ti$-$V$ system. Thus we expect the following relationship to hold.

$$( D_\beta^{\alpha-\beta} / D_\alpha^{\alpha-\beta} )^3{}_{Ti\text{-}V} = ( \Omega^\alpha . \Omega_V^\beta . \tilde{D}^\alpha X_V^\alpha ) / ( \Omega^\beta . \Omega_{Ti}^\alpha . \tilde{D}^\beta X_{Ti}^\beta )\text{-----( 34 )}$$

Furthermore the growth of particulate $\alpha$ in $Ti$-$Mn$ and $Ti$-$V$ systems should be related by:

$$( ( D_\alpha^{\alpha-\beta} )_{Ti\text{-}Mn} / ( D_\alpha^{\alpha-\beta} )_{Ti\text{-}V} )^3 = K_{Ti\text{-}Mn} / K_{Ti\text{-}V}\text{----------------------( 35 )}$$

where $K = \tilde{D}^\beta . X_{Ti}^\beta . \Omega^\beta . \Omega_{Ti}^\alpha U$. The subscripts on the $K$'s in equation ( 35 ) are the alloy systems for which the expression for $K$ is evaluated.

A similar expression as equation ( 35 ) should hold for the $\beta$ phase in the $Ti$-$Mn$ and the $Ti$-$V$ systems. Numerical checks for equations (33), (34), and (35) will be made using tracer diffusivities. But first a rationale for using tracer diffusivities is being presented below--

The tracer diffusivity of Titanium $D_{Ti}^\beta$ at 1223° K (18) is

$$D_{Ti}^\beta = 9.27 * 10^{-10} \ cm^2 / sec$$

The self diffusivity of Titanium in a 10 at % V titanium alloy, $D_{Ti}^{\beta-V}$ at 1223° K is reported by Murdock et.al (19) as

$$D_{Ti}^{\beta-V} = 5.41 * 10^{-10} \ cm^2 / sec$$

23

since the difference between $D_{Ti}{}^{\beta}$ and $D_{Ti}{}^{\beta-V}$ is small interapolated values of the tracer self diffusivity of Titanium at $973°$ K has been used in the calculations for the *Ti-Mn* and the *Ti-V* systems.

The tracer diffusivity of *V* in $\beta$ titanium, $D_V{}^{\beta}$ at $1223°$ K is given by Askill (18) as

$$D_V{}^{\beta} = 5.97 * 10^{-10} \ cm^2 / sec$$

The diffusivity of vanadium, at $1223°$ K, for a 10 at % *V* titanium alloy, $D_V{}^{\beta-V}$ is reported by Murdock et.al. (19) as:

$$D_V{}^{\beta-V} = 4.49 * 10^{-10} cm^2 / sec$$

Again one finds that $D_V{}^{\beta} \approx D_V{}^{\beta-V}$ Thus interapolated values, at $973°$ K, of the tracer diffusivity of *V* has been used for calculations.

Similarily, the tracer diffusivity of *Mn* in titanium at $1171°$ K is reported by Askill (18) as

$$D_{Mn}{}^{\beta} = 3.24 * 10^{-9} cm^2 / sec$$

A value of diffusivity of *Mn* in a 9.7 at % titanium alloy at $1171°$ K is given by Santos et.al (20) as

$$D_{Mn}{}^{\beta-Mn} = 1.86 * 10^{-9} cm^2 / sec$$

Since $D_{Mn}{}^{\beta} \approx D_{Mn}{}^{\beta-Mn}$ it is reasonalbe to use the tracer diffusivities of *Mn* in a $\beta$ titanium interapolated to $973°$ K, for all calculations.

The various tracer diffusivities interapolated to $973°$ K using data of Askill(18) are

$$D_{Mn}{}^{\beta} = 1.56 * 10^{-10} cm^2 / sec$$

$$D_{Ti}{}^{\beta} = 3.31 * 10^{-11} cm^2 / sec$$

$$D_{Ti}{}^{\alpha} = 6.944 * 10^{-14} cm^2 / sec$$

$$D_V{}^{\beta} = 1.726 * 10^{-11} cm^2 / sec$$

Fanny Dyment (21) states that the tracer diffusivity of *Mn* does not change significantly as one passes the $\beta \rightarrow \alpha$ transformation point. Thus one can safely assume the tracer diffusivity of *Mn* in $\alpha$ phase to be the tracer diffusivity of *Mn* in $\beta$ phase. Thus

$$D_{Mn}{}^{\alpha} \approx D_{Mn}{}^{\beta} = 1.56 * 10^{-10} cm^2 / sec$$

It can furthermore be assumed that the tracer diffusivity of titanium is the same in the $\alpha$ phases of the *Ti-Mn* and the *Ti-V* systems respectively (it being so for the $\beta$ phase ). Thus we can take

$$D_{Ti}^{\alpha-V} \approx D_{Ti}^{\alpha-Mn} = 6.944 * 10^{-14} cm^2 / sec$$

using the mole fractions of the components from Figs. 1 and 2 we obtain the interdiffusion coefficients as-
for the *Ti-Mn* system, we have

$$\tilde{D}_{Mn}^{\beta} = 1.42 * 10^{-10} cm^2 / sec$$

$$\tilde{D}_{Mn}^{\alpha} = 1.55 * 10^{-10} cm^2 / sec$$

and for the *Ti-V* system we obtain

$$\tilde{D}_V^{\beta} = 1.94 * 10^{-11} cm^2 / sec$$

$\tilde{D}_V^{\alpha}$ cannot be evaluated as the value of $D_V^{\alpha}$ is not available.

For a 75% matrix phase alloy, annealed for 200 hrs at $973°$ K, the left hand side of equation (33) takes on the value of .49 . The left hand side of of equation ( 35 ) takes on the value of 2.75 Only equation ( 35 ) will be used for calculations , as all the quantities on the right hand side can be evaluated. This is not true of equation ( 33 ) or ( 34 ).

At $973°$ K, the right hand side of equation (35) gives a theoretical ratio of 9.67. Thus considerations based on bulk interdiffusion predicts a much larger difference in sizes of the $\alpha$ phases in the *Ti-Mn* and *Ti-V* systems than the ones actually observed.Thus the experimental results do not seem to support the hypothesis that the coarsening kinetics might be controlled by the interdiffusion coefficient. . The failure of experimental results to completely conform to any of the above mechanism thus seem to suggest that the volume diffusion is not the major controlling mechanism and that there are other mechanisms of long range diffusion (other than volume diffusion) which transport material between the interfaces. Since the particles are located at grain boundaries (triple points), an important mechanism to consider is grain boundary diffusion. This mechanism is considered in detail in the next section.

(c) GRAIN BOUNDARY DIFFUSION

Since the interphase interfaces are intersected by $\alpha-\alpha$ and $\beta-\beta$ grain boundaries it is pertinent to inquire about the possibility of such a mechanism to be the rate controlling mechanism in $\alpha-\beta$ two phase alloys. It is known that grain boundary diffusion becomes dominant below .75 - .8 *Tm* (16). The apparent diffusion coefficient, Dapp is related to the grain boundary and bulk diffusivities by the following relation

$$D_{app}/D_l = 1 + D_b . \delta / D_l . d \text{----------------( 36 )}$$

where

$D_l$ = Diffusivity of lattice

$D_b$ = Diffusivity of boundary

$\delta$ = Effective width of boundary

$d$ = Effective mean grain size

Grain boundary control is said to exist if

$$D_b . \delta \geqslant D_l . d \text{----------------------------------}( 37 )$$

Though it is known that $D_b > D_l$ (16), the values of the grain boundary diffusivities for the alloys being studied are not available in literature. Hence equation (36) cannot be directly used to determine the possible existence of a grain boundary control of the growth kinetics. On the other hand in equation (37) a typical value of is .5 $nm$ (16)and if one assumes a typical grain size of 1 $um$. then one finds that the ratio $D_b / D_l$ required to satisfy equation (37) is $2 * 10^3$ . Thus if the grain boundary diffusivity is around 2000 times that of the bulk diffusivity, the kinetics will be controlled by grain boundary diffusion. Since a factor 2000 is a very reasonably possible number, the possibility of grain boundary control is likely. There is however, other indirect evidence whcih seem to suggest such a mechanism. The particle growth exponent for the *Ti-V* system at 973 K is .24. It has been shown ( 22 ) that under grain boundary controlled kinetics, the mean particle size evolves as

$$\overline{D}^4 . \overline{D}_0{}^4 = K . t \text{----------------------------------}( 38 )$$

where

$\overline{D}$ = mean particle size at time , t

$\overline{D}_0$ = mean initial particle size

$K$ = growth constant

$t$ = time

The close correspondence of the growth exponent of the *Ti-V* system with the theoretical values (.25) seem to suggest that in the *Ti-V* system the growth kinetics may be grain boundary controlled. Thus the apparent diffusivity differences between the Ti-Mn and the Ti-V will be much smaller than the actual lattice diffusivity differences. This has been schematically shown in Fig. 19 ( a ). In plotting the schematic shown in Fig. 19 ( a ) the assumption has been made that the contribution of the grain boundary diffusivity term to the apparent diffusivity in equation ( 36 ) is the same for the Ti-Mn and the Ti-V systems. Though the grain boundary diffusivity is expected to be smaller in the Ti-V system than the Ti-Mn system , the grain size of the Ti-V system is also smaller than the Ti-Mn system and hence the assumption of same contributions of the grain boundary term in the two systems is reasonable. A typical grain boundary structure in a titanium alloy is shown in Fig. 19 ( b ).

# V. CONCLUSIONS

1. It was found that the particle sizes of $\alpha$ and $\beta$ phases in two phase Titanium alloys could be expressed in terms of simple relationships between Time , and Volume percents of the phases.

$$D_\beta^{\alpha-\beta} = ( K_\beta / V_\alpha^{m_\alpha} ) . t^n$$

$$D_\alpha^{\alpha-\beta} = ( K_\alpha / V_\beta^{m_\beta} ) . t^n$$

2. The growth of the $\alpha$ and $\beta$ phases was attributed to a two way diffusion mechanism of the solute and the solvent.

3. Growth of $\alpha$ in $\beta$ matrix is faster than vice versa. This was attributed to the larger grain boundary diffusivities in the $\beta$ phase.

4. The particle growth kinetics cannot be explained on the basis of bulk interdiffusivity considerations alone. The growth rates predicted by considerations of bulk interdiffusion give particle size ratios between the Ti-Mn to Ti-V systems to be much larger than the ones actually observed. This was attributed to a mixed grain boundary plus bulk diffusion control in the Ti - Mn system and predominantly grain boundary diffusion control in the Ti - V system.

# VI. ACKNOWLEDGEMENTS

## ( b )  TEMPERATURE EFFECTS

In continuation of the previous particle growth studies at $973^0$ K , isothermal particle growth studies were carried out at $1023^0$ K , and  $1073^0$ K . Furthermore , to confirm the validity of the experimental procedures additional particle growth studies were carried out at $998^0$ K, and $1048^0$ K. The results of the isothermal particle growth studies carried at $1023^0$ K , and $1073^0$ K are presented in detail below :----

## ISOTHERMAL PARTICLE GROWTH STUDIES AT $1023^0$ K

The volume percents of $\alpha$, for the $\alpha$-$\beta$ Ti-Mn alloy system , varied from 18 % for alloy no. 4 to 74 % for alloy no. 2. The volume percents of $\alpha$ for the $\alpha$-$\beta$ Ti-V alloy system varied from 12 % for alloy no. 9 to 59 % for alloy no. 7. It is pertinent to note that though the volume fractions of the alloys studied are different , the chemical composition of the $\alpha$ and the $\beta$ phases is the same in all alloys in each of the two systems studied. The chemical composition of the phases , in the two systems studied are shown by the ends of the tielines drawn for $1023^0$ K , in figures ( 20 ) and ( 21 ) , respectively. The heat treatments resulted in equiaxed $\alpha$-$\beta$ microstructures. Typical equiaxed $\alpha$-$\beta$ microstructures of Ti-Mn and the Ti-V alloys heat treated at $1023^0$ K are shown in figures ( 22 ) and ( 23 ) , respectively. As expected, the $\alpha$ and the $\beta$ sizes increased as a function of time. The microstructural data for Ti-Mn and Ti-V systems is given in tables ( 3 ) to ( 5 ) and ( 6 ) to ( 8 ) , respectively. The particle sizes of the $\alpha$ and the $\beta$ phases plotted as a function of time for alloys 2, 3, and 4 of the Ti-Mn system and 7 , 8 , and 9 of the Ti- V system are shown in figures ( 24 ) to ( 27 ) . It was found that in both the Ti-Mn and the Ti-V systems, the particle growth of the $\alpha$ and the $\beta$ phases could be written in the form of equations ( 3 ) and ( 4 ) . The particle growth exponents $K_\alpha^{\alpha-\beta}$ , and $K_\beta^{\alpha-\beta}$ depended on the respective other phase volume percents. In both the Ti-Mn and the Ti-V systems , the particle growth exponents could be expressed by equations of the form ( 5 ) and ( 6 ) . The numerical data for $K_\alpha^{\alpha-\beta}$ and $K_\beta^{\alpha-\beta}$ as a function of the respective other phase is shown in table ( 9 ) for the Ti-Mn system , while table ( 10 ) shows the corresponding data for the Ti-V system. The growth constants $K_\alpha^{\alpha-\beta}$ and

$K_\beta^{\alpha-\beta}$ were plotted as a function of the respective other phase. Such plots for the Ti-Mn system are shown in figure ( 28 ) , while figure ( 29 ) shows the corresponding plots for the Ti-V system. The numerical forms of equations ( 3 ) to ( 6 ) for the Ti-Mn and the Ti-V systems are presented below---

( a )  Ti-Mn SYSTEM

28

$$D_\alpha^{\alpha-\beta} = (117/V_\alpha^{1.088}) \cdot t^{.31} \quad \gamma = .99$$

$$D_\alpha^{\alpha-\beta} = (48/V_\beta^{.852}) \cdot t^{.31} \quad \gamma = .99 \text{------}(39)$$

## ( b ) Ti- V SYSTEM

$$D_\beta^{\alpha-\beta} = (144/V_\alpha^{1.175}) \cdot t^{.27} \quad \gamma = .99$$

$$D_\alpha^{\alpha-\beta} = (15/V_\beta^{.592}) \cdot t^{.27} \quad \gamma = .99 \text{------}(40)$$

## ISOTHERMAL PARTICLE GROWTH STUDIES AT 1073 $^0$ K

The volume percents of $\alpha$, for the $\alpha$-$\beta$ Ti-Mn system, varied from 24 % for alloy no. 3 to 54 % for alloy no. 2 . The volume percents of $\alpha$ for the $\alpha$-$\beta$ Ti-V alloy system varied from 6 % for alloy no. 8 to 36 % for alloy no. 7 . The chemical composition of the phases , in the two systems , is shown by the ends of the tie lines drawn at $1073^0$ K in figures ( 20 ) and ( 21 ) respectively. Typical equiaxed $\alpha$-$\beta$ microstructures of Ti-Mn and Ti-V alloys heat treated at $1073^0$ K are shown in figures ( 30 ) and ( 31 ) respectively. The microstructural data for the Ti-Mn and the Ti-V systems is given in tables ( 11 ) to ( 14 ). The particle sizes of the $\alpha$ and the $\beta$ phases plotted as a function of time for alloys 2 , and 3 of the Ti-Mn system and 7 , and 8 of the Ti-V system are shown in figures ( 32 ) to ( 35 ) .

It was found that in both the Ti-Mn and the Ti-V systems, the particle growth of the $\alpha$ and $\beta$ phases could be expressed in the form of equations ( 3 ) and ( 4 ) . The exact numerical forms of these equations are given below for the two systems studied.

## ( a )  Ti-Mn SYSTEM

( I ) ALLOY NO. 2

$$D_\alpha^{\alpha-\beta} = 2.44 \, t^{.33} \quad \gamma = .99$$

$$D_\beta^{\alpha-\beta} = 2.08 \, t^{.33} \quad \gamma = .99 \text{------}(41)$$

( II ) ALLOY NO. 3

$$D_\alpha^{\alpha-\beta} = 1.83 \, t^{.33} \quad \gamma = .99$$

$$D_\beta^{\alpha-\beta} = 5.85 \, t^{.33} \quad \gamma = .99 \text{------}(42)$$

( b )  Ti- V SYSTEM

( I )  ALLOY NO. 7

$$D_\alpha^{\alpha-\beta} = 1.76\, t^{.28} \qquad \gamma = .99$$

$$D_\beta^{\alpha-\beta} = 3.18\, t^{.28} \qquad \gamma = .99 \text{———————(43)}$$

( II )  ALLOY NO. 8

$$D_\alpha^{\alpha-\beta} = 1.63\, t^{.29} \qquad \gamma = .99$$

$$D_\beta^{\alpha-\beta} = 22.7\, t^{.29} \qquad \gamma = .99 \text{———————(44)}$$

The studies carried out at $998^0$ K  and $1048^0$K  were essentially used as controls to confirm the validity of the data at $973^0$ K, $1023^0$ K and at $1073^0$ K.  The details of the particle growth studies at these temperatures are hence not reported here.

The parameters Ln $(( K_\alpha^{\alpha-\beta} )^{1/n})$ and Ln $(( K_\beta^{\alpha-\beta} )^{1/n})$ for given volume percents of $\beta$ ( $V_\beta$ ) , and $\alpha$ ( $V_\alpha$ ) respectively were plotted as a function of inverse temperature ( $1/T$ ) . It was found found that the normalized particle sizes $(D_\alpha^{\alpha-\beta})^{1/n}V_\alpha$ and $(D_\beta^{\alpha-\beta})^{1/n}V_\beta$ at given volume percents of $\beta( V_\beta )$ and $\alpha ( V_\alpha )$ , respectively could be written as

$$(D_\alpha^{\alpha-\beta})^{1/n}V_\alpha = K_{V_\alpha}\exp(-(Q/R.T)).t \text{ ————————(45)}$$

$$(D_\beta^{\alpha-\beta})^{1/n}V_\beta = K_{V_\beta}\exp(-(Q/R.T)).t \text{ ————————(46)}$$

The plots for the $\beta$ and the $\alpha$ phases in a 24 % $\alpha$ - 76 % $\beta$ and a 54 % $\alpha$ - 46 % $\beta$ Ti-Mn alloys are shown in figures ( 36 ) and ( 37 ) respectively. A similar plot for a 36 % $\alpha$- 64 % $\beta$ Ti- V alloy is shown in figure ( 38 ) . The activation energy , Q , determined from the above equations , for the alloys studied , varied from 32 Kcal /mole to 46 Kcal / mole . Though no clear trends could be discerned from the values of the activation energies obtained , it is pertinent to note that the activation energy values ( 32 Kcal/ mole - 46 Kcal/mole ) obtained are close to the activation energies of solute and solvent lattice diffusivities in Titanium . Though the values of the activation energies obtained does not shed any light on the rate controlling mechanisms , the fact that the growth exponent , n , increases as the temperature of isothermal annealing is increased does seem to suggest that the growth kinetics in the Ti-Mn and the Ti-V tend toward " bulk control " as the temperature is increased. The growth exponent of .33 in the Ti-Mn system , for example, does indicate that at $1073^0$ K the long range diffusion occurs predominantly through the bulk. In addition the activation plots in Figs.

( 36 ) and ( 38 ) indicate that there is a trend of increasing activation energy ( slope of the plots ) as the temperature increases . This is consistent with the fact that the diffusion mechanism may be shifting to bulk diffusion as the temperature is increased.

# REFERENCES

1. D. S. Clark and W. R. Varney, "Metallurgy for Engineers, Second Edition", *D. Van Nostrand Company, New York*, 1973 , P. 309.

2. S. G.Byrnes, "Recovery, Recrystallization and Grain Growth", *MacMillan Co.*, 1965, P. 100.

3. C. Zener, "Private Communication Cited in C. S. Smith" , *Trans. - AIME,* 1948, Vol. 175, P. 15

4. E., I. Levine, Greenhut, and H. Margolin, Met Trans, 1973 , Vol. 4 , P. 2519

5. S. Ankem and H. Margolin, Met. Trans. A, 1977 , Vol. 8A , P. 1320

6. S. Ankem and H. Margolin, "Grain Growth Relationship in Two - phase Titanium Alloys, presented at the fifth International Conference on Titanium", held at Munich, W. Germany, September 1984.

7. M. Lifshitz and V. V. Slyosov, *J. Phy. Chem. Solids*, 1961 , Vol. 19 , P. 35.

8. C. Wagner, Electrochem, 1961 , Vol. 65 , P. 581.

9. A. J. Ardell, Acta Met., 1972 , Vol. 20 , P. 61.

10. C. K. L. Davies, P. Nash and R. N. Stevens, Acta Met. , 1980 , Vol. 28 , P. 179.

11. A. D. Brailsford and P. Wynblatt, Acta. Met., 1979 , Vol. 27 , P. 489.

12. Tsumuraya and Y. Miyata, Acta Met., 1983 , Vol. 31 , P. 437

13. G. F. Vander Voort , Metallography , Principles and Practice , McGraw - Hill book company , 1984

14. R. P. Elliot, "Constitution of Binary Alloys, First Supplement", *McGraw - Hill Inc.*, New York, 1965 , P. 617.

15. ASM - Metals Handbook , 8th Edition , Metallography and Phase Diagrams , ASM , Metals Park , OH.

16. Porter and Esterling , Phase Transformations in Metals and Alloys , Van Nostrand , UK Company ltd. , 1986.

17. H. Margolin , Private Communication , 1987

18. Handbook of Chemistry and Physics. 64th Edition , R. C. Weast ed.; CRC Press Inc.,

1983-84.

19.  J.F. Murdock and C.J.McHargue , Acta Met. , 1968, Vol. 16 , P. 493.

20.  E. Santos and F. Dyment , Phil. Mag , 31 ( 1975 ) , 809.

21.  F. Dyment , " Titanium 1980 , Science and Technology " , AIME ( 1980 ) 520.

22.   Martin and Doherty , Stability of Microstructure in Metallic Systems , Cambridge University Press., 1976.

TABLE 1: The Aim Compositions
and the Actual Ingot Chemistry
of Ti-Mn Alloys

| Alloy No. | Compositions | | | | | |
|-----------|------|------|------|------|------|------|
| | AIM | ACTUAL COMPOSITIONS OF INGOTS | | | | |
| | %Mn | Mn | Fe | O* | N | C |
| 1 | 0.6 | .4 | 0.02 | 0.071 | 0.01 | 0.02 |
| 2 | 2.7 | 3.0 | 0.01 | 0.086 | 0.01 | 0.02 |
| 3 | 4.9 | 4.8 | 0.01 | 0.082 | 0.006 | 0.01 |
| 4 | 7.1 | 6.0 | 0.01 | 0.083 | 0.008 | 0.01 |
| 5 | 9.3 | 9.4 | 0.02 | 0.100 | 0.10 | 0.02 |
| 6 | 11.5 | 13 | 0.01 | 0.116 | 0.012 | 0.02 |

* Oxygen content of final product.

## TABLE 2: The Aim Composition
## and the Actual Ingot Chemistry of Ti-V Alloys

| Alloy No. | Compositions | | | | | |
|---|---|---|---|---|---|---|
| | AIM | ACTUAL COMPOSITIONS OF INGOTS | | | | |
| | %V | V | Fe | O* | N | C |
| 7 | 3.9 | 4.3 | 0.01 | 0.078 | 0.017 | 0.02 |
| 8 | 6.0 | 6.2 | 0.01 | 0.063 | 0.015 | 0.01 |
| 9 | 8.3 | 8.1 | 0.01 | 0.082 | 0.016 | 0.02 |
| 10 | 10.5 | 10.6 | 0.01 | 0.075 | 0.020 | 0.02 |
| 11 | 12.8 | 12.6 | 0.01 | 0.083 | 0.019 | 0.02 |
| 12 | 15.0 | 14.8 | 0.01 | 0.092 | 0.021 | 0.02 |

* Oxygen content of final product.

Table 3: Isothermal Growth Data for Alloy No.2 (74% α–26%ß, Ti-Mn Alloy, Annealed at 1023 K, WQ

| Time t (hrs) | log t | Dα (um) | log Dα | Dß (um) | Log Dß |
|---|---|---|---|---|---|
| 25. | 1.3979 | 8.2390 | .91587 | 2.8576 | .45600 |
| 50. | 1.6989 | 9.3975 | .97301 | 3.2595 | .51315 |
| 100. | 2. | 12.4879 | 1.0964 | 4.3314 | .63662 |
| 200. | 2.3010 | 15.4769 | 1.1896 | 5.3325 | .72693 |
| 400. | 2.6020 | 18.9278 | 1.27710 | 6.5651 | .81724 |

$D_\alpha \times^{-\alpha} = 2.9276t^{.31}$       $= .99$

$D_\alpha \times^{-\alpha} = 1.01849t^{.31}$       $= .99$

36

Table 4: Isothermal Growth Data for Alloy No.3 (49% α-51%β, Ti-Mn Alloy,
Annealed at 1023 K, WQ

| Time t (hrs) | log t | Dα (um) | log Dα | Dβ (um) | Log Dβ |
|---|---|---|---|---|---|
| 25. | 1.3979 | 4.8527 | .68597 | 4.9606 | .6955 |
| 50. | 1.6989 | 5.9712 | .77606 | 6.10411 | .7856 |
| 100. | 2. | 7.9472 | .90021 | 8.1240 | .7097 |
| 200. | 2.3010 | 9.6489 | .9844 | 9.8636 | .7940 |
| 400. | 2.6020 | 11.4124 | 1.0573 | 11.6663 | 1.06693 |

$$D_{\alpha}{}^{x=0} = 1.7736t^{.317} \qquad = .99$$

$$D_{\alpha}{}^{x=0} = 1.81280t^{.317} \qquad = .99$$

Table 5:  Isothermal Growth Data for Alloy No.4 (18% α-82%β, Ti-Mn Alloy.
Annealed at 1023 K, WQ

| Time t (hrs) | log t | Dα (um) | log Dα | Dβ (um) | Log Dβ |
|---|---|---|---|---|---|
| 25. | 1.3979 | 3.1330 | .49597 | 14.0909 | 1.14893 |
| 50. | 1.6989 | 4.1762 | .62078 | 18.7826 | 1.27375 |
| 100. | 2. | 4.5037 | .65356 | 20.2558 | 1.30654 |
| 200. | 2.3010 | 6.4057 | .80656 | 28.81011 | 1.45954 |
| 400. | 2.6020 | 7.9596 | .900890 | 35.7987 | 1.55386 |

$$D_{\alpha} = 1.081 t^{.325} \qquad = .987$$

$$D_{\beta} = 4.864 t^{.325} \qquad = .987$$

Table 6:  Isothermal Growth Data for Alloy No.7 (59% α-41%ß, Ti-V Alloy,
         Annealed at 1023° K, WQ

| Time t (hrs) | log t | Dα (um) | log Dα | Dß (um) | Log Dß |
|---|---|---|---|---|---|
| 25. | 1.3979 | 3.91545 | .5927 | 2.7277 | .43579 |
| 50. | 1.6989 | 4.72128 | .674059 | 3.2890 | .51706 |
| 100. | 2. | 5.69296 | .75533 | 3.9659 | .59834 |
| 200. | 2.3010 | 6.8646 | .83661 | 4.7821 | .67961 |
| 400. | 2.6020 | 8.2774 | .91789 | 5.7663 | .76089 |

$$D_\alpha{}^{\alpha-\alpha} = 1.641 t^{.132} \qquad = .99$$

$$D_\alpha{}^{\alpha-\alpha} = 1.1438 t^{.132} \qquad = .99$$

39

Table 7: Isothermal Growth Data for Alloy No.8 (39% α-61%ß, Ti-V Alloy,
Annealed at 1023 K, WQ

| Time t (hrs) | log t | Dα (um) | log Dα | Dß (um) | Log Dß |
|---|---|---|---|---|---|
| 25. | 1.3979 | 3.2439 | .51106 | 4.9852 | .69768 |
| 50. | 1.6989 | 3.9387 | .59535 | 6.0529 | .78196 |
| 100. | 2. | 4.78246 | .67965 | 7.3496 | .86626 |
| 200. | 2.3010 | 5.8068 | .76393 | 8.9238 | .95065 |
| 400. | 2.6020 | 7.05063 | .848220 | 10.8354 | 1.03424 |

$$D_\alpha = 1.3172t^{.000} \qquad = .99$$
$$D_{\alpha-\beta} = 2.024t^{..} \qquad = .99$$

Table 8:   Isothermal Growth Data for Alloy No.9 (12% α-88%β. Ti-V Allo..
Annealed at 1023 K, WQ

| Time t (hrs) | log t | Dα (um) | log Dα | Dβ (um) | Log Dβ |
|---|---|---|---|---|---|
| 25. | 1.3979 | 2.4820 | .39480 | 17.779 | 1.2499 |
| 50. | 1.6989 | 2.9928 | .4760 | 21.4388 | 1.3312 |
| 100. | 2. | 3.6088 | .55736 | 25.8546 | 1.4125 |
| 200. | 2.3010 | 4.3515 | .63863 | 31.1714 | 1.4737 |
| 400. | 2.6020 | 5.2471 | .719910 | 37.5861 | 1.5750 |

$$D_\alpha = 1.0408t \qquad = .99$$
$$D_\beta = 7.455t \qquad = .99$$

41

Table 9: Isothermal Growth Parameters $K_{\nu}\times\eta$ and $k_{\alpha}\times\eta$ for the various Ti - Mn Alloys, at 1023°K

| Alloy No. | $V_{\nu}$ | log $V_{\nu}$ | $K_{\alpha}\times\eta$ | log $k_{\alpha}\times\eta$ | $V_{\alpha}$ | log $V_{\alpha}$ | $k_{\nu}\times\eta$ | log $k_{\nu}\times\eta$ |
|---|---|---|---|---|---|---|---|---|
| 2 | 74.24 | 1.8706 | 1.018 | .0079568 | 25.76 | 1.4109 | 2.92 | .46539 |
| 3 | 49.45 | 1.6941 | 1.8128 | .25834 | 50.55 | 1.7037 | 1.7736 | .2428 |
| 4 | 18.19 | 1.2598 | 4.864 | .6869 | 81.81 | 1.9128 | 1.081 | .03382 |

$$K_{\alpha}\times\eta = \frac{117}{V_{\nu}^{1.08804}} \qquad = .99$$

$$K_{\nu}\times\eta = \frac{48}{V_{\alpha}^{.89210}} \qquad = .99$$

Table 10:  Isothermal Growth Parameters $K_\beta^{x-\alpha}$ and $K_\alpha^{x-\alpha}$ for the various
Ti – V Alloys, at 1023°K

| Alloy No. | $V_\beta$ | log $V_\beta$ | $K_\alpha^{x-\alpha}$ | log $K_\alpha^{x-\alpha}$ | $V_\alpha$ | log $V_\alpha$ | $K_\beta^{x-\alpha}$ | log $K_\beta^{x-\alpha}$ |
|---|---|---|---|---|---|---|---|---|
| 7 | 58.94 | 1.7704 | 1.14385 | .05836 | 41.06 | 1.6134 | 1.541 | .2151 |
| 8 | 39.42 | 1.5957 | 2.024 | .30621 | 60.58 | 1.7823 | 1.3172 | .1196 |
| 9 | 12.25 | 1.0881 | 7.4559 | .8725 | 87.75 | 1.9432 | 1.0408 | .01736 |

$$K_\alpha^{x-\alpha} = \frac{144}{V_\beta^{1.172}} \qquad = .99$$

$$K_\beta^{x-\alpha} = \frac{15}{V_\alpha^{.5592}} \qquad = .99$$

Table 11: Isothermal Growth Data for Alloy No.2 (54% α-46%β, Ti-Mn Alloy,
Annealed at 1073 K, WQ

| Time t (hrs) | log t | $D\alpha$ (um) | log $D\alpha$ | $D\beta$ (um) | log $D\beta$ |
|---|---|---|---|---|---|
| 12½ | 1.0969 | 5.8538 | .76743 | 4.90887 | .69098 |
| 25. | 1.3979 | 6.9776 | .843706 | 6.0030 | .77836 |
| 50. | 1.6789 | 9.1400 | .960946 | 7.66456 | .88448 |
| 100. | 2. | 10.4287 | 1.01823 | 8.74524 | .94177 |
| 200. | 2.3010 | 13.9757 | 1.14537 | 11.7196 | 1.06891 |
| 400. | 2.6020 | 18.77964 | 1.2736 | 15.7432 | 1.9783 |

$$D_\alpha^{1/n} = 3.4455 t^{1/n} \qquad = .39$$

$$D_\beta^{1/n} = 3.03719 t^{1/n} \qquad = .39$$

44

Table 12: Isothermal Growth Data for Alloy No.3 (24% α-76%β, Ti-Mn Al.c.)
Annealed at 1073 K, WQ

| Time t (hrs) | log t | Dα (um) | log Dα | Dβ (um) | Log Dβ |
|---|---|---|---|---|---|
| 12½ | 1.0969 | 4.0766 | .610298 | 12.9974 | 1.1135 |
| 25. | 1.3979 | 5.7854 | .762333 | 18.4315 | 1.2655 |
| 50. | 1.6989 | 6.74659 | .829084 | 21.4936 | 1.3323 |
| 100. | 2. | 8.39247 | .92388 | 26.73521 | 1.42709 |
| 200. | 2.3010 | 11.2323 | 1.05046 | 35.79465 | 1.5536 |
| 400. | 2.5120 | 13.30895 | 1.12414 | 42.40373 | 1.62736 |

$$D_\alpha = 1.83653t^{...} \qquad = .33$$

$$D_\beta = 5.85049t^{...} \qquad = .33$$

45

Table 13: Isothermal Growth Data for Alloy No.7 (36% α—54%β, Ti-V Alloy..
Annealed at 1073 K. WQ

| Time t (hrs) | log t | Dα (um) | log Dα | Dβ (um) | Log Dβ |
|---|---|---|---|---|---|
| 12½ | 1.0969 | 3.6352 | .5605 | 6.57751 | .8180ₔ |
| 25. | 1.3979 | 4.4338 | .64677 | 8.02250 | .904309 |
| 50. | 1.6989 | 5.49977 | .740346 | 9.9533 | .9979ₔ |
| 100. | 2. | 6.5958 | .3192 | 11.9343 | 1.07679 |
| 200. | 2.3010 | 7.65418 | .88369 | 13.85238 | 1.14152 |
| 400. | 2.6020 | 10.1479 | 1.00637 | 18.3655 | 1.2540₁ |

$$D_\alpha = 1.76250t^{...}$$  = .99

$$D_\beta = 3.18875t^{...}$$  = .99

Table 14: Isothermal Growth Data for Alloy No.8 (6% α-94%β, Ti-V Alloy).
Annealed at 1073 K, WQ

| Time t (hrs) | log t | Dα (um) | log Dα | Dβ (um) | Log Dβ |
|---|---|---|---|---|---|
| 12½ | 1.0969 | 3.39113 | .530366 | 47.3371 | 1.67520 |
| 25. | 1.3979 | 4.1461 | .617639 | 57.857 | 1.76235 |
| 50. | 1.6989 | 5.0692 | .70493 | 70.7381 | 1.8495 |
| 100. | 2. | 6.1979 | .79224 | 86.4804 | 1.93695 |
| 200. | 2.3010 | 7.5779 | .87954 | 105.7451 | 2.02426 |
| 400. | 2.6020 | 9.2648 | .96683 | 129.3971 | 3.11158 |

$$D_\alpha^{*m} = 1.63019 t^{.....} \qquad = .99$$
$$D_\beta^{*m} = 22.744 t^{.....} \qquad = .99$$
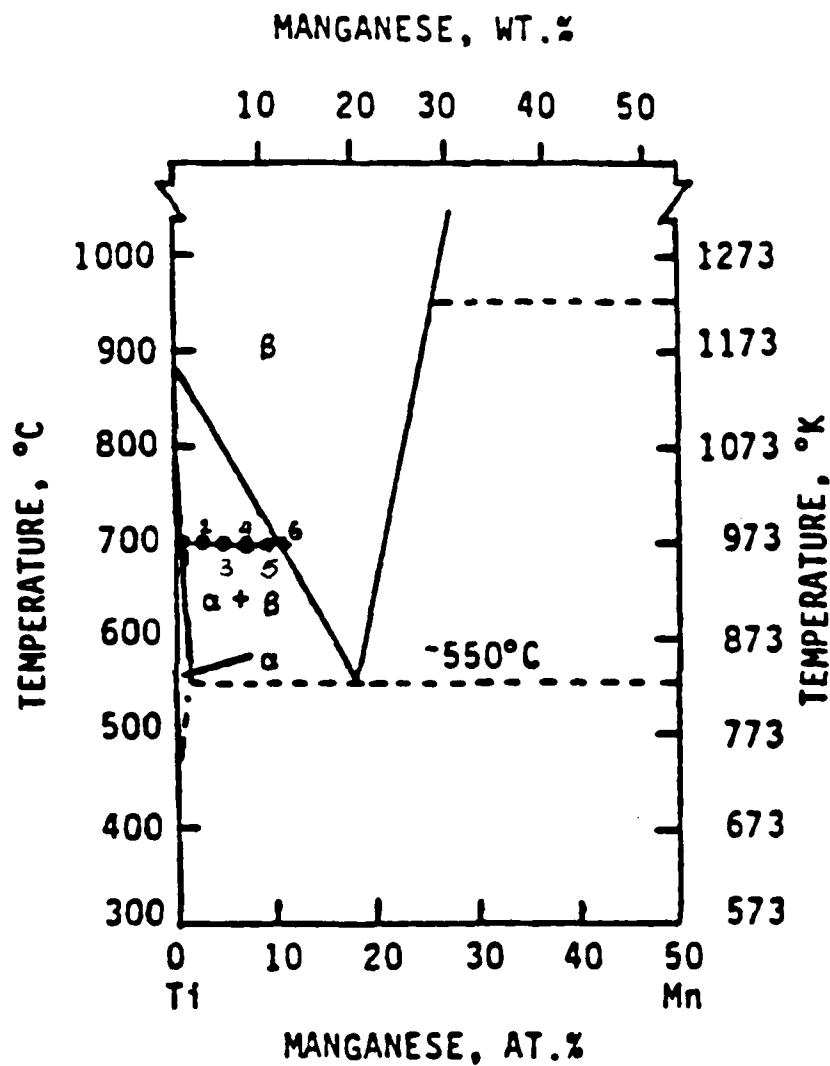
Fig. 1 : PARTIAL Ti END OF THE Ti - Mn PHASE DIAGRAM.
THE AIM COMPOSITIONS OF ALLOYS 1 - 6 ARE
INDICATED WITH SOLID CIRCLES. [ 14 ]
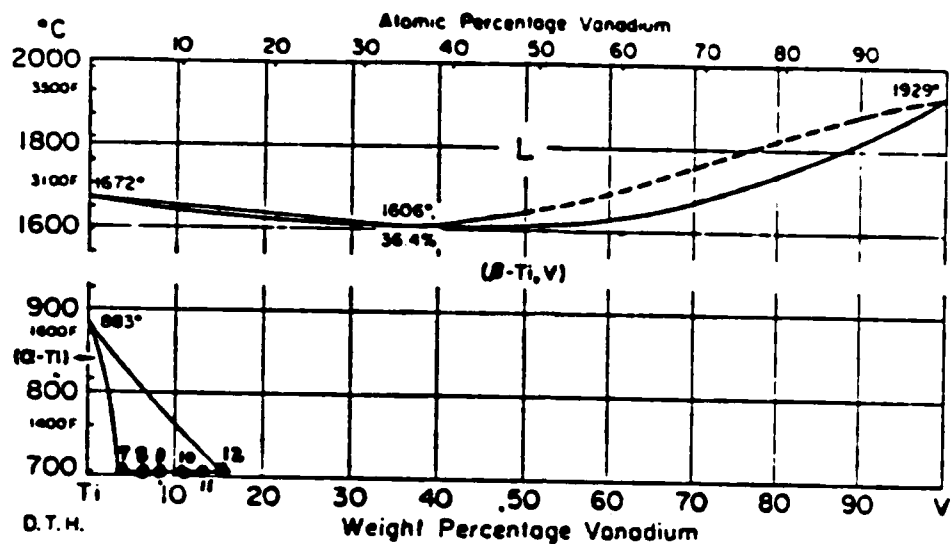
Fig. 2 : THE Ti - V PHASE DIAGRAM.    THE AIM COMPOSI-
TIONS OF ALLOYS 7 - 12 ARE INDICATED WITH
SOLID CIRCLES.[ 15 ]

63 % α – 37 % β

10% α   90 % β

79 % α – 21 % β

45 % α   55 % β

Fig. 3 :   MICROSTRUCTURES OF VARIOUS α – β Ti – Mn
ALLOYS ANNEALED FOR 200 HRS. AT 973 K , W. Q.

50 HRS.

400 HRS.

25 HRS.
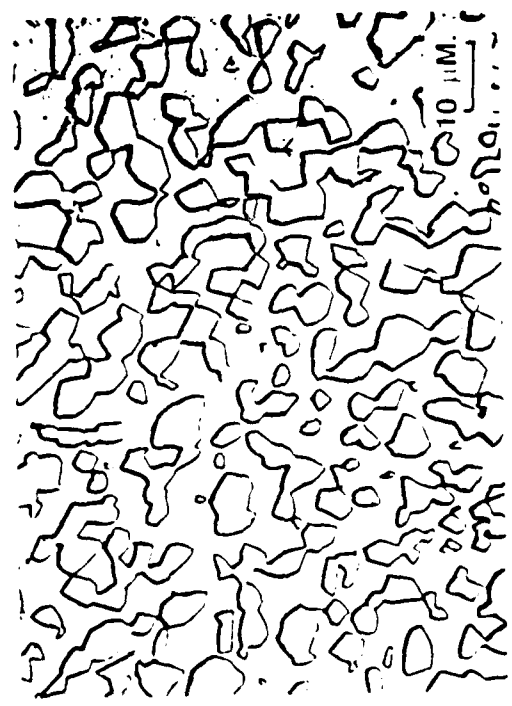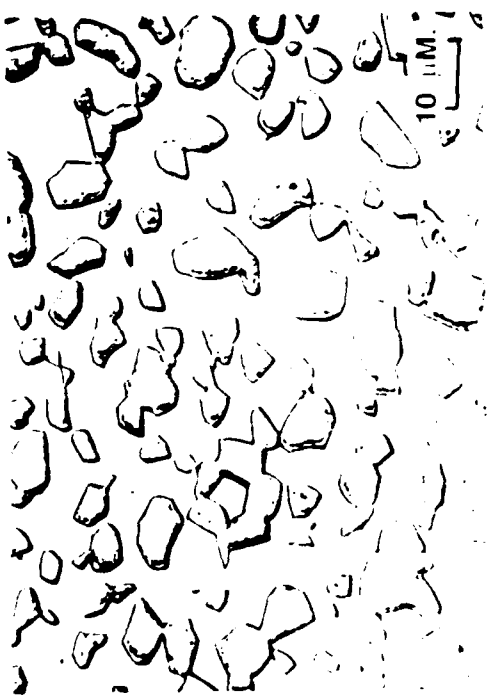
100 HRS.

**Fig. 4(a):** EFFECT OF TIME ON PARTICLE SIZES OF A 45% $\alpha$ - 55% $\beta$ ALLOY, ANNEALED AT 973 K FOR VARI-OUS TIMES.

45 % α - 55 % β Ti - Mn ALLOY

44 % α - 56 % β Ti - V ALLOY

Fig. 4 (b) : COMPARISON OF THE PARTICLE SIZES OF α β
Ti - Mn AND Ti - V ALLOYS ANNEALED FOR 400
HRS. AT 973 K , W. Q.
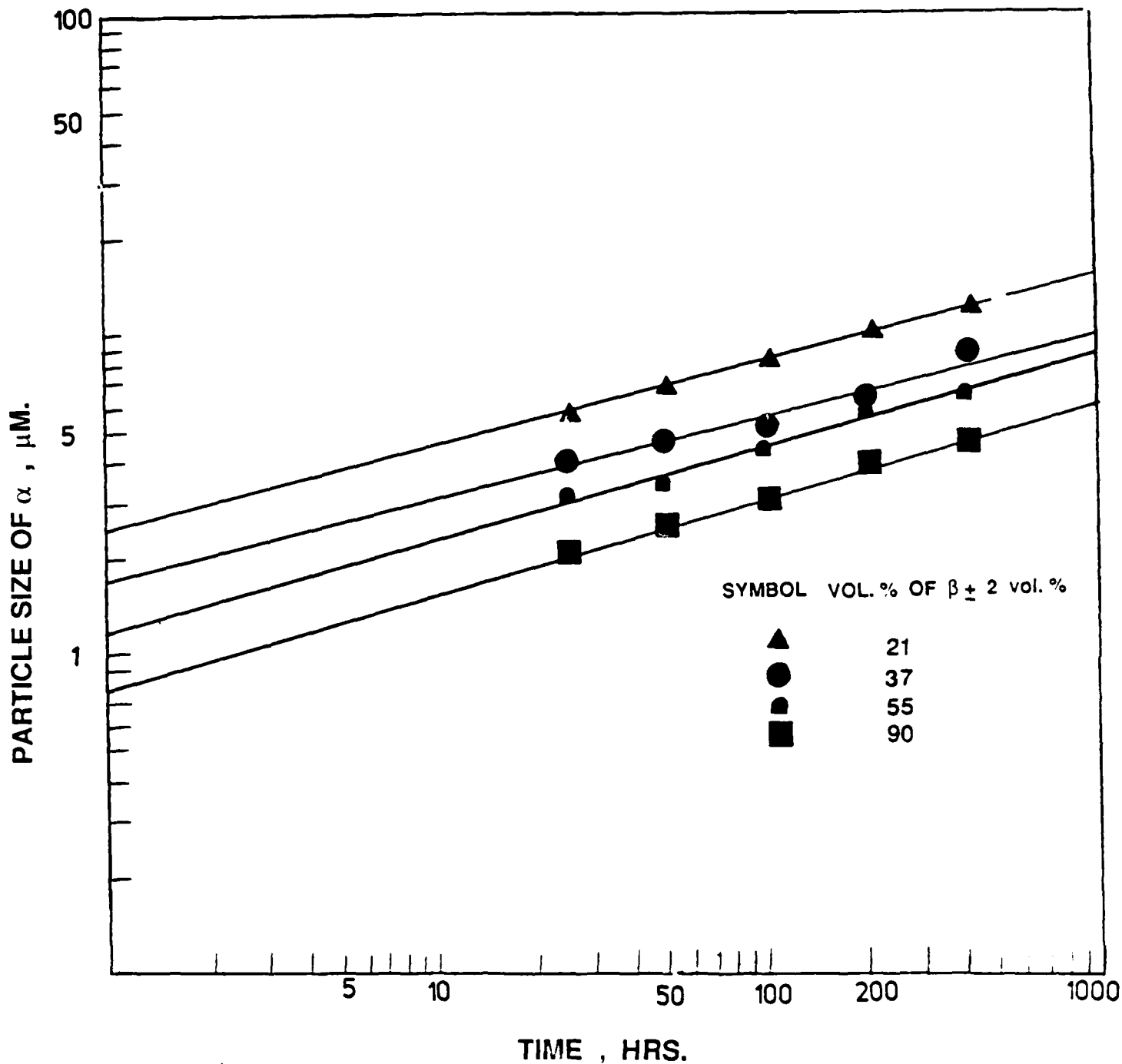
Fig. 5 : PARTICLE SIZES OF $\alpha$ – PHASE IN $\alpha$ – $\beta$ Ti - Mn ALLOYS. THE ALLOYS WERE ANNEALED FOR VARIOUS TIMES AT 973 K , W. Q.
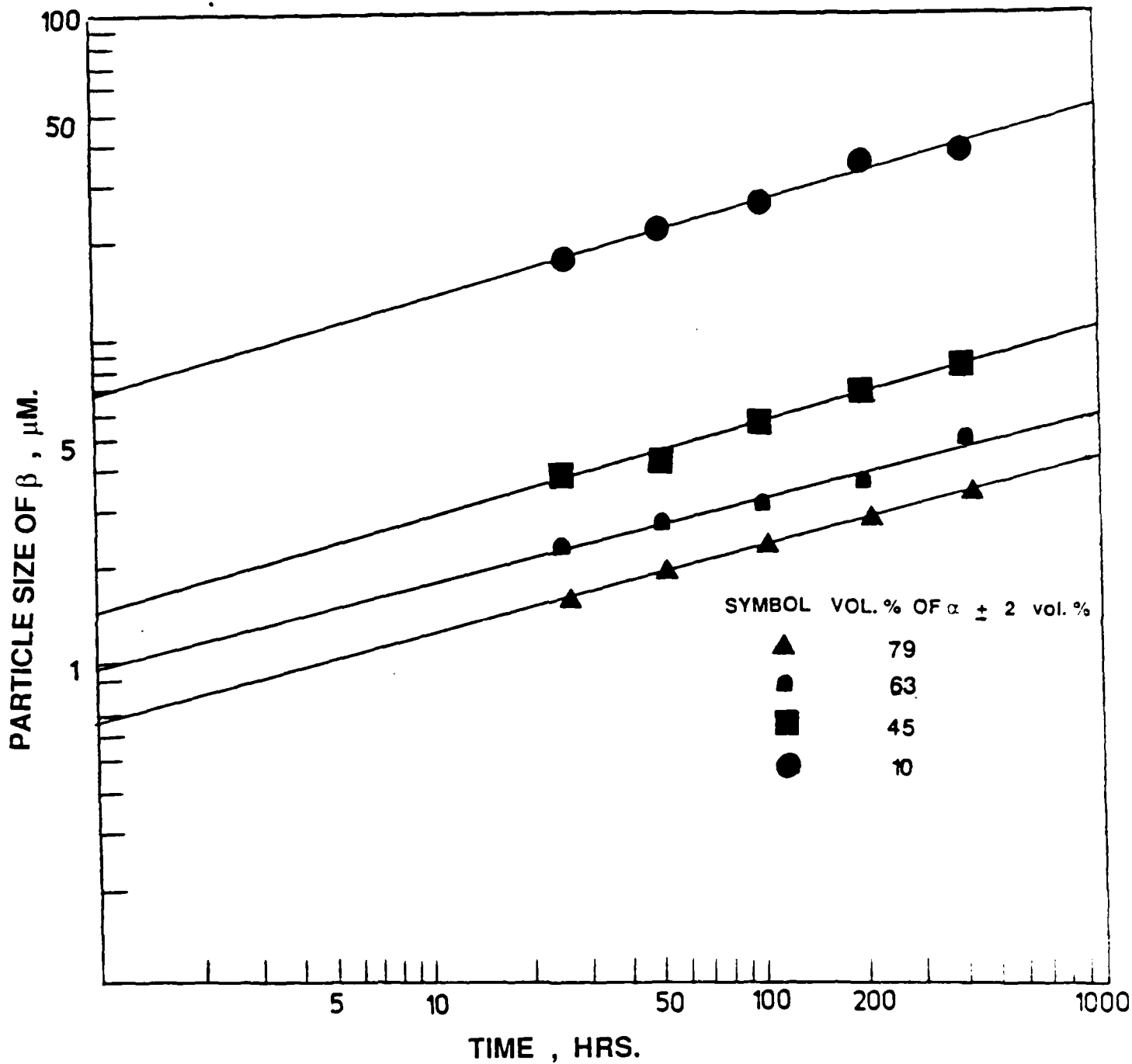
Fig. 6: PARTICLE SIZES OF β – PHASE IN α – β Ti - Mn ALLOYS. THE ALLOYS WERE ANNEALED FOR VARIOUS TIMES AT 973 K , W. Q.
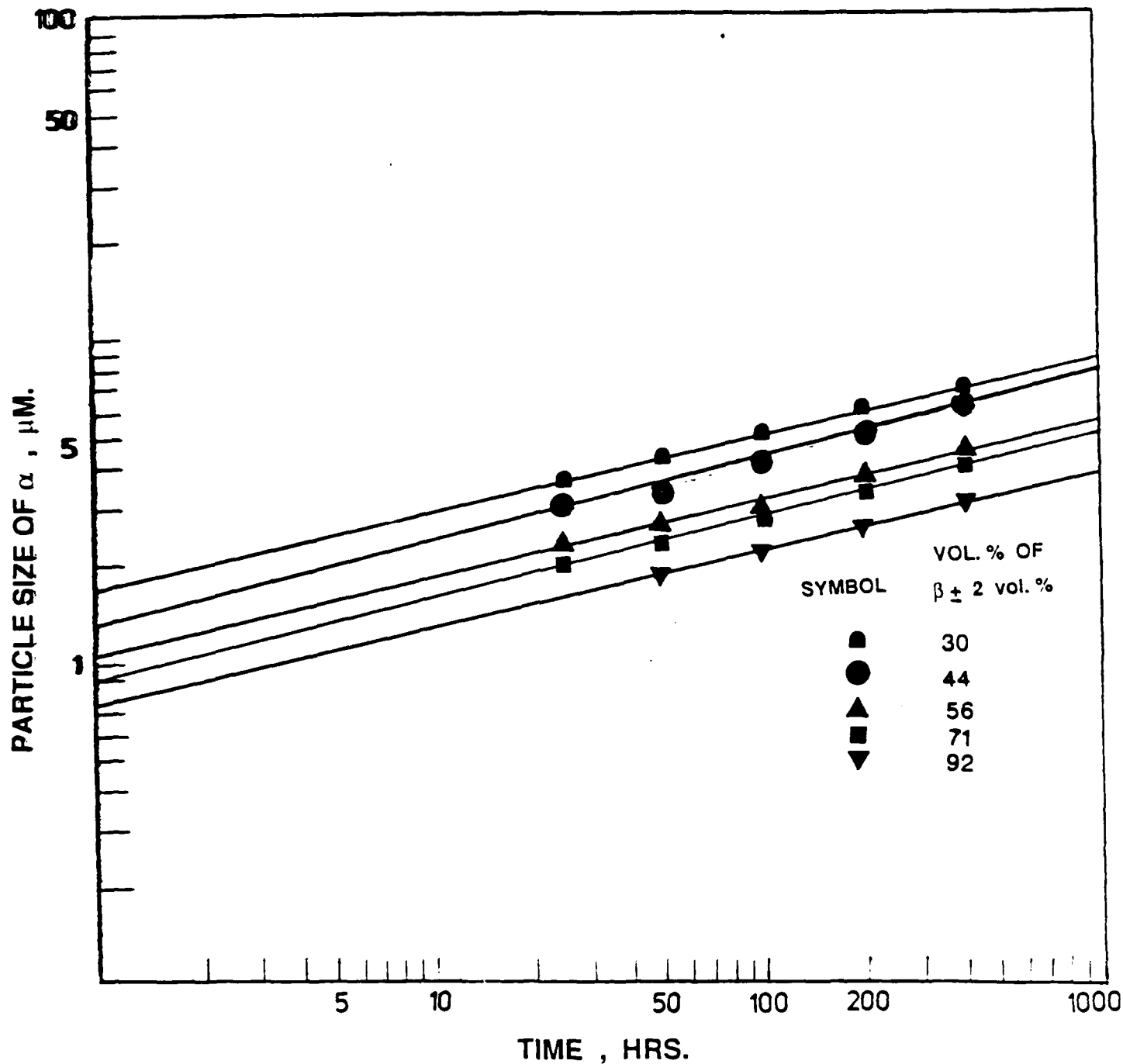
**Fig. 7:** PARTICLE SIZES OF $\alpha$ – PHASE IN $\alpha$ – $\beta$ Ti - V ALLOYS. THE ALLOYS WERE ANNEALED FOR VARIOUS TIMES AT 973 K , W. Q.
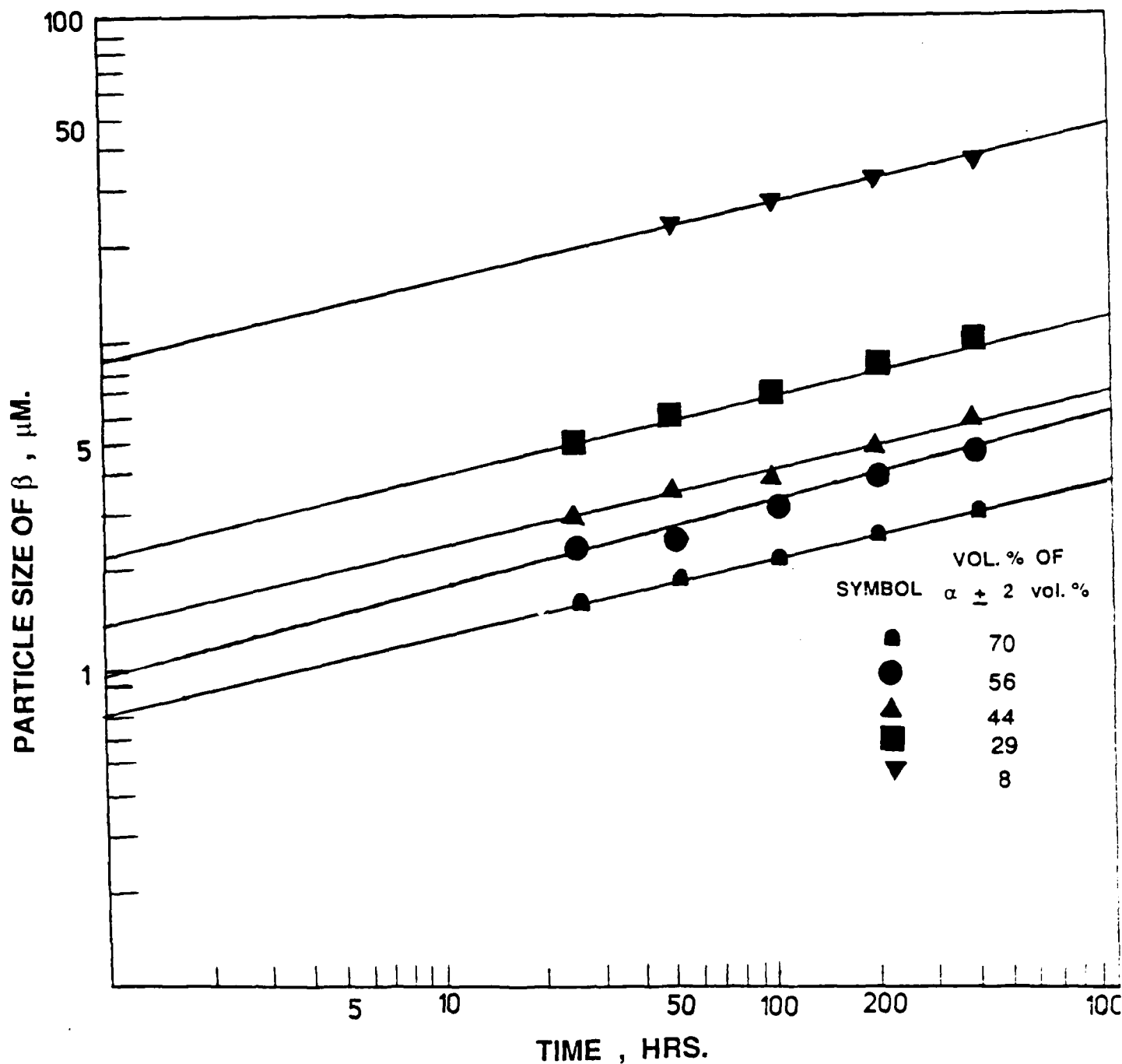
Fig. 8 : PARTICLE SIZES OF β – PHASE IN α – β Ti - V ALLOYS. THE ALLOYS WERE ANNEALED FOR VARIOUS TIMES AT 973 K , W. Q.
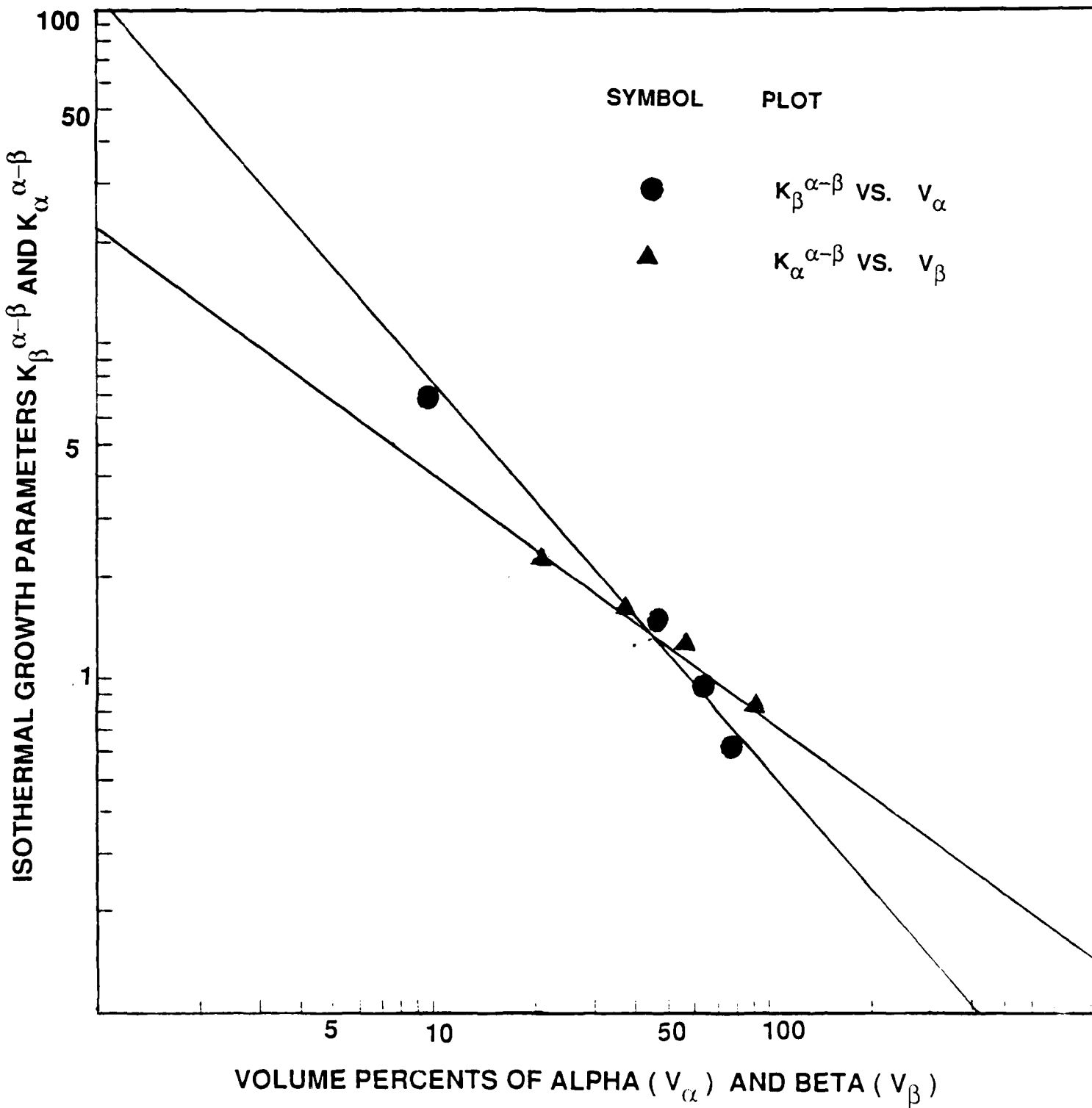
Fig. 9(a) : DEPENDENCY OF THE GROWTH PARAMETERS $\dot{K}_\alpha^{\alpha-\beta}$ AND $K_\beta^{\alpha-\beta}$ ON VOLUME PERCENTS OF $\beta$ ($V_\beta$) AND $\alpha$ ($V_\alpha$), RESPECTIVELY, FOR THE Ti - Mn SYSTEM AT 973 K
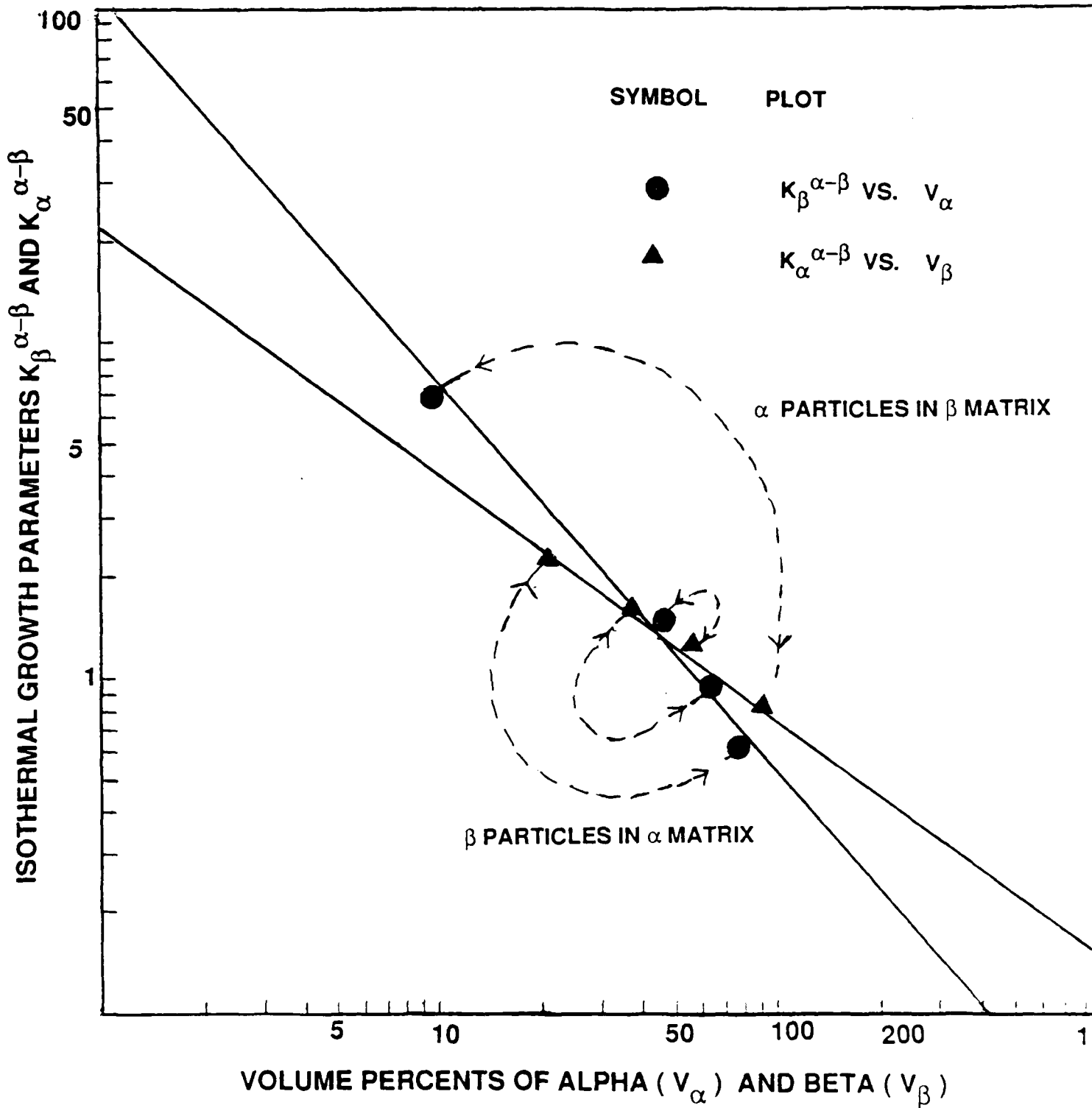
Fig. 9(b) : DEPENDENCY OF THE GROWTH PARAMETERS $K_\alpha^{\alpha-\beta}$ AND $K_\beta^{\alpha-\beta}$ ON VOLUME PERCENTS OF $\beta$ ($V_\beta$) AND $\alpha$ ($V_\alpha$), RESPECTIVELY, FOR THE Ti - Mn SYSTEM AT 973 K
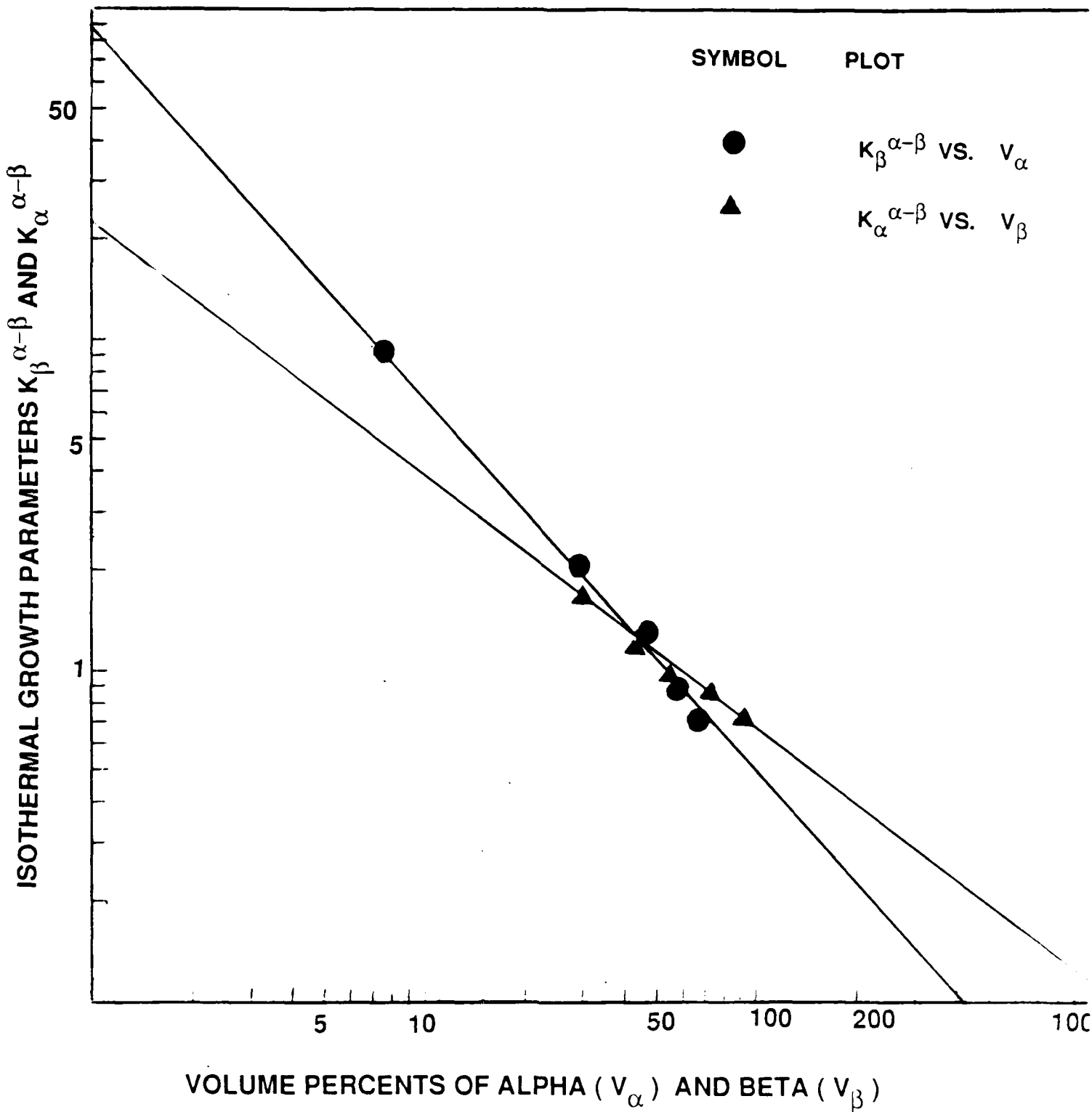
Fig. 10(a) : DEPENDENCY OF THE GROWTH PARAMETERS $K_\alpha^{\alpha-\beta}$ AND $K_\beta^{\alpha-\beta}$ ON VOLUME PERCENTS OF $\beta$ ($V_\beta$) AND $\alpha$ ($V_\alpha$), RESPECTIVELY, FOR THE Ti - V SYSTEM AT 973 K

59
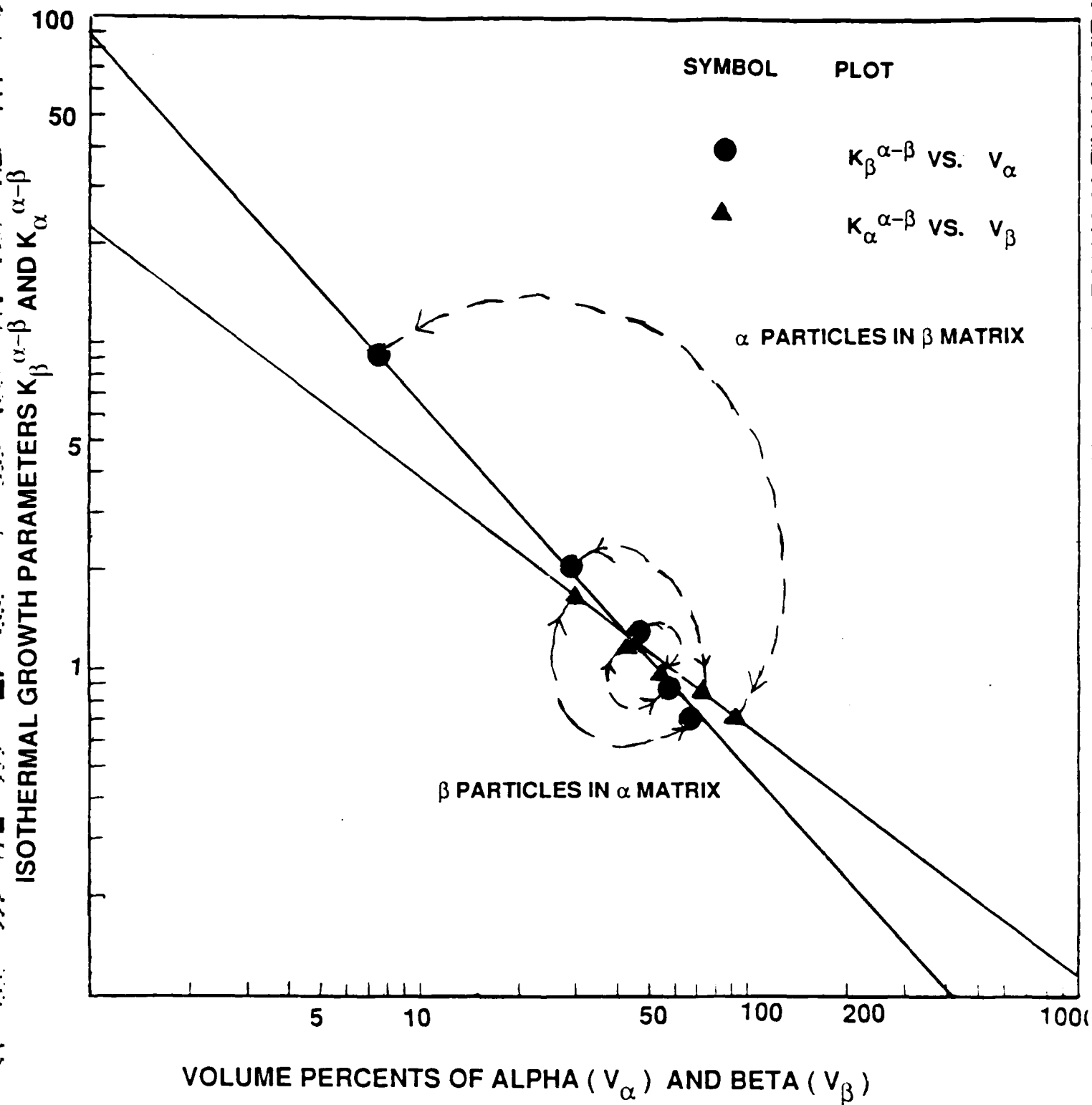
Fig.10(b): DEPENDENCY OF THE GROWTH PARAMETERS $K_\alpha^{\alpha-\beta}$ AND $K_\beta^{\alpha-\beta}$ ON VOLUME PERCENTS OF $\beta$ $(V_\beta)$ AND $\alpha$ $(V_\alpha)$, RESPECTIVELY, FOR THE Ti - V SYSTEM AT 973 K

60
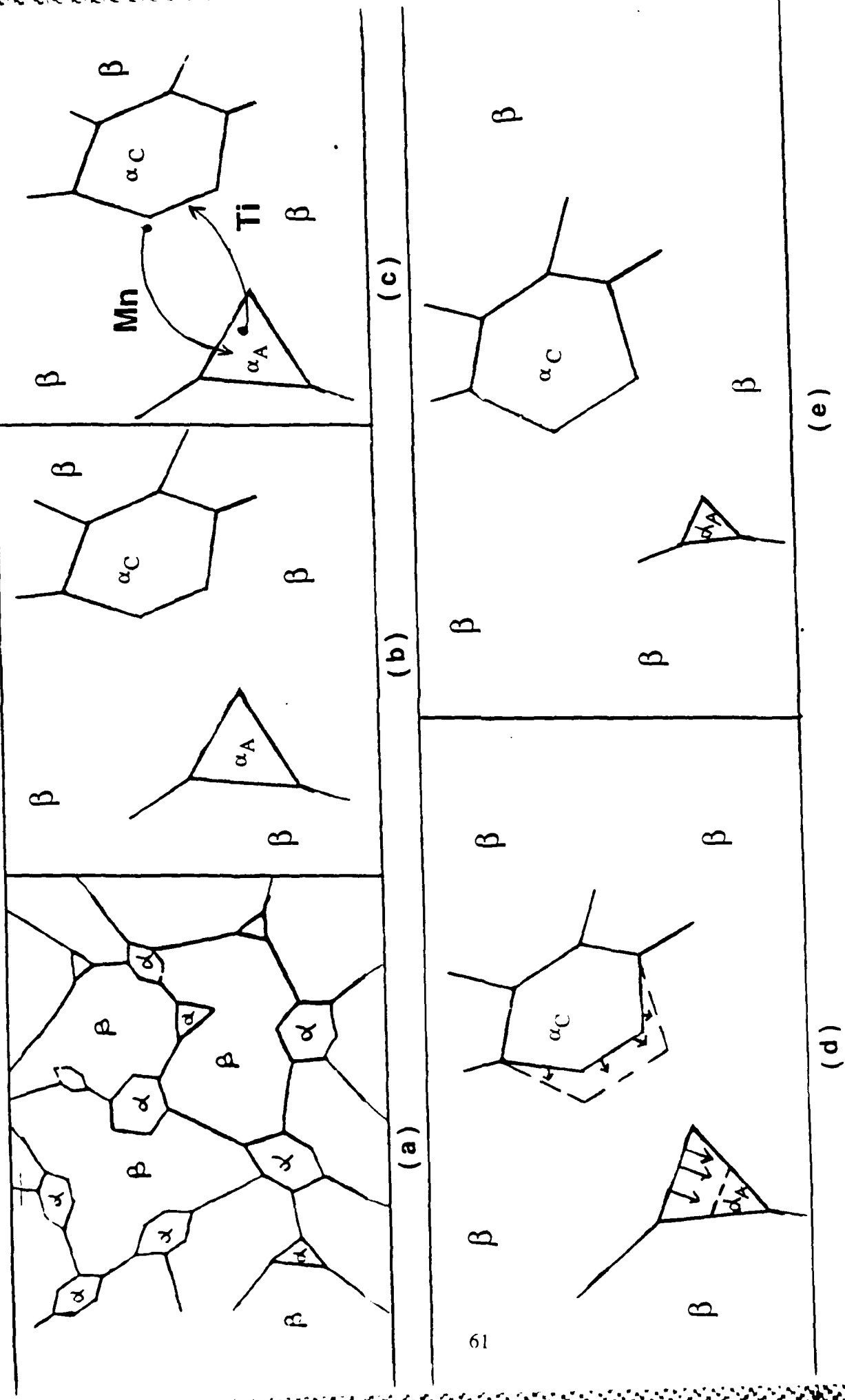
Fig. 11: A SCHEMATIC OF PARTICLE GROWTH IN TYPE 1 ( ALPHA IN BETA MATRIX ) MICROSTRUCTURES.

61
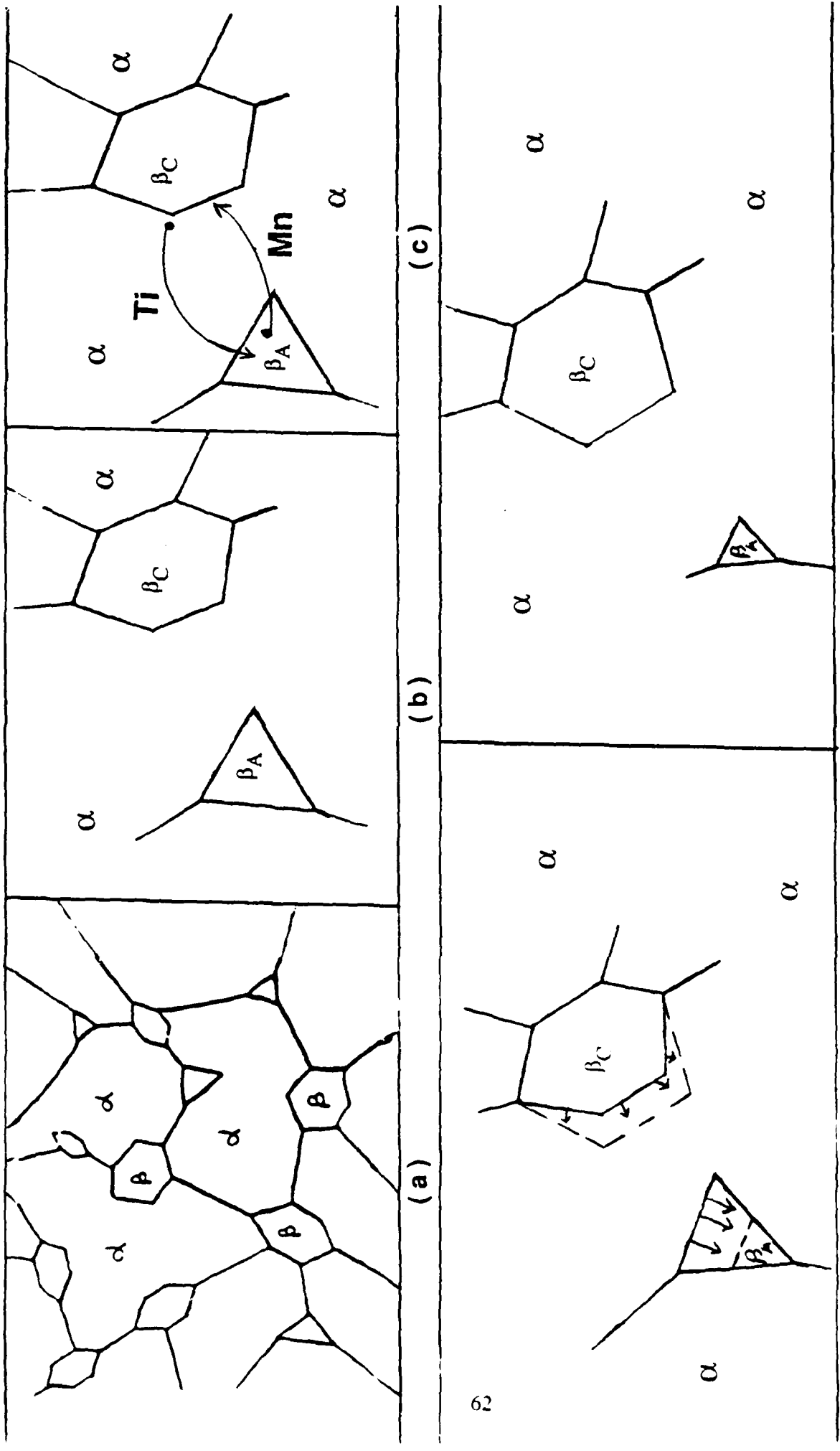
Fig. 12 : A SCHEMATIC OF PARTICLE GROWTH IN TYPE 2 ( BETA IN ALPHA MATRIX ) MICROSTRUCTURES.

62
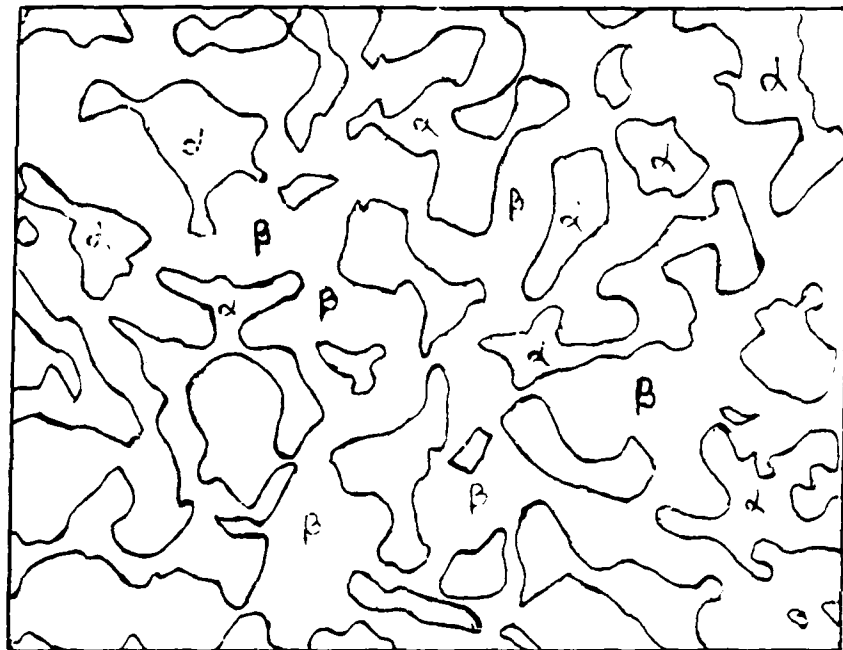
(a)
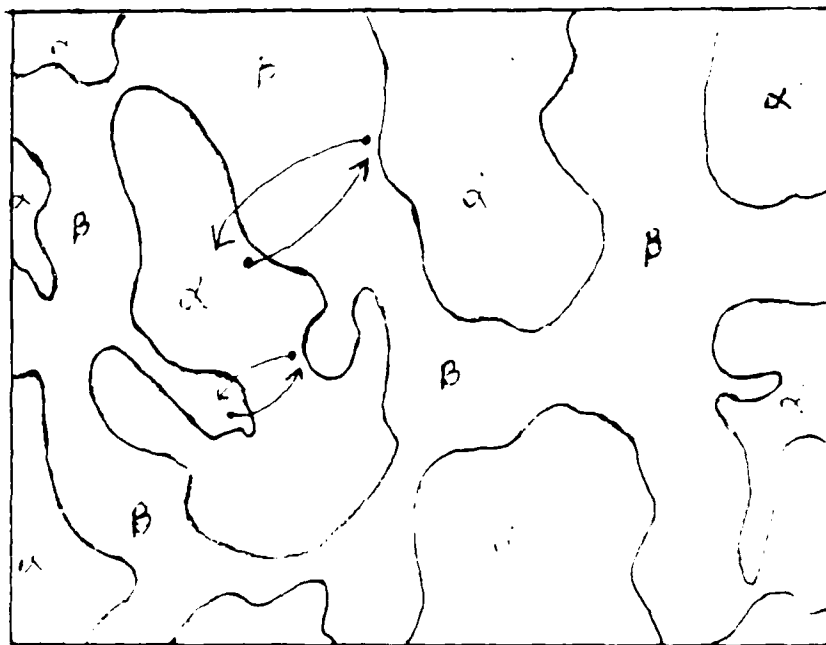
(b)

Fig. 13 :  A SCHEMATIC OF DIFFUSION PATHS IN TYPE 3
( NEARLY EQUIVALENT VOLUME PERCENTS OF $\alpha$
AND $\beta$ ) MICROSTRUCTURES.
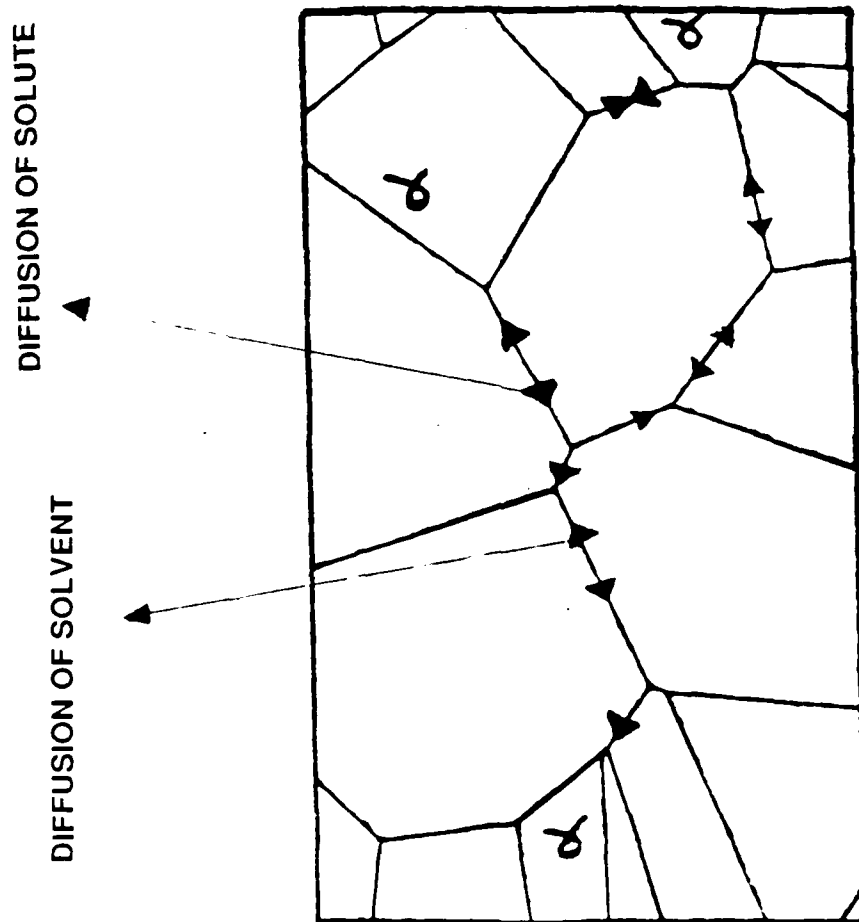
Fig. 14 : AN ALTERNATE MECHANISM OF BULK DIFFUSION VIA
β β GRAIN BOUNDARIES IN CLASS 1 MICROSTRUCTURES.

**FLUX EXCHANGE**

Tracking boundaries for interface AB

Tracking boundaries for interface ED
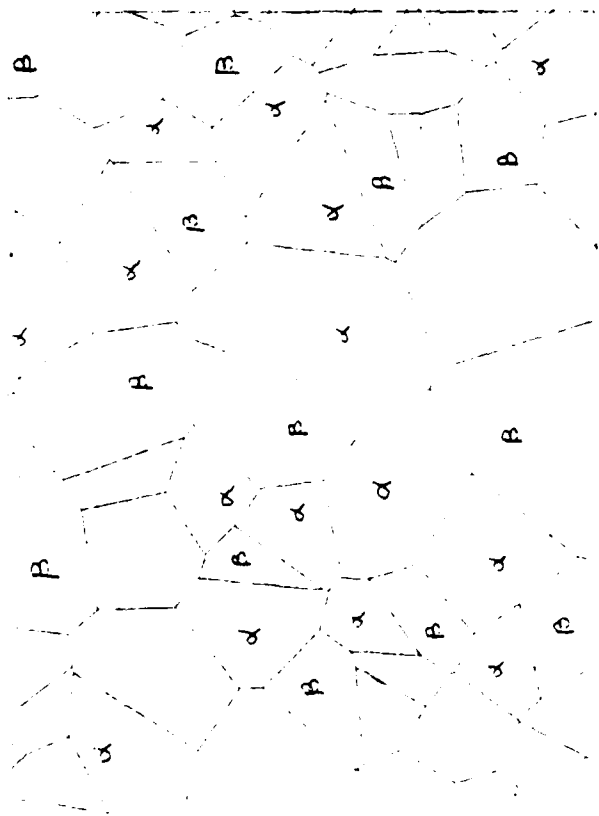
(a)
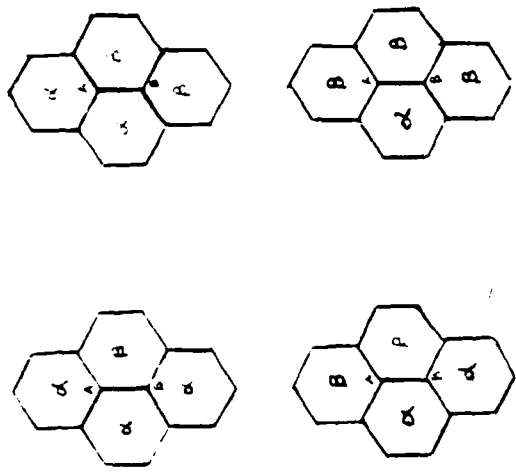
(b)
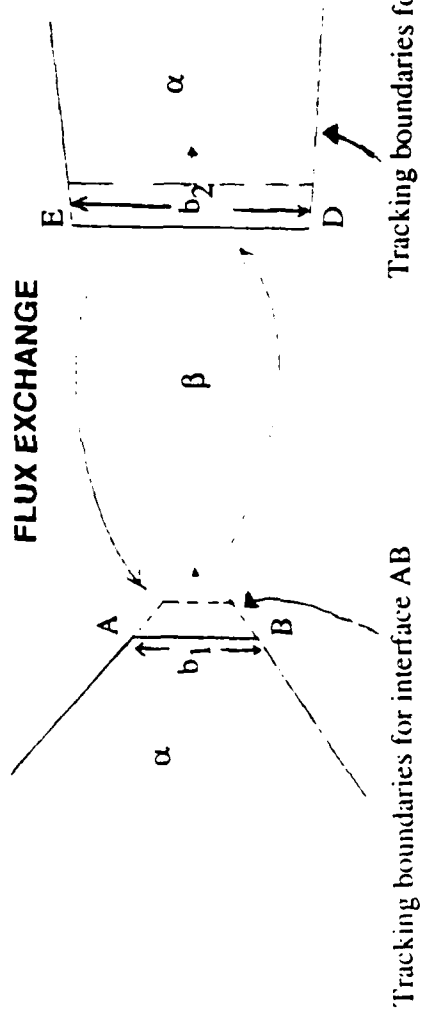
(c)

Fig. 15 : (a) A NETWORK OF $\alpha$ AND $\beta$ GRAINS IN A $\alpha - \beta$ TWO PHASE ALLOY (b) TYPICAL NEAREST NEIGHBOURS IN A $\alpha - \beta$ TWO PHASE ALLOY. (c) AN EXPLODED VIEW OF TWO INTER-ACTING INTERFACES.
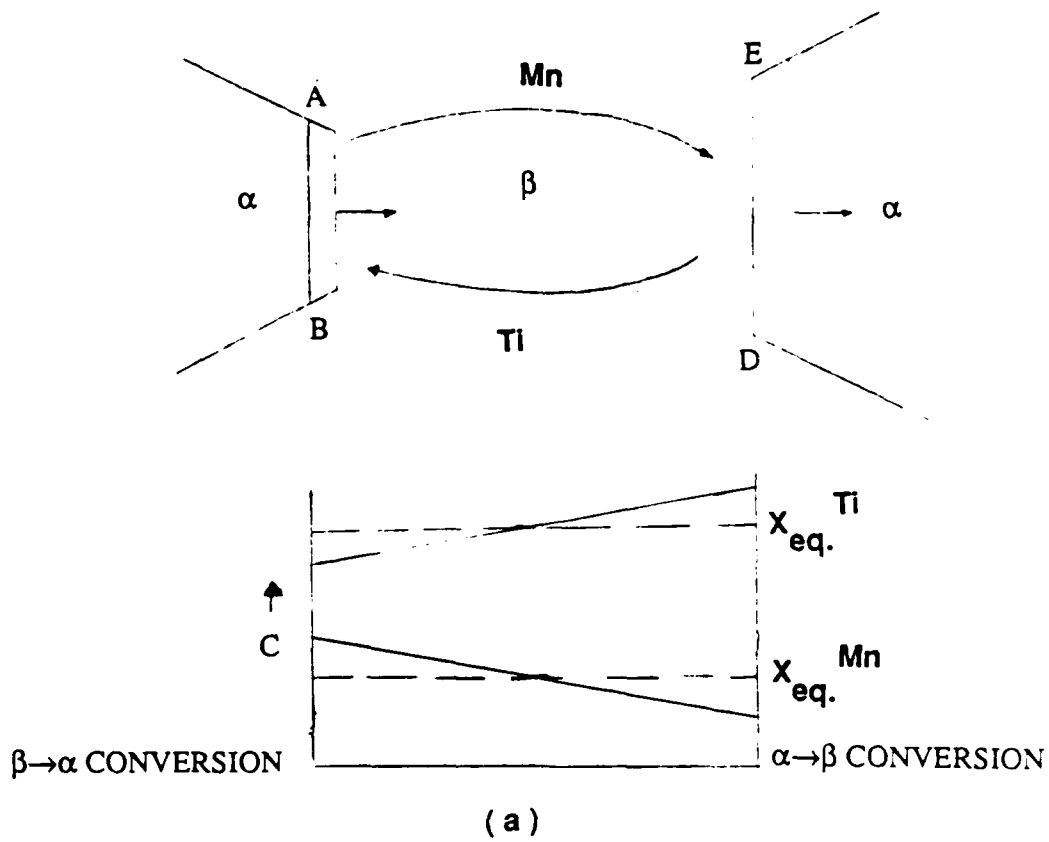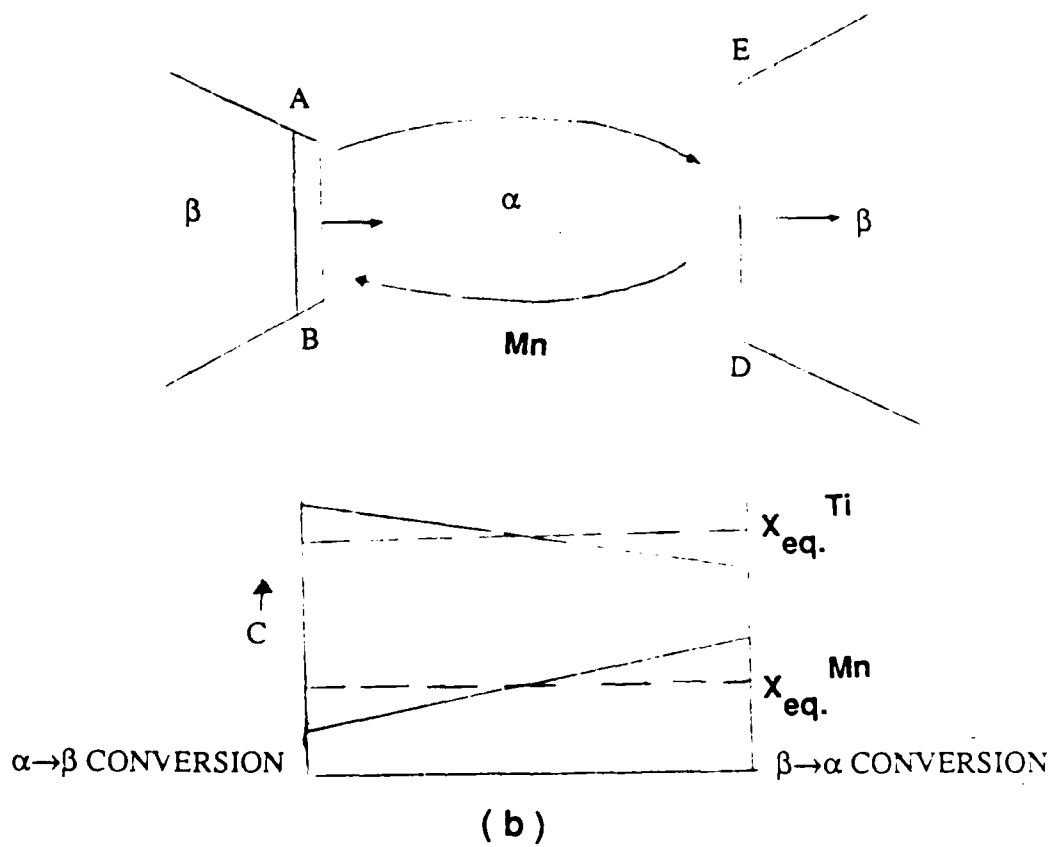
Fig. 16 : ( a ) TYPICAL CONCENTRATION GRADIENTS OF Ti AND Mn IN MATRIX IN CLASS 1 MICROSTRUCTURES. ( b ) TYPICAL CONCENTRATION GRADIENTS IN MATRIX IN CLASS 2 MICROSTRUCTURES.

66

(b)

(a)

10 μM.

Fig. 17 : TYPICAL PLANAR ( a ) AND CURVED ( b ) INTERFACES IN $\alpha$-$\beta$ TITANIUM ALLOYS.
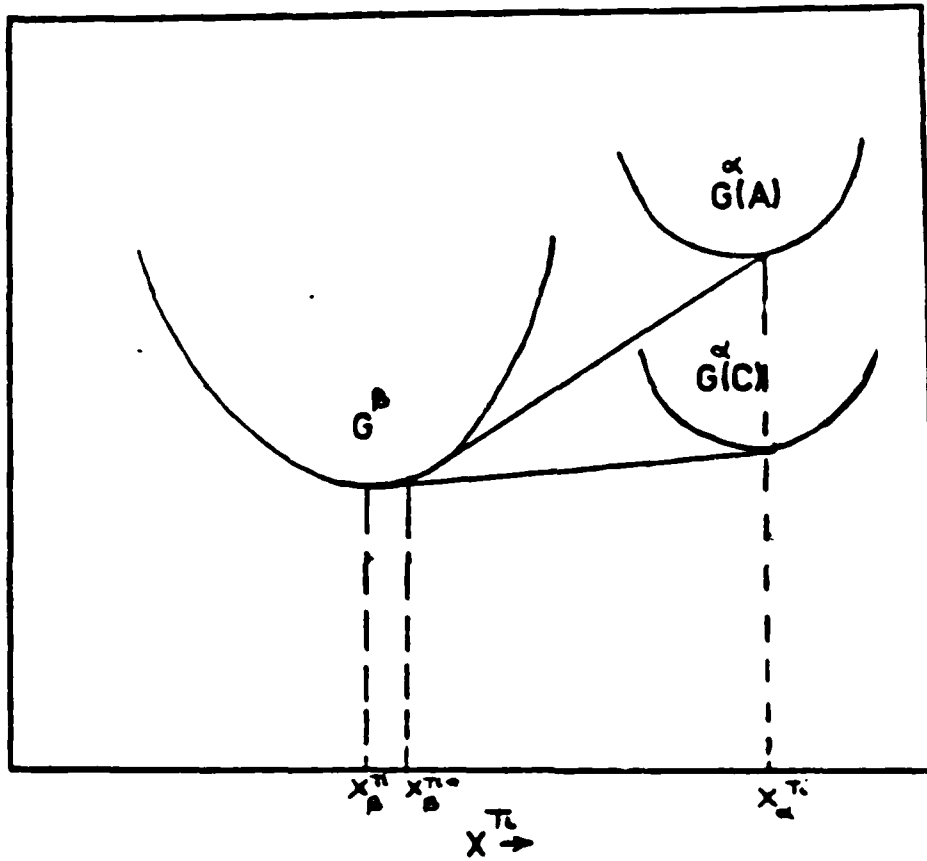
Fig. 18 ( a) :   MOLAR FREE ENERGY PLOTS OF PARTICLE AND
MATRIX PHASES IN CLASS 1 MICROSTRUCTURES.
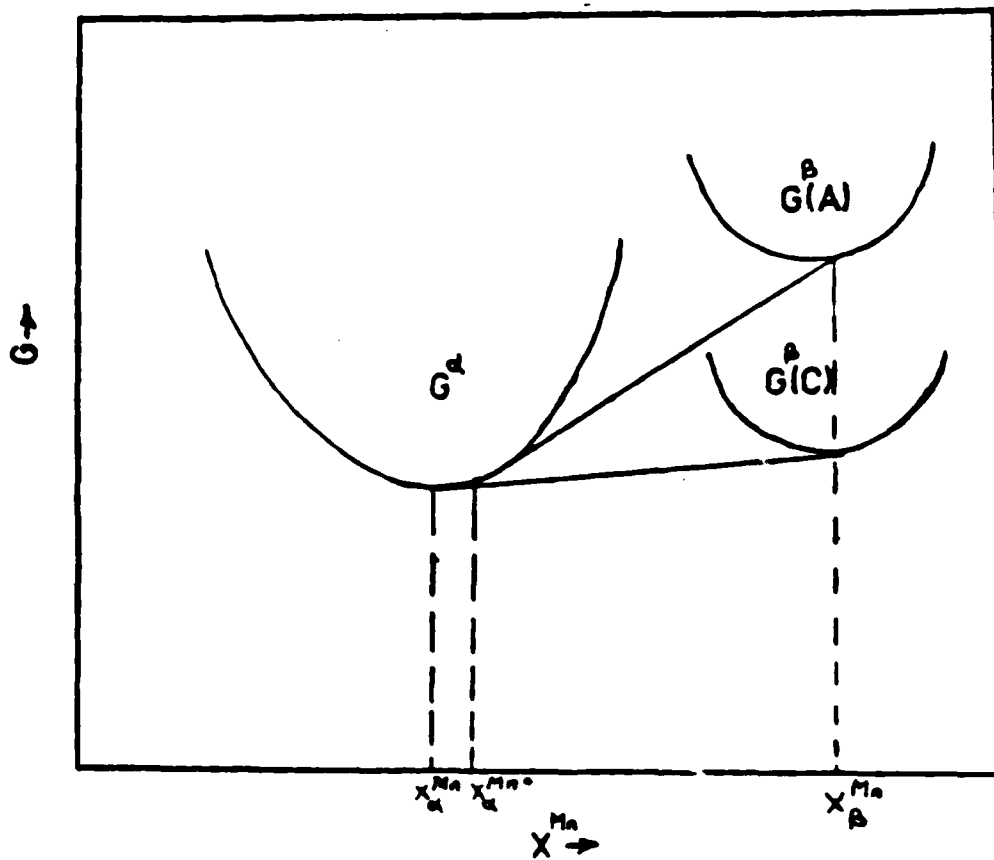
Fig. 18 (b): MOLAR FREE ENERGY PLOTS OF PARTICLE AND MATRIX PHASES IN CLASS 2 MICROSTRUCTURES.
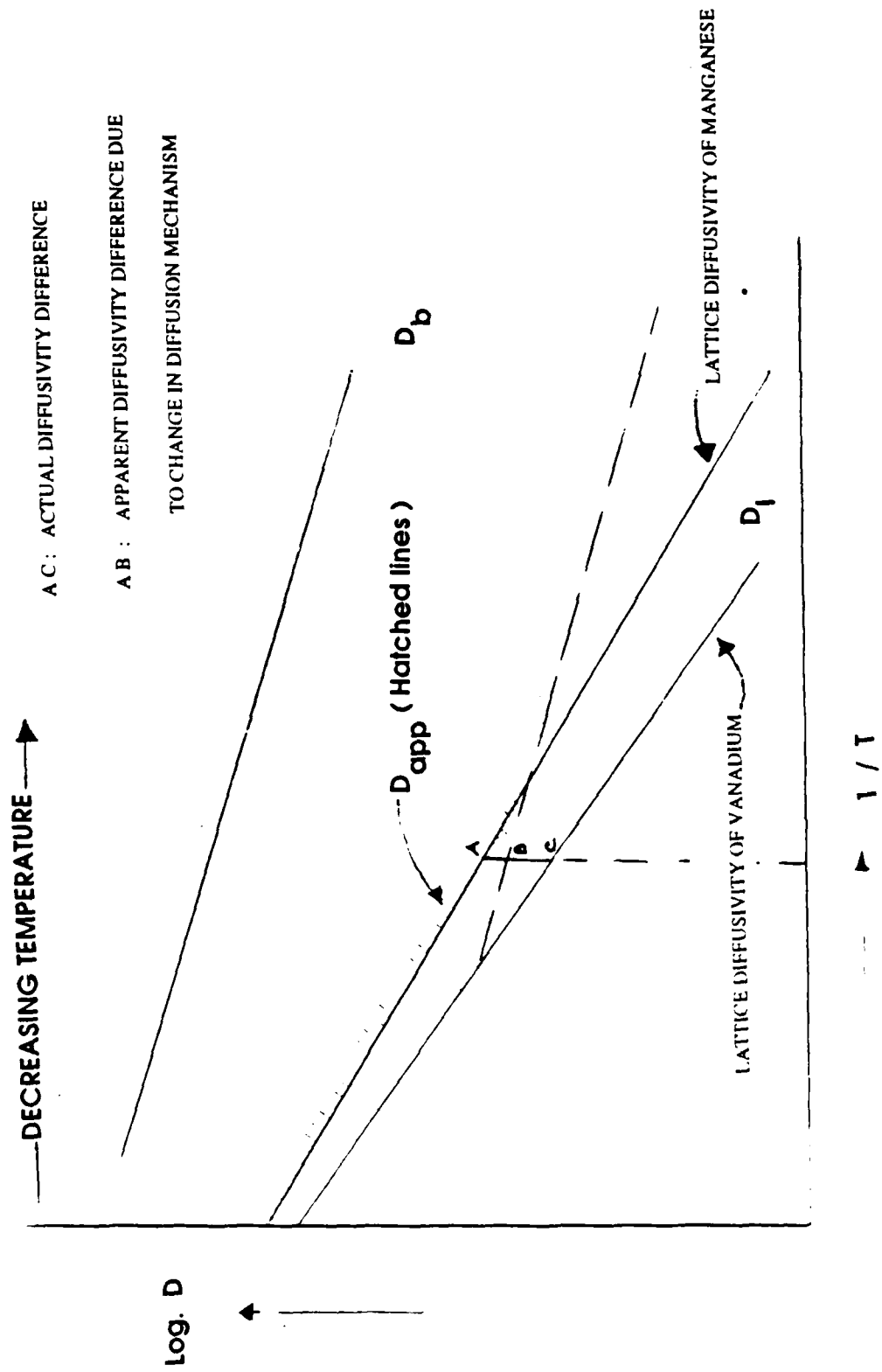
Fig. 19 (a) :  ACTUAL AND APPARENT DIFFUSIVITY DIFFERENCES IN
Ti - Mn AND Ti - V ALLOY SYSTEMS.
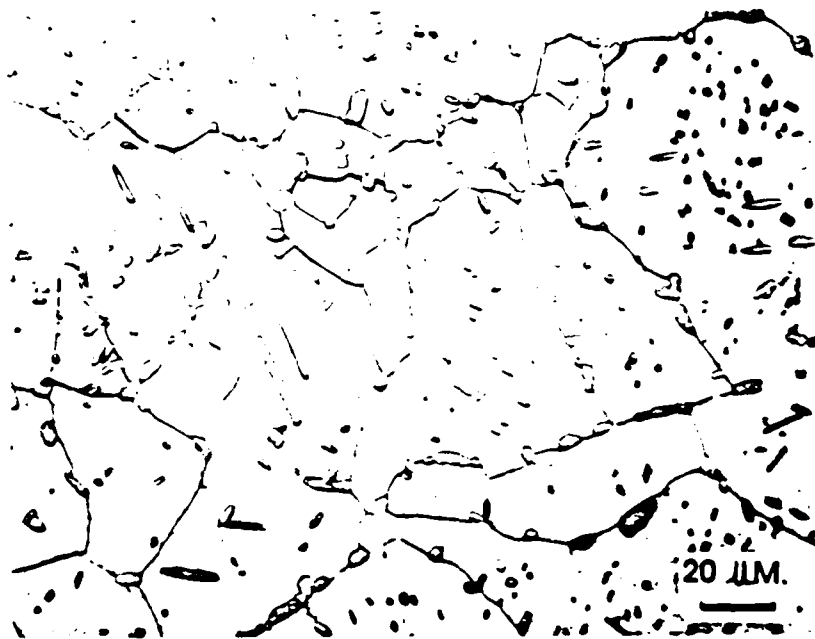
**Fig. 19 (b) :** A TYPICAL GRAIN BOUNDARY STRUCTURE IN AN (α-β)
ALLOY.

Fig. 20 : PARTIAL Ti END OF THE Ti - Mn PHASE DIAGRAM.
THE AIM COMPOSITIONS OF ALLOYS ARE
INDICATED WITH SOLID CIRCLES.
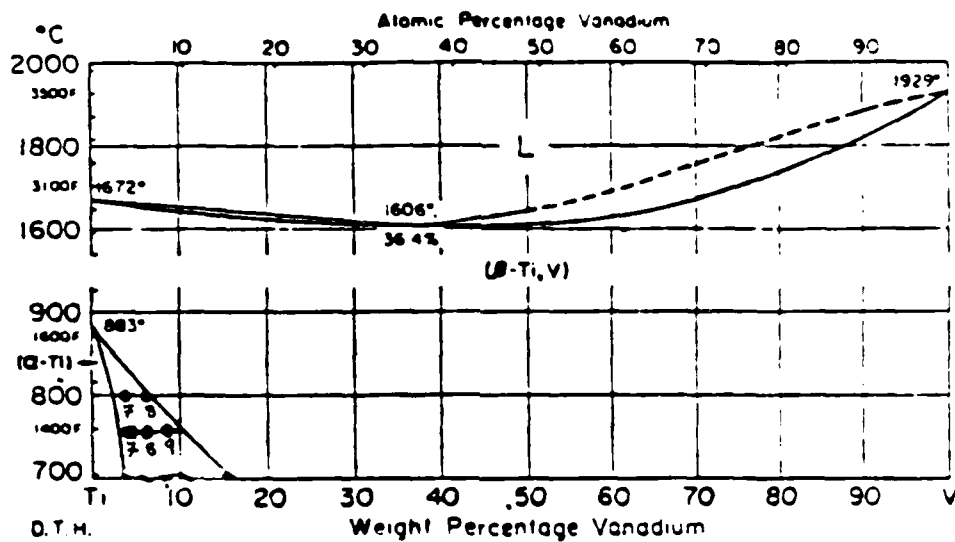
Fig. 21 : THE Ti - V PHASE DIAGRAM.    THE AIM COMPOSI-
TIONS OF ALLOYS ARE INDICATED WITH
SOLID CIRCLES.

49 % α - 51 % β

74 % α - 26 % β

18 % α - 82 % β
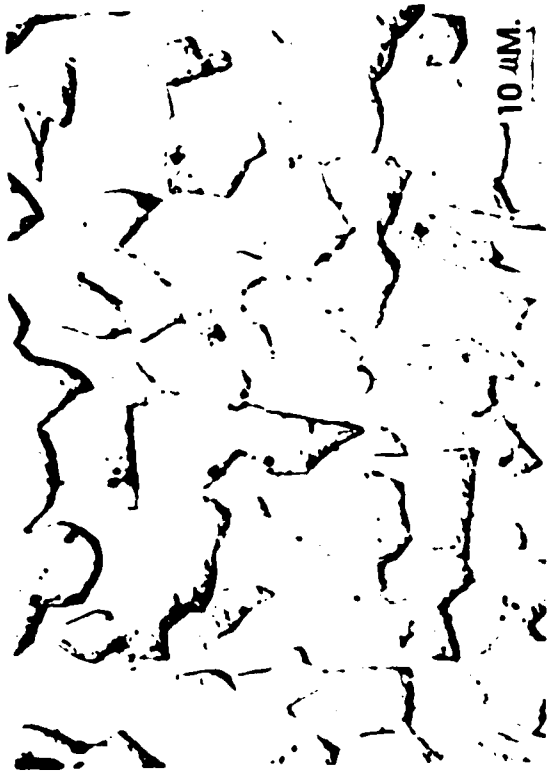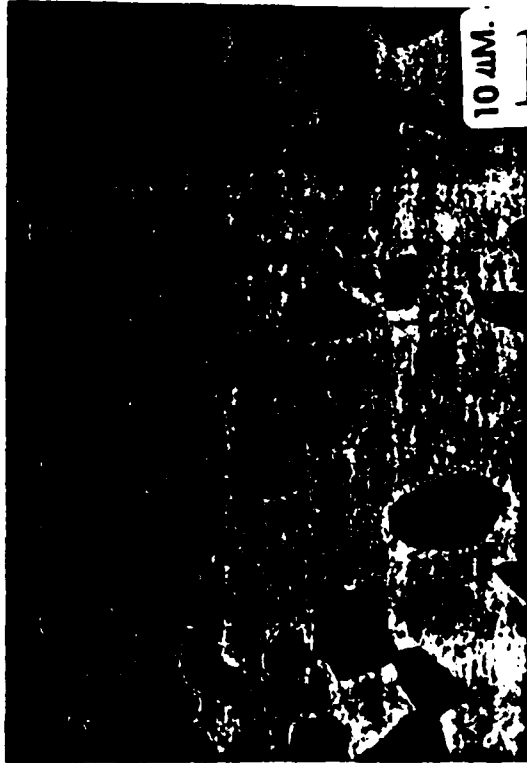
Fig. 22 : MICROSTRUCTURES OF VARIOUS α–β Ti-Mn ALLOYS ANNEALED FOR 200 HRS AT 1023° K

39% α - 61% β

59% α - 41% β

12% α - 88% β

Fig. 23 :  MICROSTRUCTURES OF VARIOUS α β Ti-V ALLOYS
ANNEALED FOR 200 HRS. AT 1023° K
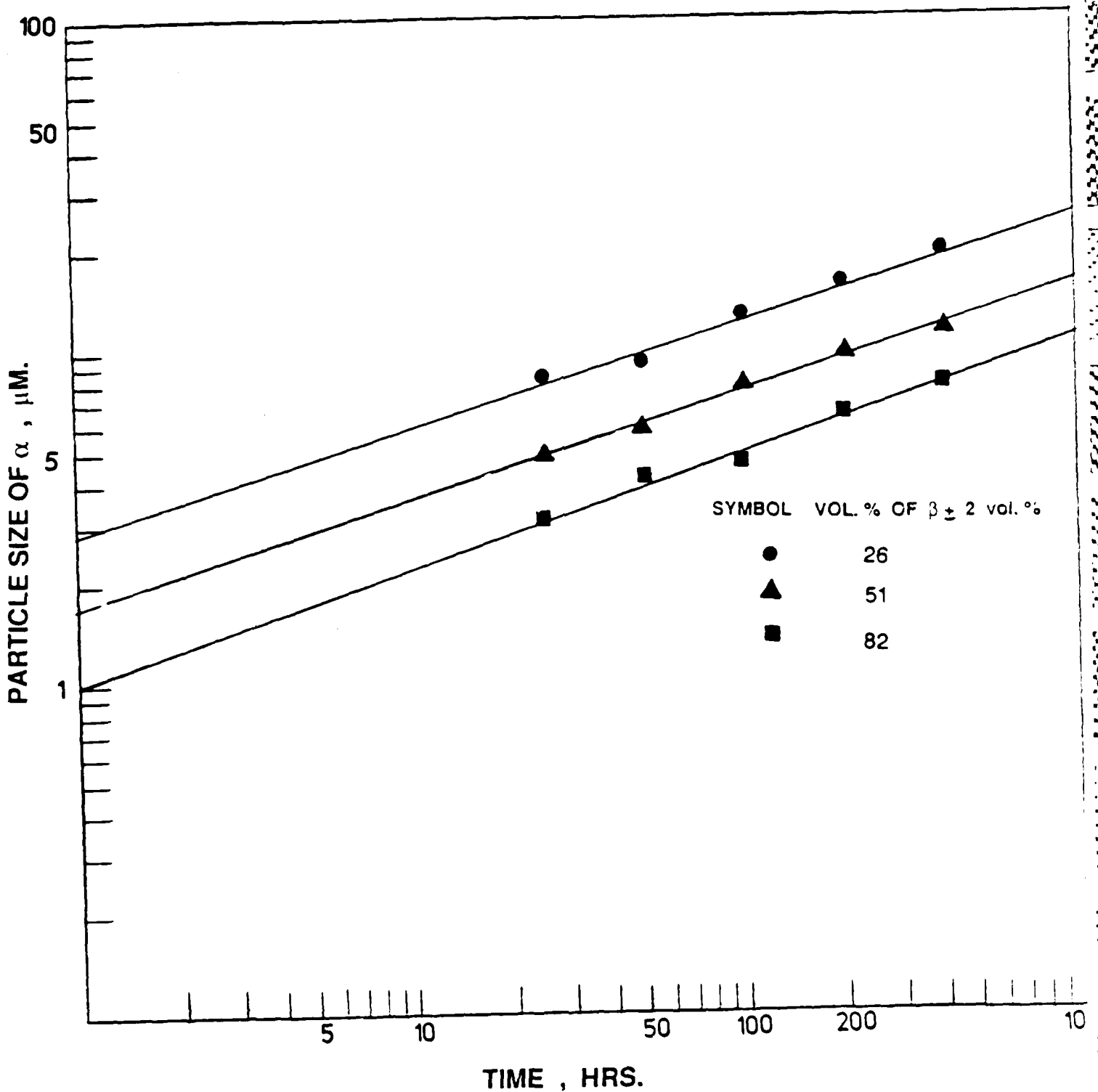
Fig. 24 : PARTICLE SIZES OF $\alpha$ – PHASE IN $\alpha$ – $\beta$ Ti - Mn ALLOYS. THE ALLOYS WERE ANNEALED FOR VARIOUS TIMES AT 1023 K , W. Q.
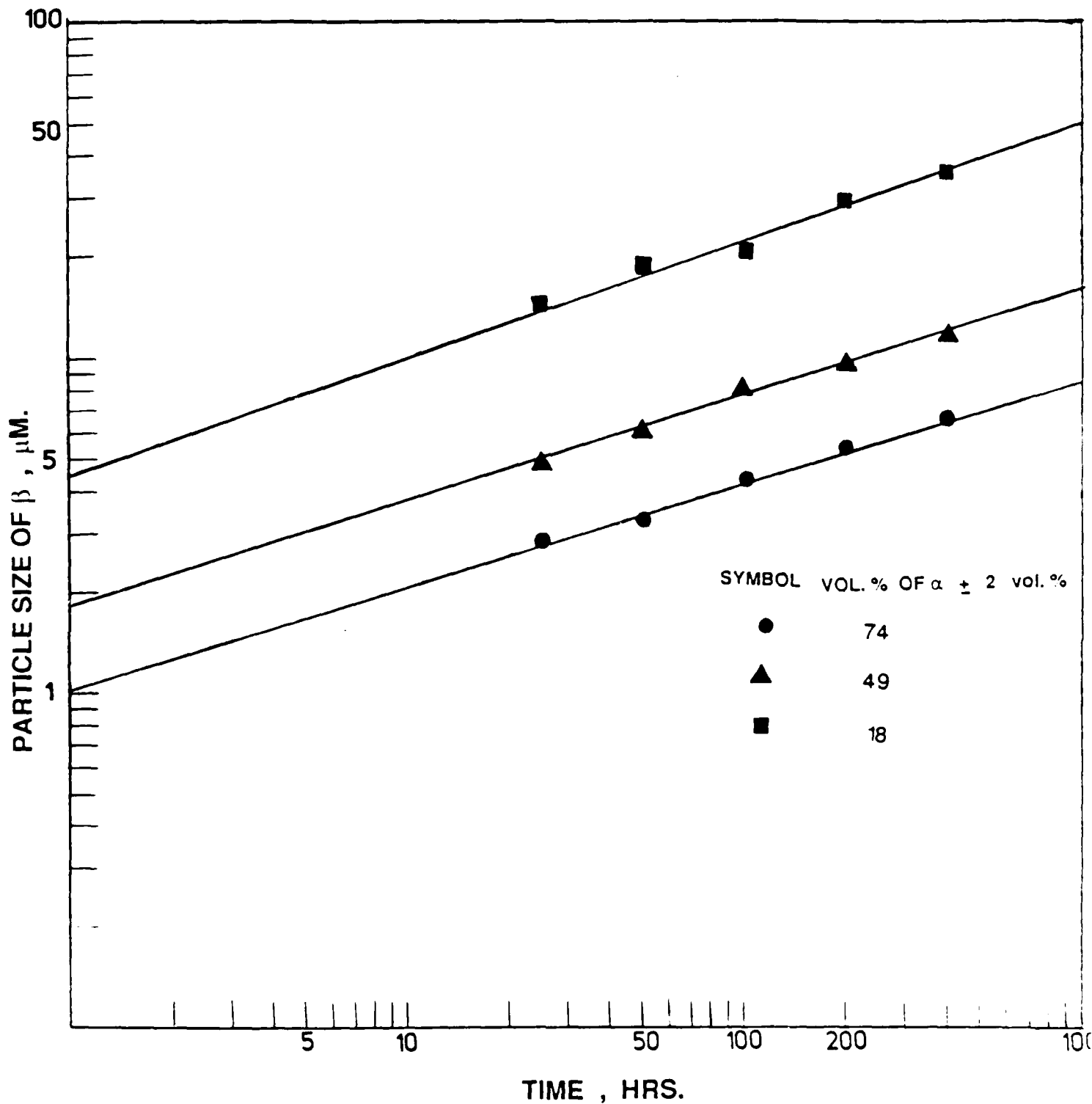
Fig. 25 : PARTICLE SIZES OF $\beta$ – PHASE IN $\alpha$ – $\beta$ Ti - Mn ALLOYS. THE ALLOYS WERE ANNEALED FOR VARIOUS TIMES AT 1023 K , W. Q.
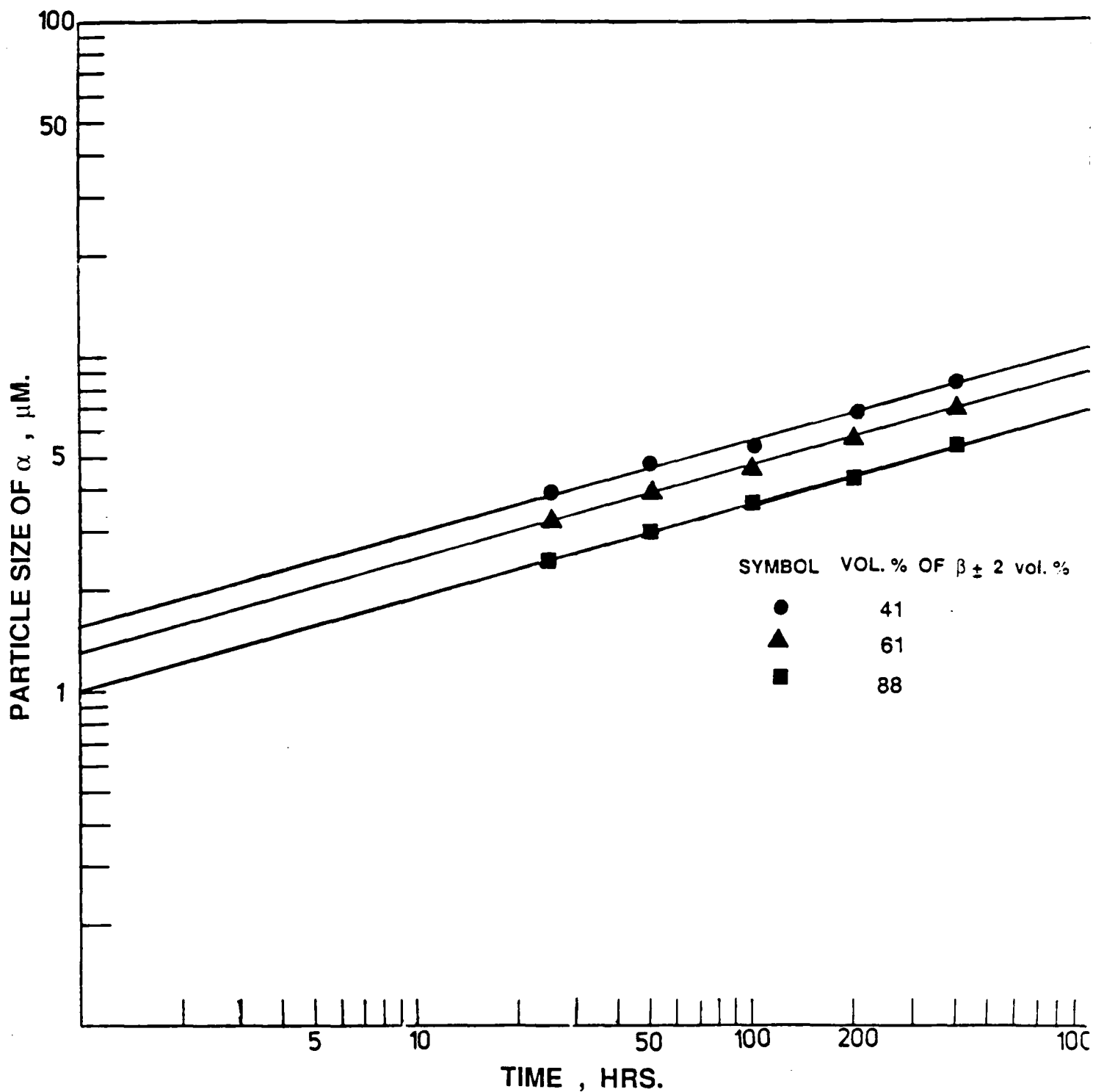
Fig. 26 : PARTICLE SIZES OF $\alpha$ – PHASE IN $\alpha$ – $\beta$ Ti - V ALLOYS. THE ALLOYS WERE ANNEALED FOR VARIOUS TIMES AT 1023 K , W. Q.
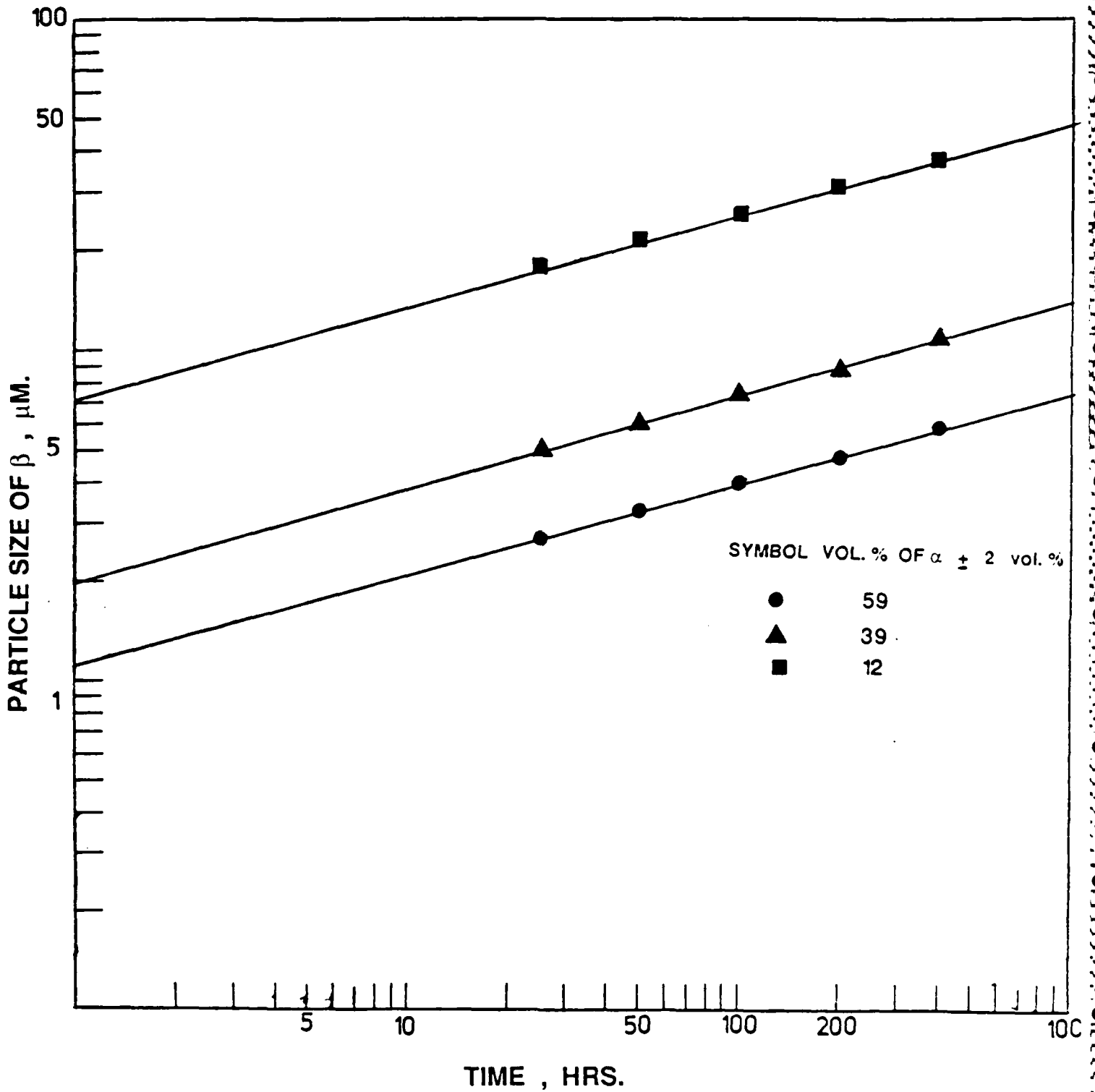
Fig. 27: PARTICLE SIZES OF β – PHASE IN α – β Ti - V ALLOYS. THE ALLOYS WERE ANNEALED FOR VARIOUS TIMES AT 1023 K , W. Q.
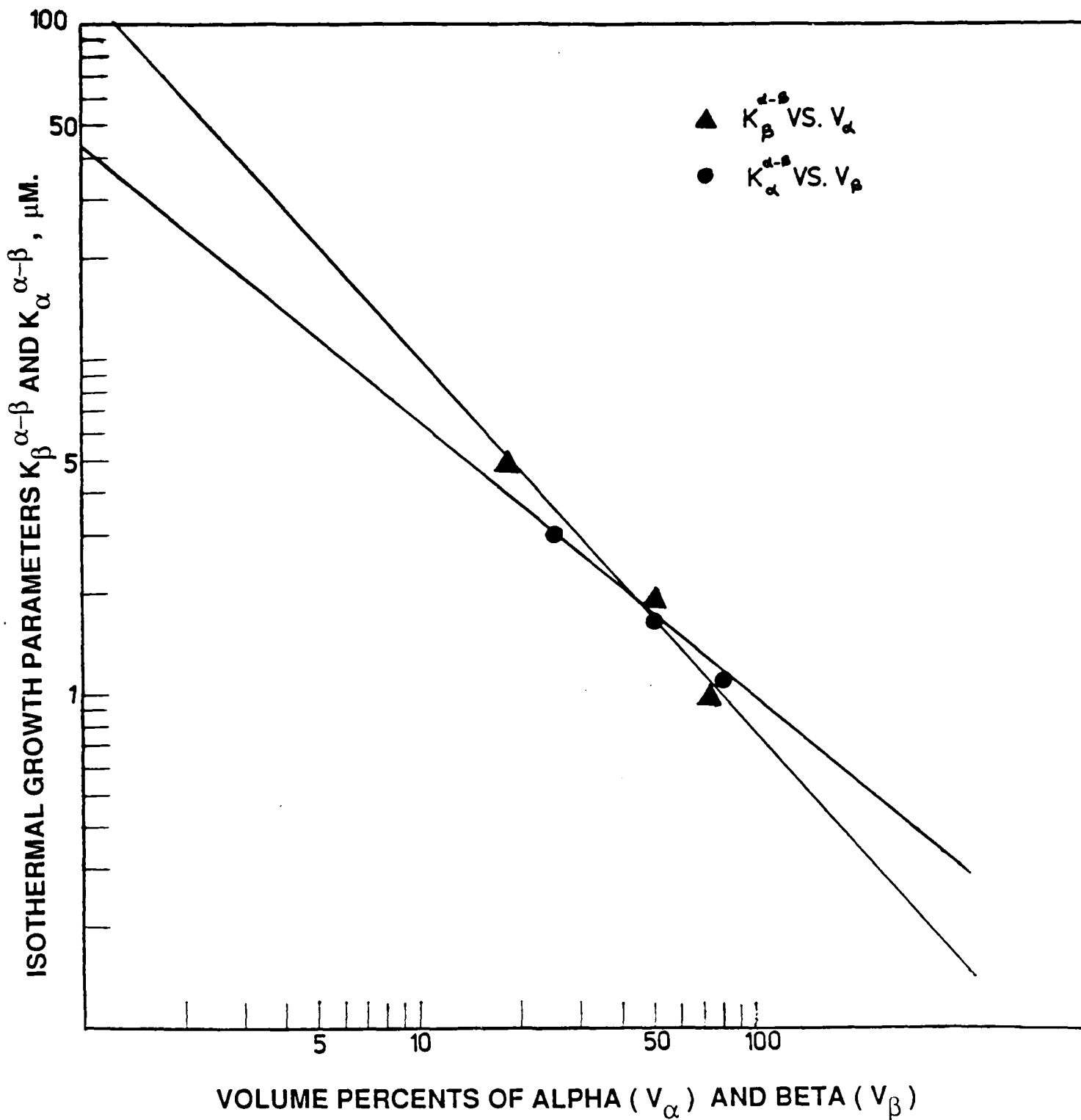
Fig. 28: DEPENDENCY OF THE GROWTH PARAMETERS $K_\alpha^{\alpha-\beta}$ AND $K_\beta^{\alpha-\beta}$ ON VOLUME PERCENTS OF $\beta$ ($V_\beta$) AND $\alpha$ ($V_\alpha$), RESPECTIVELY, FOR THE Ti - Mn SYSTEM AT 1023 K

80
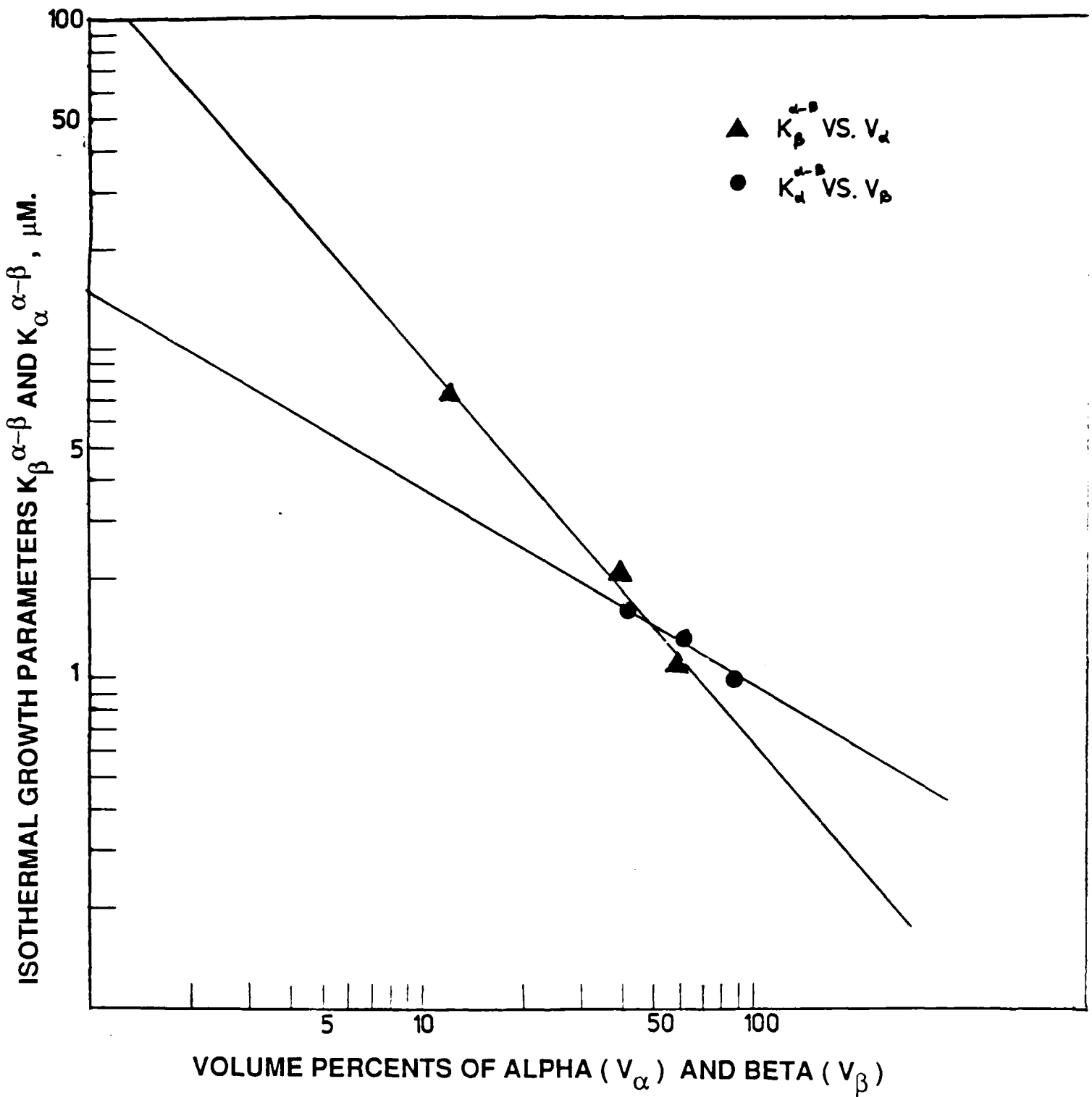
Fig. 29: DEPENDENCY OF THE GROWTH PARAMETERS $K_\alpha^{\alpha-\beta}$ AND $K_\beta^{\alpha-\beta}$ ON VOLUME PERCENTS OF $\beta$ ($V_\beta$) AND $\alpha$ ($V_\alpha$), RESPECTIVELY, FOR THE Ti - V SYSTEM AT 1023 K

81

54 % α -46 % β

24 % α -76 % β
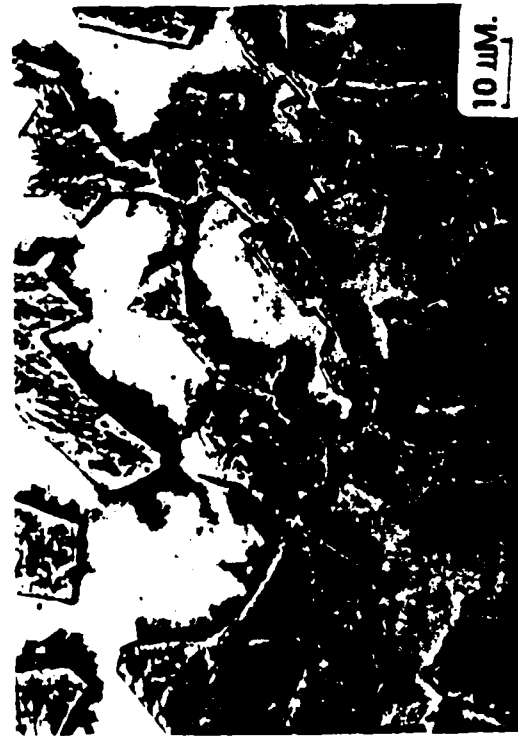
Fig. 30 : MICROSTRUCTURES OF VARIOUS α–β Ti-Mn ALLOYS ANNEALED FOR 200 HRS. AT 1073° K

82

6 % α - 94 % β

36 % α - 64 % β

Fig. 31 : MICROSTRUCTURES OF VARIOUS α–β Ti-V ALLOYS
ANNEALED FOR 200 HRS. AT 1073° K

83
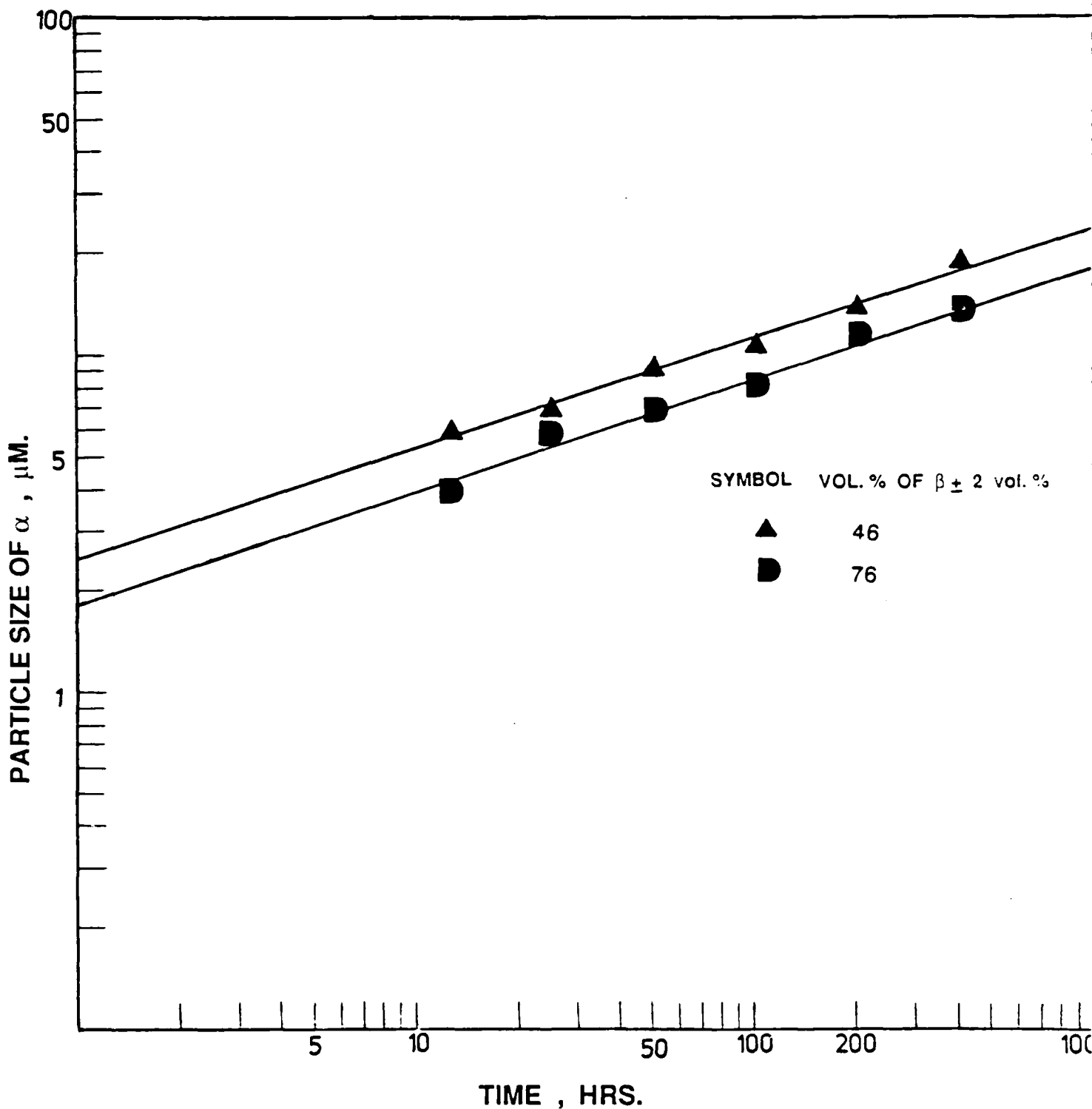
Fig. 32: PARTICLE SIZES OF $\alpha$ – PHASE IN $\alpha$ – $\beta$ Ti - Mn ALLOYS. THE ALLOYS WERE ANNEALED FOR VARIOUS TIMES AT 1073 K , W. Q.

84
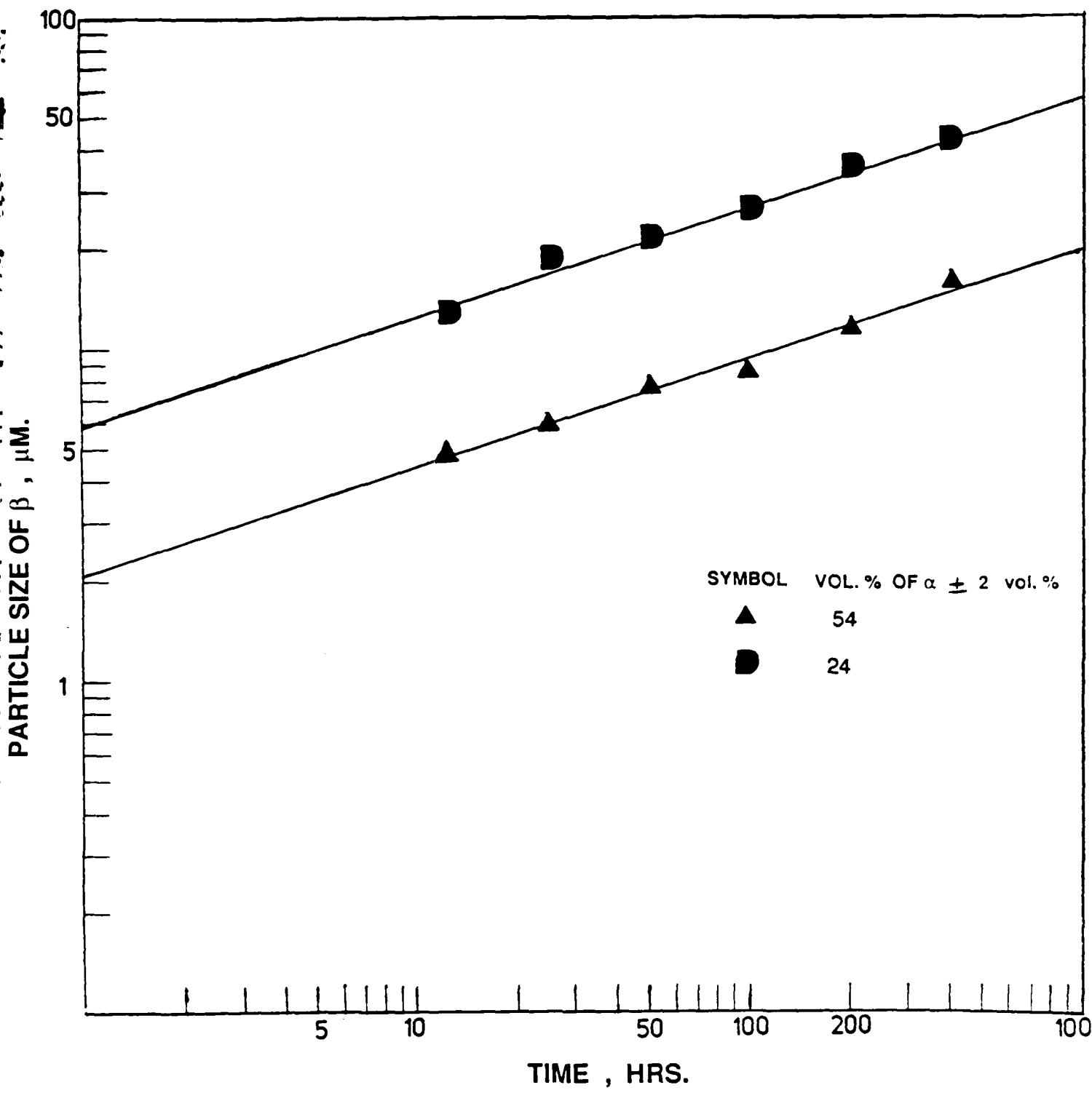
Fig. 33: PARTICLE SIZES OF $\beta$ – PHASE IN $\alpha - \beta$ Ti - Mn ALLOYS. THE ALLOYS WERE ANNEALED FOR VARIOUS TIMES AT 1073 K , W. Q.

85
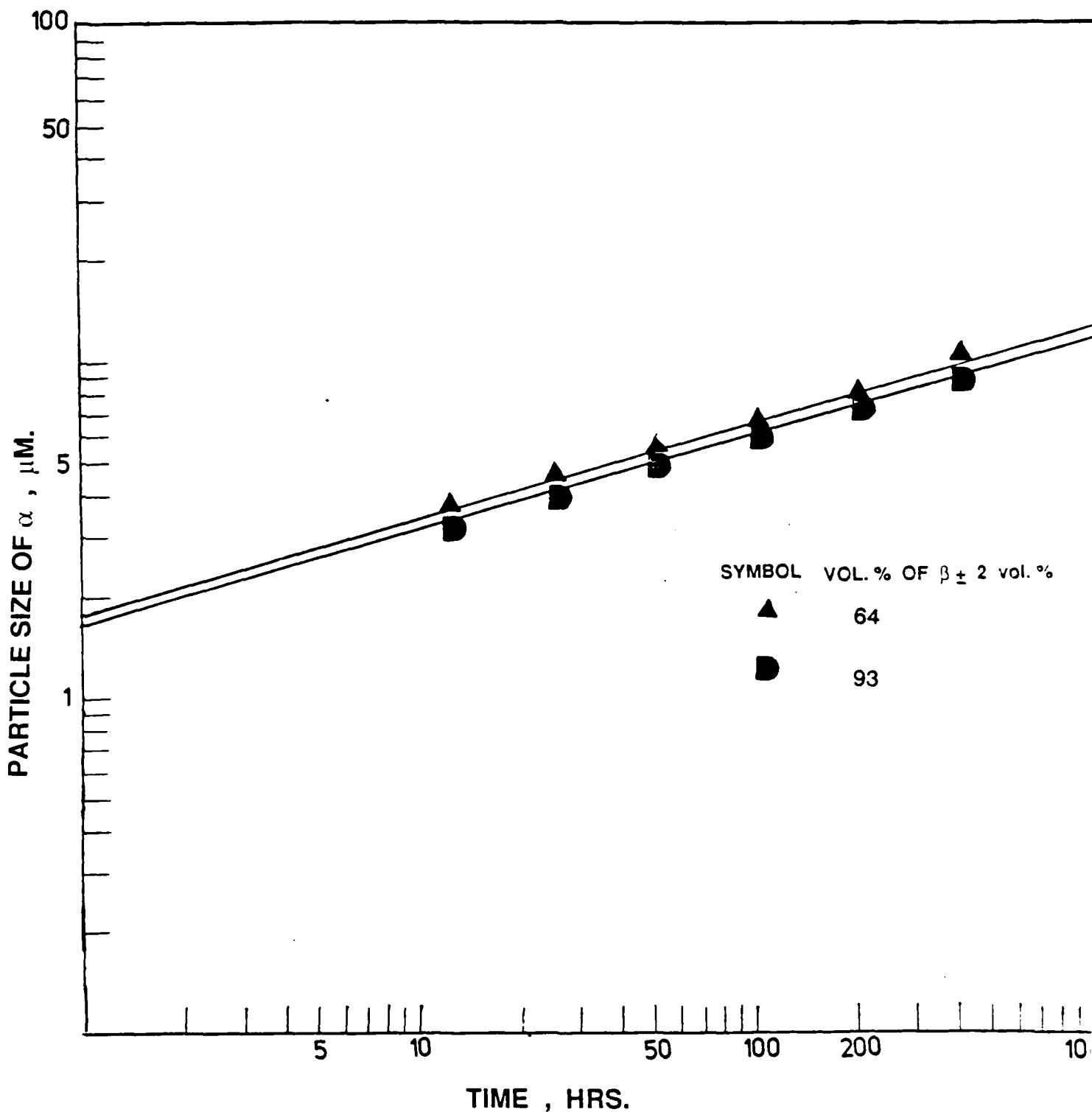
Fig. 34: PARTICLE SIZES OF $\alpha$ – PHASE IN $\alpha$ – $\beta$ Ti - V ALLOYS. THE ALLOYS WERE ANNEALED FOR VARIOUS TIMES AT 1073 K , W. Q.
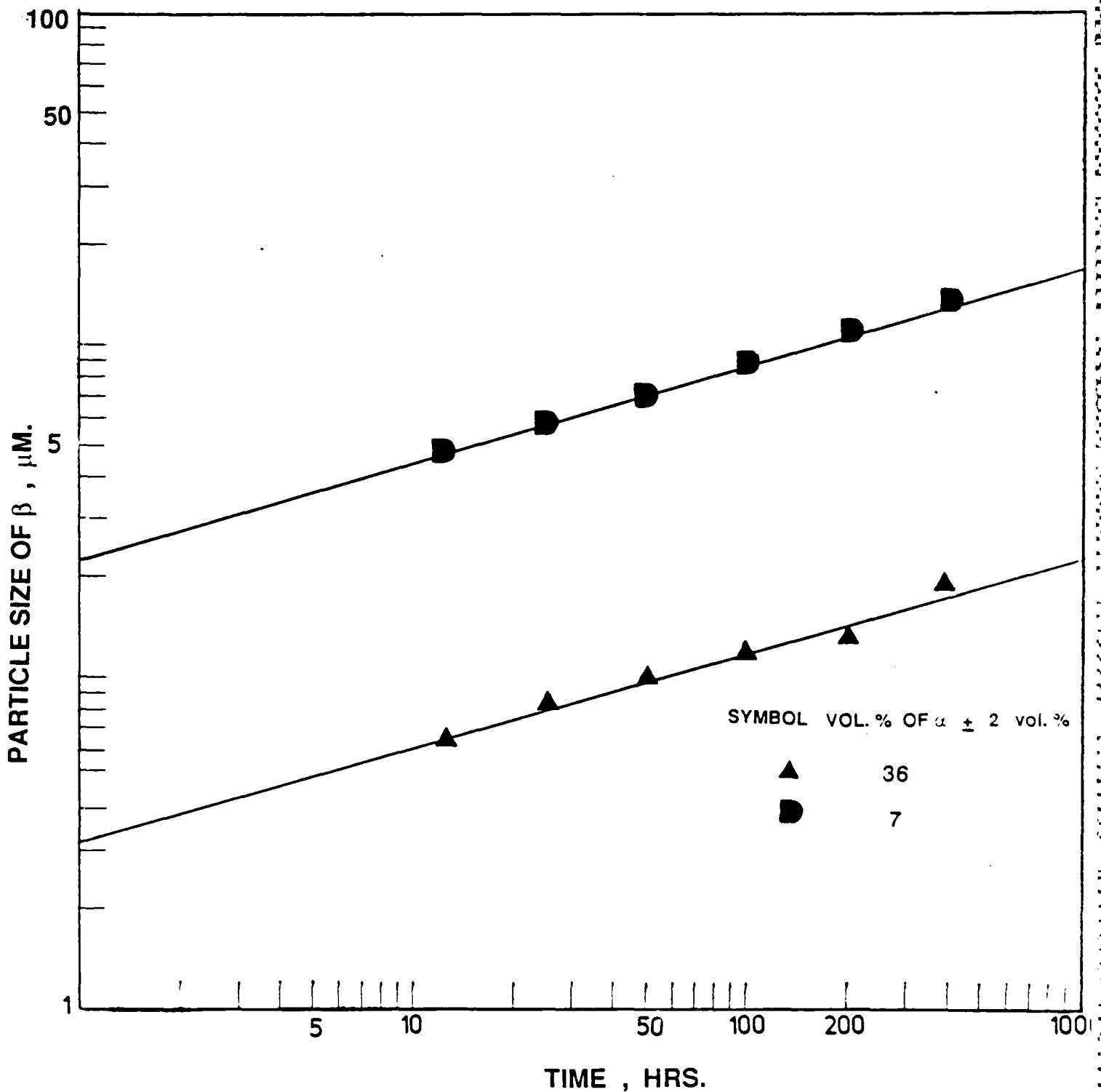
Fig. 35: PARTICLE SIZES OF β – PHASE IN α – β Ti - V ALLOYS. THE ALLOYS WERE ANNEALED FOR VARIOUS TIMES AT 1073 K , W. Q.
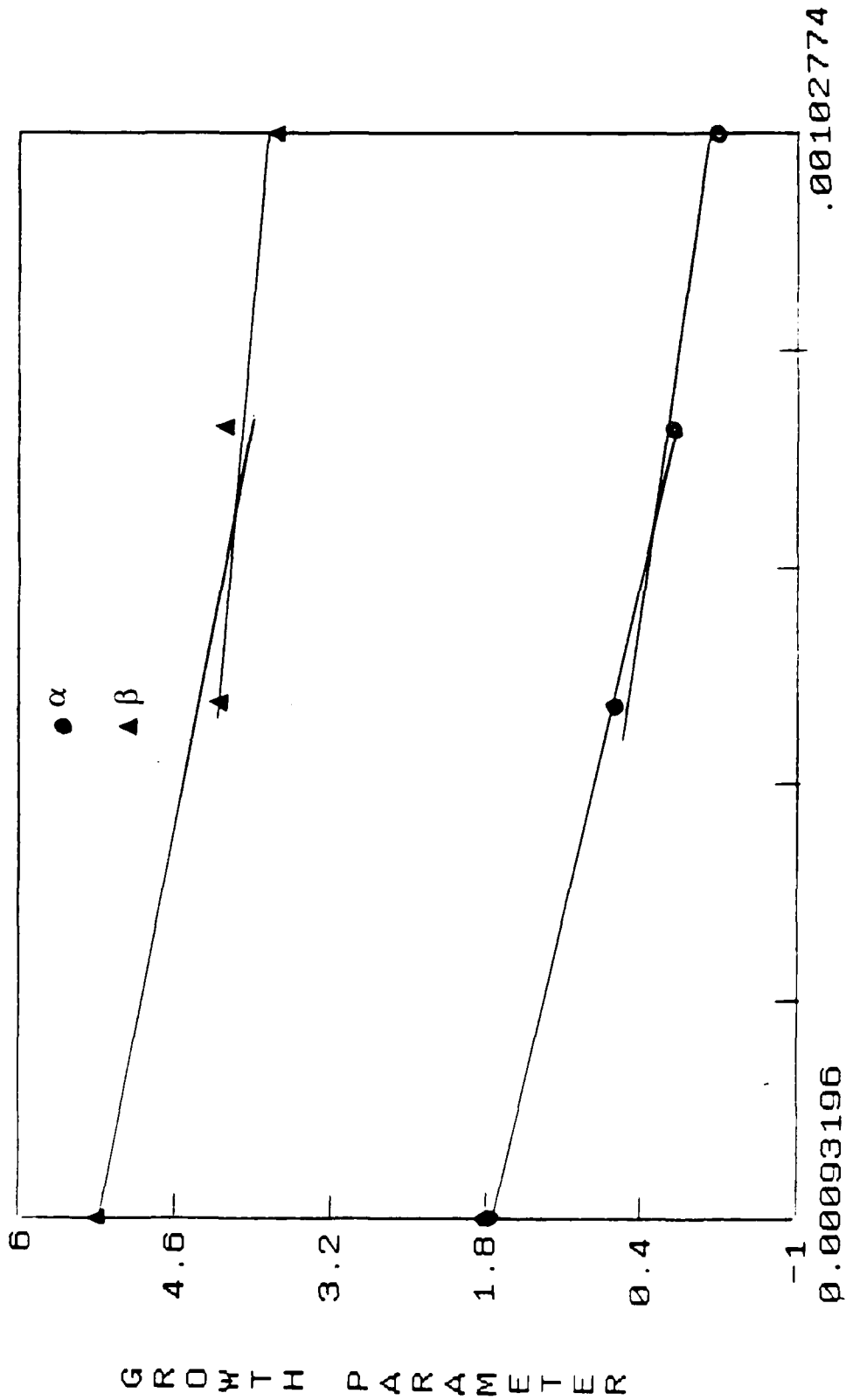
INVERSE TEMP. (1/T)

Fig. 36 : **DEPENDENCY OF GROWTH PARAMETERS $K_\alpha^{\alpha-\beta}$ AND $K_\beta^{\alpha-\beta}$ ON TEMPERATURE FOR A 24 % $\alpha$ – 76 % $\beta$ Ti-Mn ALLOY.**

88
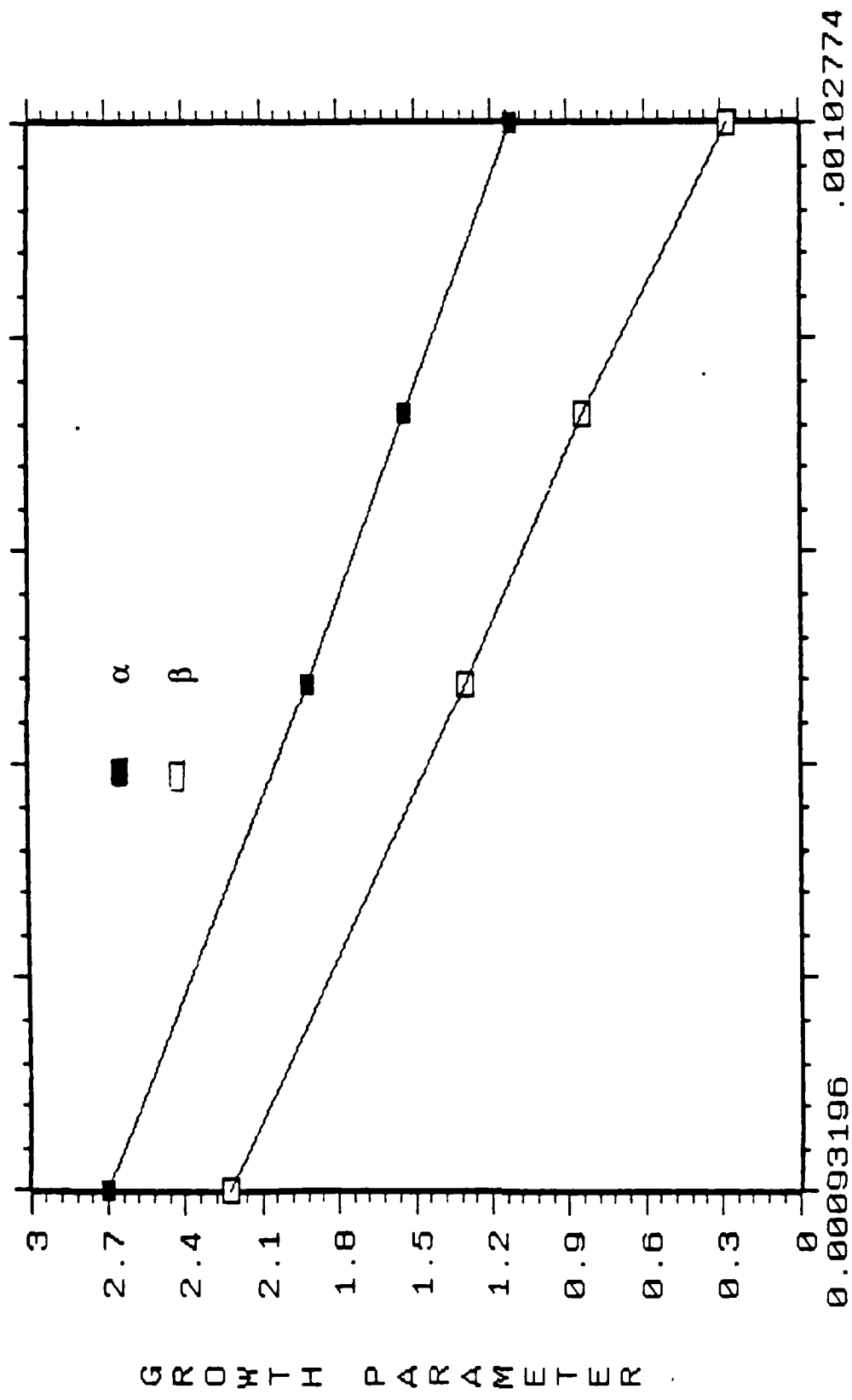
Fig. 37 : DEPENDENCY OF GROWTH PARAMETERS $K_\alpha^{\alpha-\beta}$ AND $K_\beta^{\alpha-\beta}$ ON
TEMPERATURE FOR A 54 % $\alpha$ – 46 %$\beta$ Ti-Mn ALLOY.
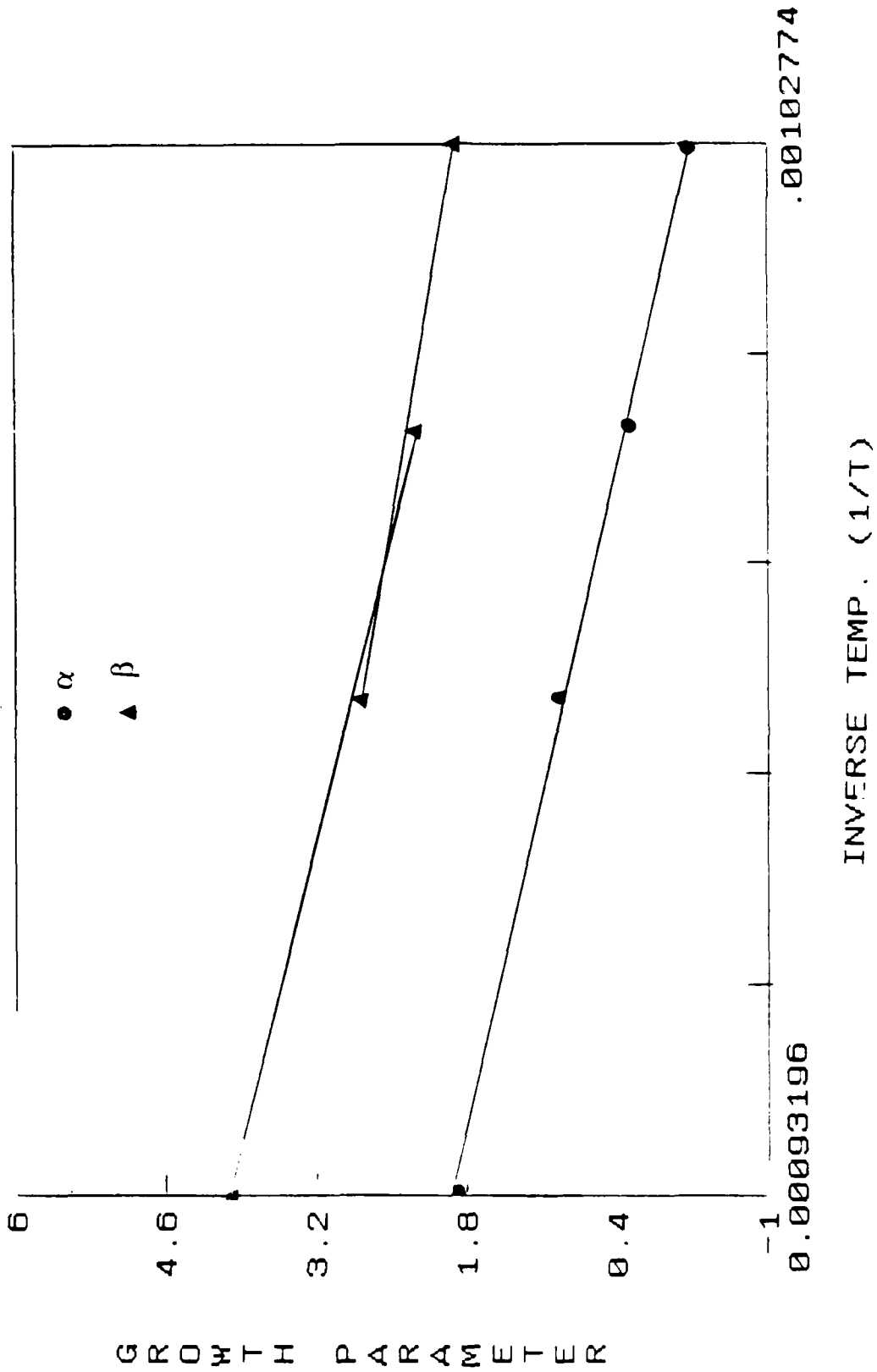
Fig. 38 : DEPENDENCY OF GROWTH PARAMETERS $K_\alpha^{\alpha-\beta}$ AND $K_\beta^{\alpha-\beta}$ ON TEMPERATURE FOR A 36 % $\alpha$ – 64 %$\beta$ Ti-V ALLOY.

90

## B. HIGH TEMPERATURE DEFORMATION STUDIES

### (a). EXPERIMENTAL

Six Ti-Mn alloys were selected for the high temperature deformation study. The intended and actual compositions of the six alloys are listed in Table 1 of the previous section on Particle Coarsening Studies.

### Heat Treatment and Microstructure

Specimens were cut from the as-received bars into sections about 3.5 inch (8.89 cm) in length. These were vacuum annealed in the alpha+beta field at 973 K and at 923 K for 200 hours followed by water quenching. This resulted in an equiaxed microstructure. Typical microstructures were presented in the previous section dealing with Particle Coarsening Studies. Vacuum was better than 10 millitorr during the annealing process. Upon completion of heat treatment helium gas was let into the chamber to produce a slightly positive pressure before being opened to air. The heat treatments were carried out so as to completely recrystallize the alloys, and to obtain equiaxed microstructures.

### Specimen Preperation

The annealed bars were machined with brazed carbide tools with a semi-cylindrical tip of 3/16 inch radius. Special specimens complying with ASTM standards were prepared were fabricated using a high temperature material which has a .2% YS about 8 times higher than the alloy.
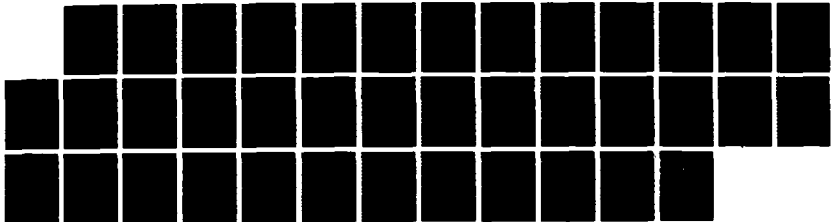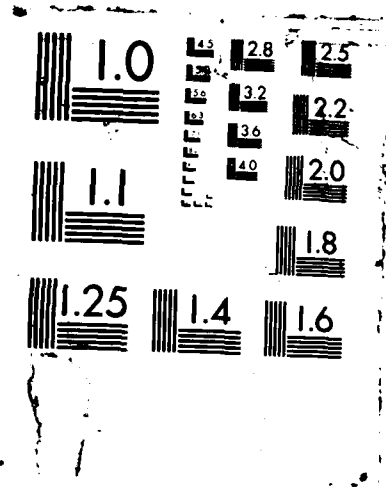
## High Temperature Tensile Test Apparatus

Tensile tests were carried out in an Instron testing machine capable of various constant cross-head velocities between 5 cm/min and 0.005 cm/min. Semi-cylindrical resistance heating elements with a constant temperature zone approximately 2 inch long were used. The furnace was surrounded by a ceramic fiber insulation to improve the heating efficiency and ensure temperature stability. Tensile tests were conducted at two different temperatures, 973 K and 923 K, in a vacuum chamber equipped with a set of mechanical and turbo pumps. Vacuum was better than 10 millitor. The temperature of the specimen was controlled by a feed back temperature controller. All the Ti-Mn alloys were tested at four different engineering strain rates, 1.1 * E-4/Sec, 2.6 * E-4/Sec, 2.6 * E-3/Sec, 2.6 * E-2/Sec. Each test was repeated under identical conditions to check for reproducibility. The variation was found to be in the range of + 5 percent. A schematic of the vacuum chamber used for the high temperature tensile test is shown in fig.1.

## Computation of Experimental Data

The load-elongation plots obtained from the Instron machine was digitised on a Hicomscan, Hitachi digitiser. A computer program was developed for converting the load elongation data into true stress-true strain data. The program also calculated the offset flow stresses and the strain rate sensitivity. The alpha and beta volume fractions were determined by the linear intercept method (1) according to the procedure described in the previous section dealing with Particle Coarsening Studies.

## (b). RESULTS AND DISCUSSION

As indicated in Tables 1 and 2, the beta volume percent increases as the Manganese content increases. Alpha phase is the matrix phase in alloy 2 and beta is the matrix in alloy 5.In the case of alloys 3 and 4 none of the two phases can be regarded as completely continuous.

### Stress-Strain behavior in alloys 1 and 2

Alpha phase has a hcp structure with c/a ratio about 2% less than the ideal value of 1.633 (2). the operative slip systems in alpha Titanium alloys are $(1\bar{1}00)$ $[11\bar{2}0]$ (3, 4), (0001) $[11\bar{2}0]$ (5) and $(10\bar{1}1)$ $[11\bar{2}0]$ (6). In addition to the "grown-in" dislocation sources, there are some dislocation generators coming into play because of the interaction between the dislocations of different slip systems, i.e. multiple slip. Dislocations are generated in an accelerating manner with increasing strain which results in the strain hardening behavior of alloy 1. The extent of work hardening at elevated temperatures is not so evident as that of the alloys tested at room temperature (7). Longo (8) explained the temperature dependence of the work hardening in terms of a thermal softening superimposed on an athermal hardening process. The effect of the strain rate would vary the time available for the action of the recovery mechanism. This theory is substantiated from our experimental data given in fig. 2 (973 K) and fig. 14 (923 K) where the strain hardening is more evident at the higher strain rates.

The offset flow stress versus beta volume percent, figs. 8 to 12 (973 K) and figs. 20 to 24 (923 K ) indicate that the offset

93

flow stress increases from alloy 1 to alloy 2 at all the strain rates for both 973 K and 923 K. This is as one would expect since alloy 2 contains the hard beta phase whereas alloy 1 is nearly 100 % alpha. In addition , the grain size of alpha decreases with the addition of beta and this also contributes to the higher flow stress of alloy 2.


## Interface Sliding in Alpha-Beta Alloys

It has been found that interface sliding in alpha-beta titanium alloys may be an important model of deformation even at room temperature (9,10). Ankem and Margolin studied the deformation of alpha- beta titanium alloy specimens with aluminum grid lines on polished surface and found that the plastic straining of the alpha grains in the vicinity of the sliding is more evident than strain in the beta grains. They (9) also pointed out that an alpha-beta interface need not be a flat plane for sliding to take place. In alloy 3 and alloy 4, both at 973 K and 923 K, the alpha-beta interfaces per unit volume are much higher than that in alloys 1, 2, 5 and 6. Therefore, there is a greater chance for interface sliding to take place in alloys 3 and 4. Between alloys 3 and 4 the particles of alloy 4 are more equiaxed which is ideal for interface sliding. Also, alloy 4 has lower flow stresses at 923 K than at 973 K, compare fig. 5 with fig. 17 for a strain rate of $1.1 * E - 4$/Sec. This can be explained by the interface sliding mechanism. Optical microscopic observations indicated that the microstructure is finer at 923 K than it is at 973 K. Hence this enhances the interface sliding

activity. Since interface sliding was observed at room temperature, it is reasonable to assume that interface sliding will be more pronounced at elevated termperatures because thermally induced vibrations of the crystal atoms accelerate the diffusional process (11,12).

Ashby and Verrall (12) suggested a threshold stress which controls sliding behavior of materials at high temperatures. At low strain rates, there is sufficient time for diffusion to occur therefore, less external stress is required to initiate sliding. Higher stress must be applied before sliding comes into play at high strain rates. Our experimental data shown in fig.5 (973 K) and fig 17. (923 K) substantiates this theory. Also, the offset flow stress versus beta volume percent plots, figs.8 to 12 (973 K) and figs.20 to 24 (923 K) show a drop at alloy 4 at the lower strain rates. Moreover, as mentioned above, the offset flow stresses at 973 K are higher than that at 923 K for alloy 4 at lower strain rates. This strongly suggests that interface sliding must be the dominating mechanism in this alloy. Experiments are underway to check if indeed interface sliding occurs in this alloy at these temperatures and strain rates.

## Sharp Flow Stress Drops in Near Beta Alloys

Beta-phase (bcc) is the dominant phase in alloy 5 and alloy 6 both at 973 K and 923 K. This implies that beta phase is responsible for the unusual behavior for the abrupt flow stress drops at small strains and the flow softening behavior. Flow softening has been observed in Ti-C (13), Zr-Nb (14) and Zr-Mo (15) systems. Jonas, Heritier and Luton (14) have shown that for

Zr-Nb (15% Nb) the flow softening is due to the declustering phenomenon. Paton and Hamilton (16) however attribute the flow softening and sharp drop in flow stress to the formation of sub grains due to the occurance of dynamic recovery. They have studied the post deformation microstructure, both by optical and transmission electron microscopy, and have shown the existance of subgrains in the microstructure. Optical micrographs of deformed specimens does tend to indicate the existance of subgrains. However, transmission electron microscopy will have to be used to confirm that dynamic recovery is the operating mechanism in the case of near beta alloys. Flow stress of alloy 6 at both 973 K and 923 K, fig. 7 (973 K) and fig. 19 (923 K), is higher than that for alloy 5, fig. 6 (973 K) and fig. 18 (923 K). This is due to the higher beta content of alloy 6. The offset flow stress versus beta volume percent also indicate similar trends for the same reasons. Experiments are underway to determine the mechanism of flow softening in alloy 6.

Comparison of Calculated and Experimental Data

Theoretical calculations were made to predict the stress-strain behavior of alpha-beta alloys based on the iso-strain model for the four different strain rates, not shown here. All the calculated flow stresses of alloy 4 were consistently higher than the experimental stresses. This can be interpreted as being due to a negative contribution by the interaction term (17) due to significant amount of interface sliding.

The calculated stress-strain curves were sometimes lower and sometimes higher than the experimental data suggesting that the assumption of constant strain is not valid and interactions are

96

expected as suggested by Ankem and Margolin (17).

### Strain Rate Sensitivity Determination

Strain rate sensitivity can be determined by various methods as outlined by Hart (18), Backofen, Turner and Avery (19), Hedworth and Stowell (20),and by Gibbs (21). However, the method adopted for determining strain rate sensitivity (m) in our case was similar to the one formulated by Hedworth and Stowell (20). The difference between their (20) method and ours is that they (20) determined the strain rate sensitivity by a velocity change experiment on a single specimen whereas in our case separate specimens were used for each data point.

Flow stress for a given total plastic strain, 0.001, was determined for each alloy for four different strain rates for both the test temperatures i.e. 973 K and 923 K. The slope of the plot of log (flow stress) versus log (strain rate) was the strain rate sensitivity, m. The correlation co-efficient obtained (> 0.97) indicate the validity of this method of determining strain rate sensitivity.

The strain rate sensitivity versus beta volume percent plots for both 973 K and 923 K, fig. 13 (973 K) and fig. 25 (923 K) indicates similar trends. The strain rate sensitivity shows a drop at about 20 volume percent beta and a peak at around 50 volume percent beta at 973 K as well as at 923 K. Moreover, the strain rate sensitivity at about 50 volume percent beta (alloy 4) at 923 K is higher than at 973 K.

### (c). SUMMARY

The flow stress behavior of the Ti-Mn alloys investigated

97

indicated similar trends at both the test temperatures i.e. 973 K and 923 K. This implies that the operating mechanisms may be similar. At Manganese contents greater than 3 wt. % (alloys 3 to 6) the Ti-Mn alloys exhibited strain softening and flow stress drops at both test temperatures. The magnitude of the flow stress drop increased with increasing strain rate for a given beta volume percent. Also, the flow stress drop increased with an increase in the beta volume percent.

The fact that the offset flow stresses do not vary linearly with beta volume percent at the lower two strain rates indicates that a change in mechanism occurs with a change in beta volume percent. Smaller flow stresses in alloys with nearly equal volume percents of the alpha and beta phases can be utilized by the Titanium industry with great advantages for fabrication of these alloys.

Further work will be conducted to check if indeed interface sliding occurs in the alpha-beta alloys at low strain rates. The Ti-Mn alloys will be tested at one more temperature, 1023 K, at the four strain rates. Similar series of tests will be conducted on Ti-V alloys. The outcome of these investigations should enable us in understanding how the various factors namely strain rate, temperature and the volume percent of the second phase effect the high temperature deformation behavior of two phase alloys. Theoretical modelling will also done by the FEM method to predict the deformation behavior of various two phase materials.

## REFERENCES

1.  G.F.Vander Voort : "Metallography Principles and Practice", McGraw-Hill Book Co., 1984.

2.  M.B.Robert, W.P.Alan and B.G.Robert : "Structure and Properties of Engineering Materials", 4th ed., McGraw-Hill Book Co., 1977.

3.  A.T.Churchman : Proc. R. Soc., 1954, A226, 216.

4.  M.A.Greenfield and H.Margolin : Met. Trans., 1972, 3, p2649.

5.  F.D.Rosi, C.A.Dube and B.H.Alexander : AIME, J.Metals, 1953, 5, p257.

6.  R.W.K.Honeycombe : "The Plastic Deformation of Metals", 2nd ed., Edward Arnold Ltd., 1984.

7.  S.Ankem and H.Margolin : Met. Trans. A, 1982, 13A, p595.

8.  W.P.Longo : "Work Softening in Polycrysttaline Metals", University of Florida, Thesis, 1970.

9.  S.Ankem and H.Margolin : Met. Trans. A, 1983, 14A, p500.

10. W.A.Baeslack III and Y.Mahajan : Met. Trans. A, 1980, 11A, p1234.

11. R.C.Gifrins : J. Mater. Sci., 1978, 13, p1926.

12. R.C.Gifrins : Met. Trans., 1976, 7A, p1225.

13. H.R.Ogden, R.I.Jaffee and F.C.Holden : J. of Metals, Jan. 1955.

14. J.J.Jonas, B.Heritier and M.J.Luton : Met. Trans., 1979, 10A, p611.

15. B.Heritier and J.J.Jonas : Met. Trans., 1979, 10A, p557.

16. N.E.Paton and C.H.Hamilton : "Superplasticity in Titanium Alloys", Proc. of the V International Conference on Titanium, 1985, Vol. 2, P. 649

17. S.Ankem and H.Margolin : Met. Trans. A, 1986, 17A, p2209.

18. E.W.Hart: Acta Metall., 1976, 15, 351.

19. W.A.Backofen, I.R.Turner and D.H.Avery : Trans. of ASM, 1964, 57, p980.

20. J.Hedworth and M.J.Stowell : J. Mater. Sci., 1971, 6, p1061.

21. G.B.Gibbs : Phil. Mag., 1966, 13, p317.

```
================================================================
TABLE 1.   VOLUME PERCENTS OF ALPHA AND BETA PHASES.   H.T.  973 K,
200 HRS. W.Q.
================================================================
```

| ALLOY NO. | ALPHA VOLUME PERCENT | BETA VOLUME PERCENT |
|-----------|---------------------|---------------------|
| 1 | 100 | 0 |
| 2 | 79 | 21 |
| 3 | 63 | 37 |
| 4 | 45 | 55 |
| 5 | 11 | 89 |
| 6 | 0 | 100 |

```
================================================================
TABLE 2.    VOLUME PERCENTS OF ALPHA AND BETA PHASES.  H.T. 923 K,
200 HRS. W.Q.
================================================================
```

| ALLOY NO. | ALPHA VOLUME PERCENT | BETA VOLUME PERCENT |
|-----------|---------------------|---------------------|
| 1 | 100 | 0 |
| 2 | 95.6 | 6.4 |
| 3 | 68.4 | 31.6 |
| 4 | 56.7 | 43.3 |
| 5 | 24.4 | 75.6 |
| 6 | 12.1 | 87.9 |
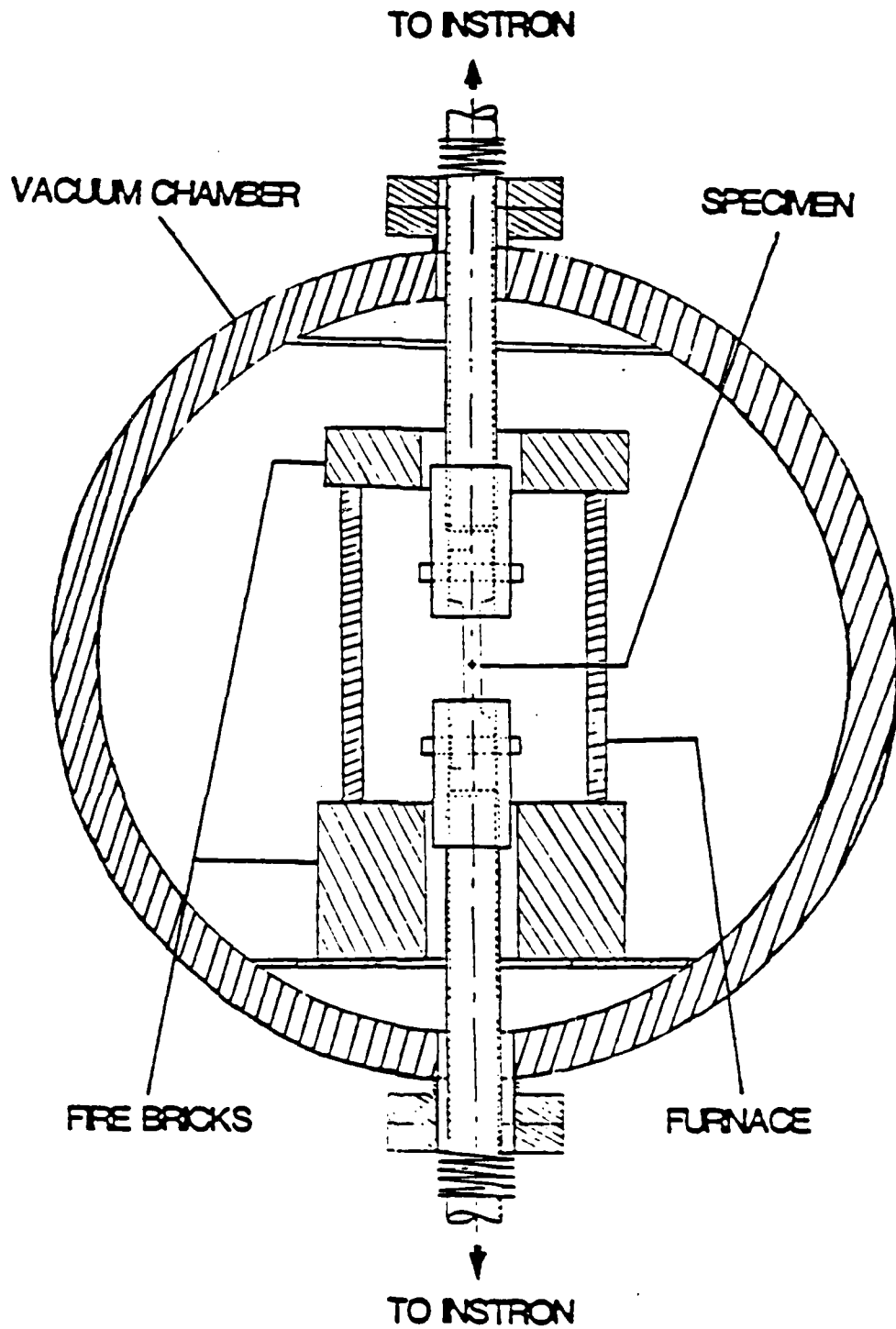
FIG 1: A SCHEMATIC OF THE HIGH TEMPERATURE VACUUM CHAMBER USED FOR THE TENSILE TEST.

102

**FIG 2 : TRUE STRESS - TRUE STRAIN CURVES OF ALLOY 1 ( 100 %α , Ti-Mn ALLOY) TESTED IN VACUUM AT 973 °K AT DIFFERENT STRAIN RATES.**

TEST CONDITIONS : 700 °C , VACUUM

STRAIN RATE :

● -- ~ $2.6 * 10^{-2}$/Sec
■ -- ~ $2.6 * 10^{-3}$/Sec
⬣ -- ~ $2.6 * 10^{-4}$/Sec
▲ -- ~ $1.1 * 10^{-4}$/Sec

ALLOY 1

TRUE STRESS , KSI

45
40.5
36
31.5
27
22.5
18
13.5
9
4.5
0

0   0.05   0.1   0.15   0.2   0.25
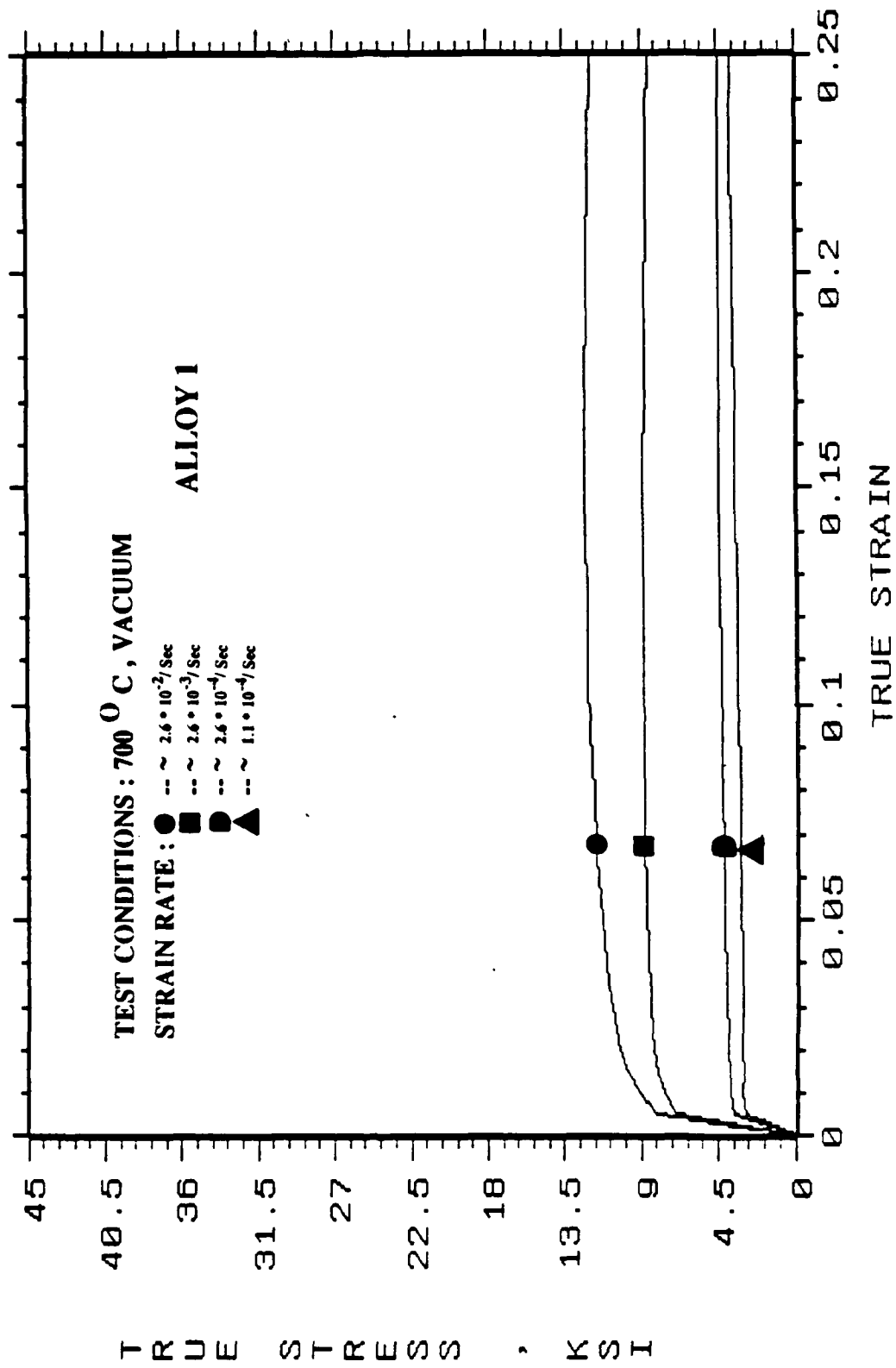
TRUE STRAIN

**FIG 3 : TRUE STRESS - TRUE STRAIN CURVES OF ALLOY 2( 79 %α - 21 % β , Ti-Mn ALLOY)**
**TESTED IN VACUUM AT 973 °K AT DIFFERENT STRAIN RATES.**



TEST CONDITIONS : 700 °C , VACUUM

STRAIN RATE :

● -- ~ 2.6 * 10⁻²/Sec
■ -- ~ 2.6 * 10⁻³/Sec
● -- ~ 2.6 * 10⁻⁴/Sec
▲ -- ~ 1.1 * 10⁻⁴/Sec

ALLOY 2

TRUE STRESS , KSI
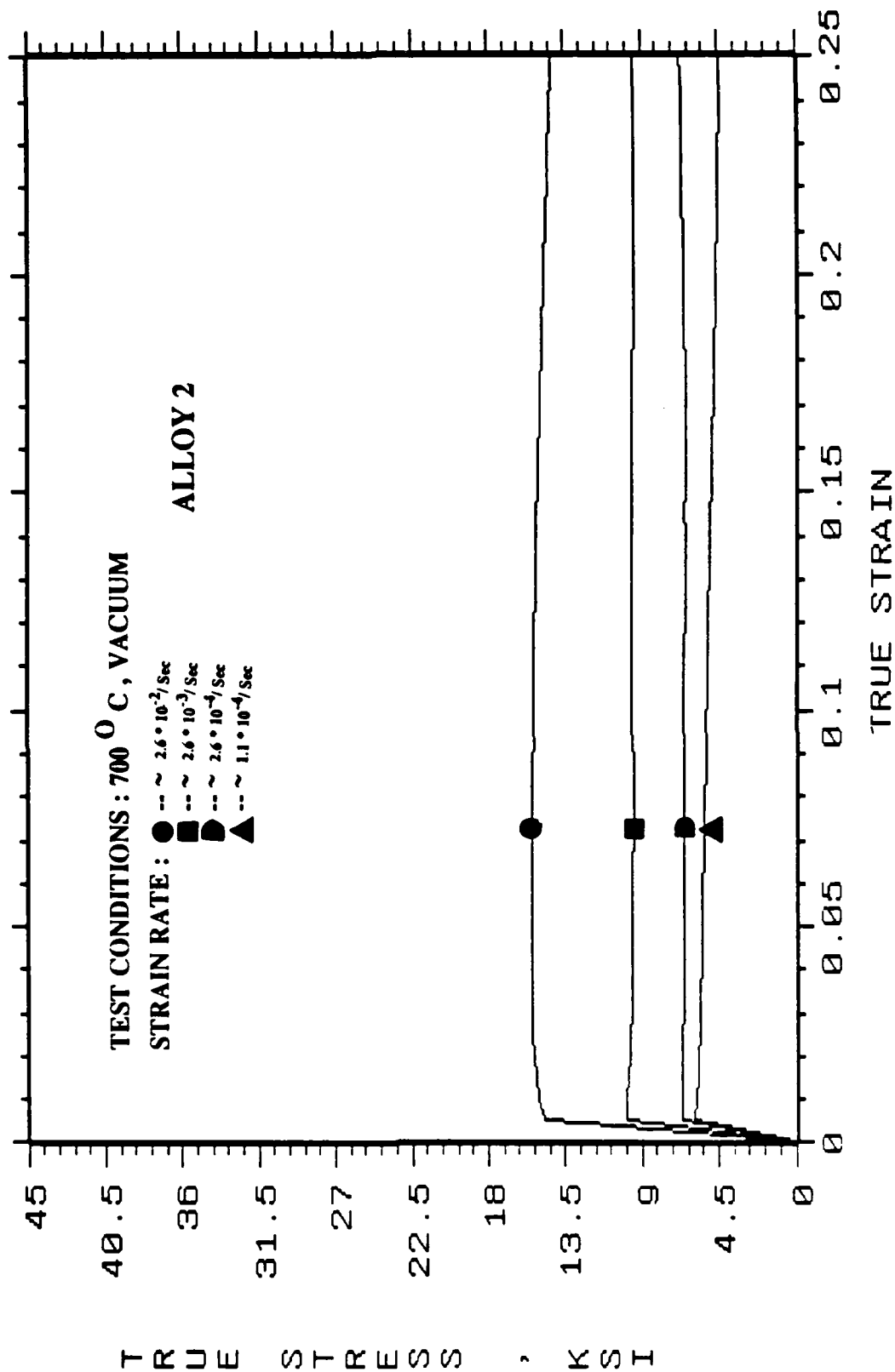
TRUE STRAIN

FIG 4 : TRUE STRESS-TRUE STRAIN CURVES OF ALLOY 3 ( 63 % α - 37 % β, Ti - Mn ALLOY )
TESTED IN VACUUM AT 973°K AT DIFFERENT STRAIN RATES.

FIG 5 : TRUE STRESS-TRUE STRAIN CURVES OF ALLOY 4 ( 45 % α - 55 % β, Ti - Mn ALLOY )
TESTED IN VACUUM AT 973°K AT DIFFERENT STRAIN RATES.

TEST CONDITIONS : 700°C , VACUUM

STRAIN RATES :

● ~ $2.6 \cdot 10^{-2}$/Sec
■ ~ $2.6 \cdot 10^{-3}$/Sec
▲ ~ $2.6 \cdot 10^{-4}$/Sec
▲ ~ $1.1 \cdot 10^{-4}$/Sec
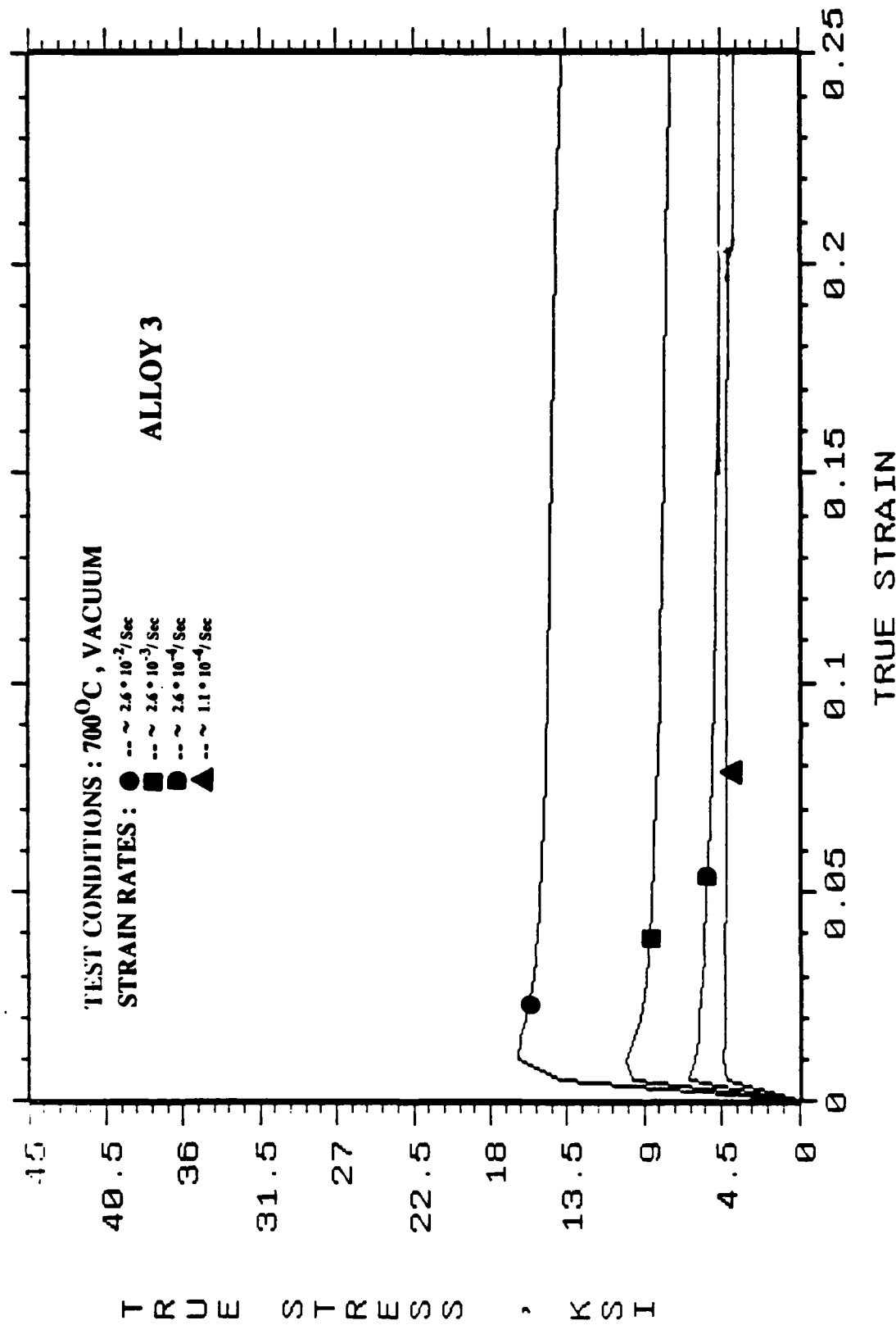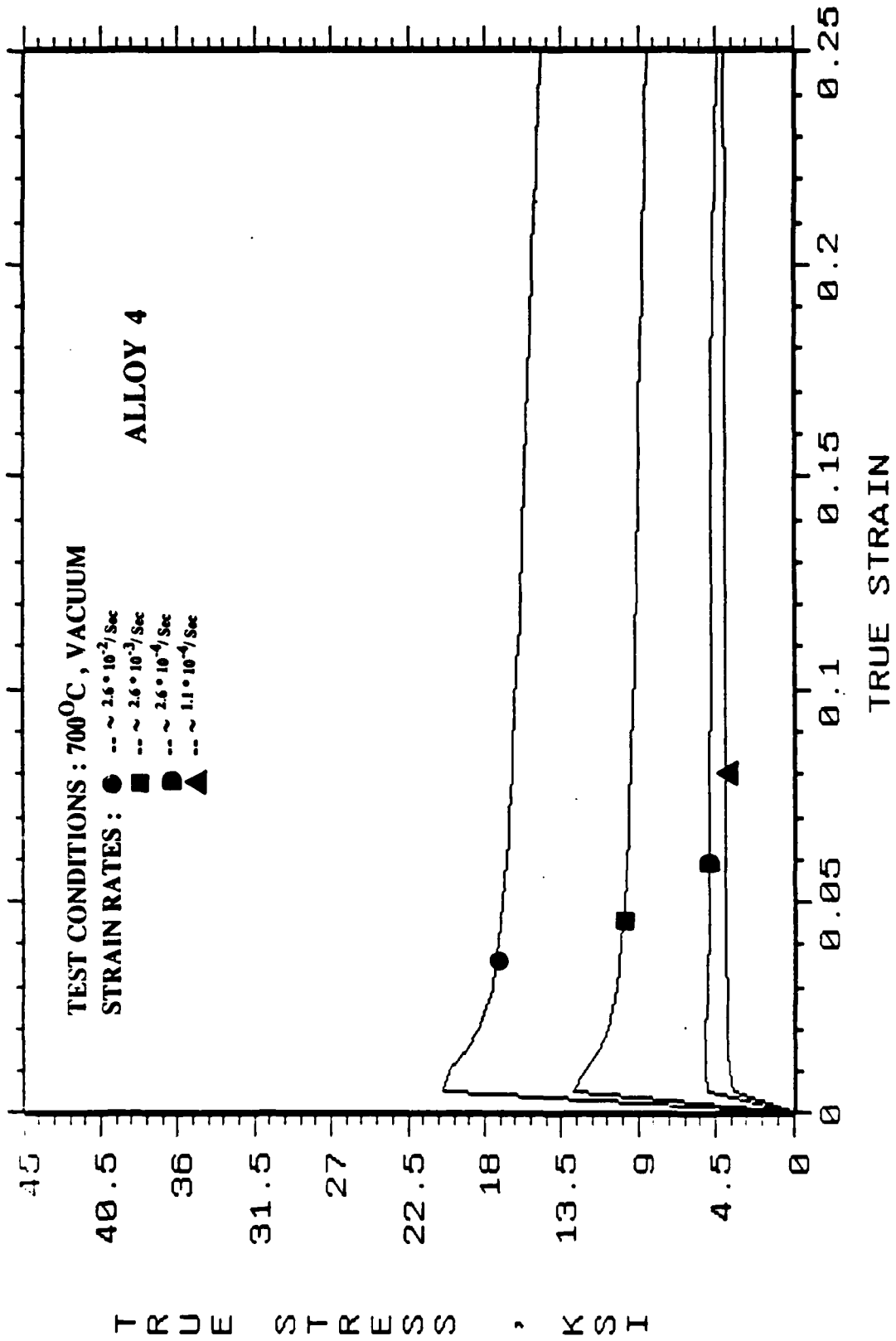
ALLOY 4

TRUE STRAIN

FIG 6 : TRUE STRESS - TRUE STRAIN CURVES OF ALLOY 5( 10 %α - 90 % β , Ti-Mn ALLOY)
TESTED IN VACUUM AT 973 °K AT DIFFERENT STRAIN RATES.

107
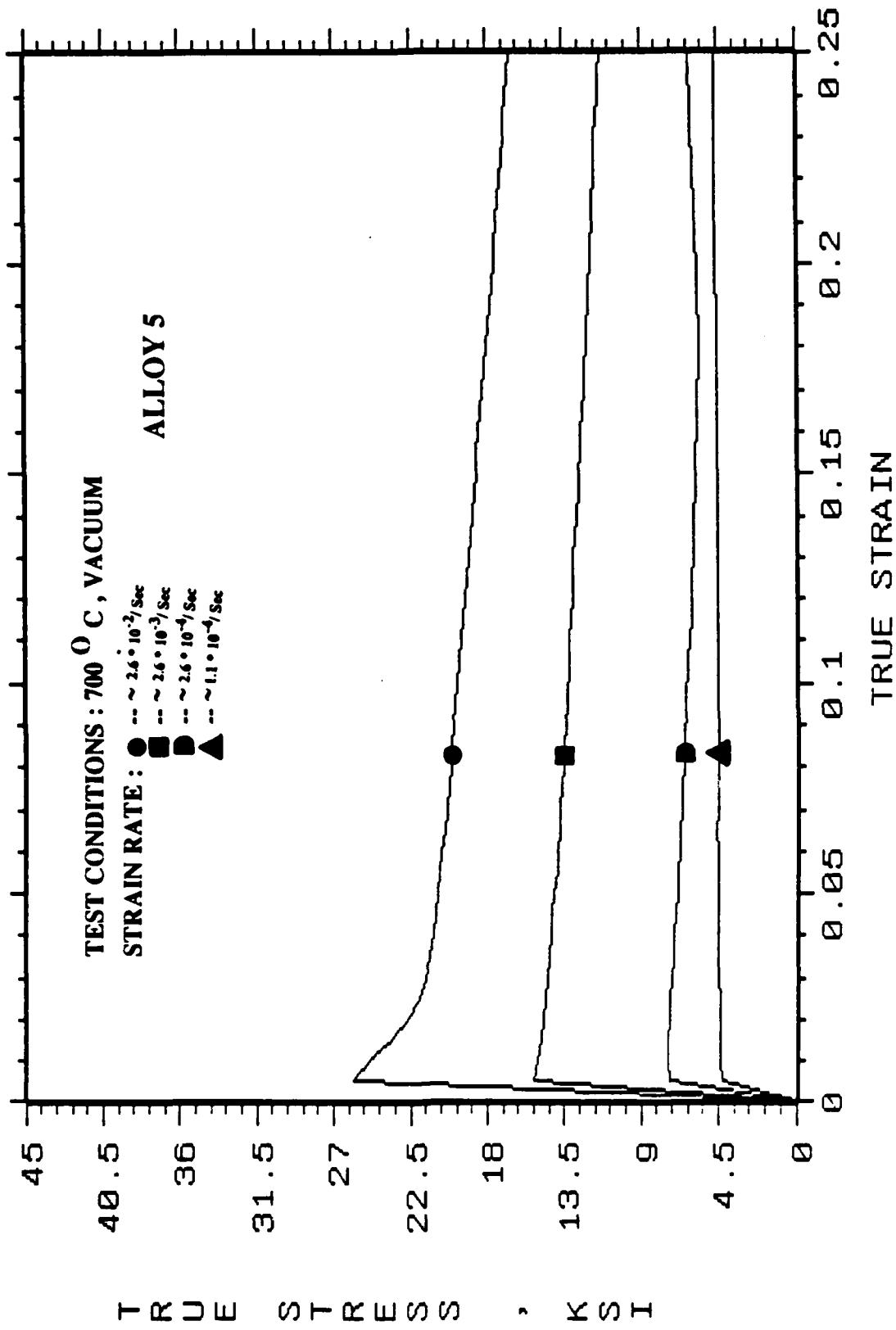
FIG 7: TRUE STRESS - TRUE STRAIN CURVES OF ALLOY 6( 100% β , Ti-Mn ALLOY) TESTED IN VACUUM AT 973 °K AT DIFFERENT STRAIN RATES.
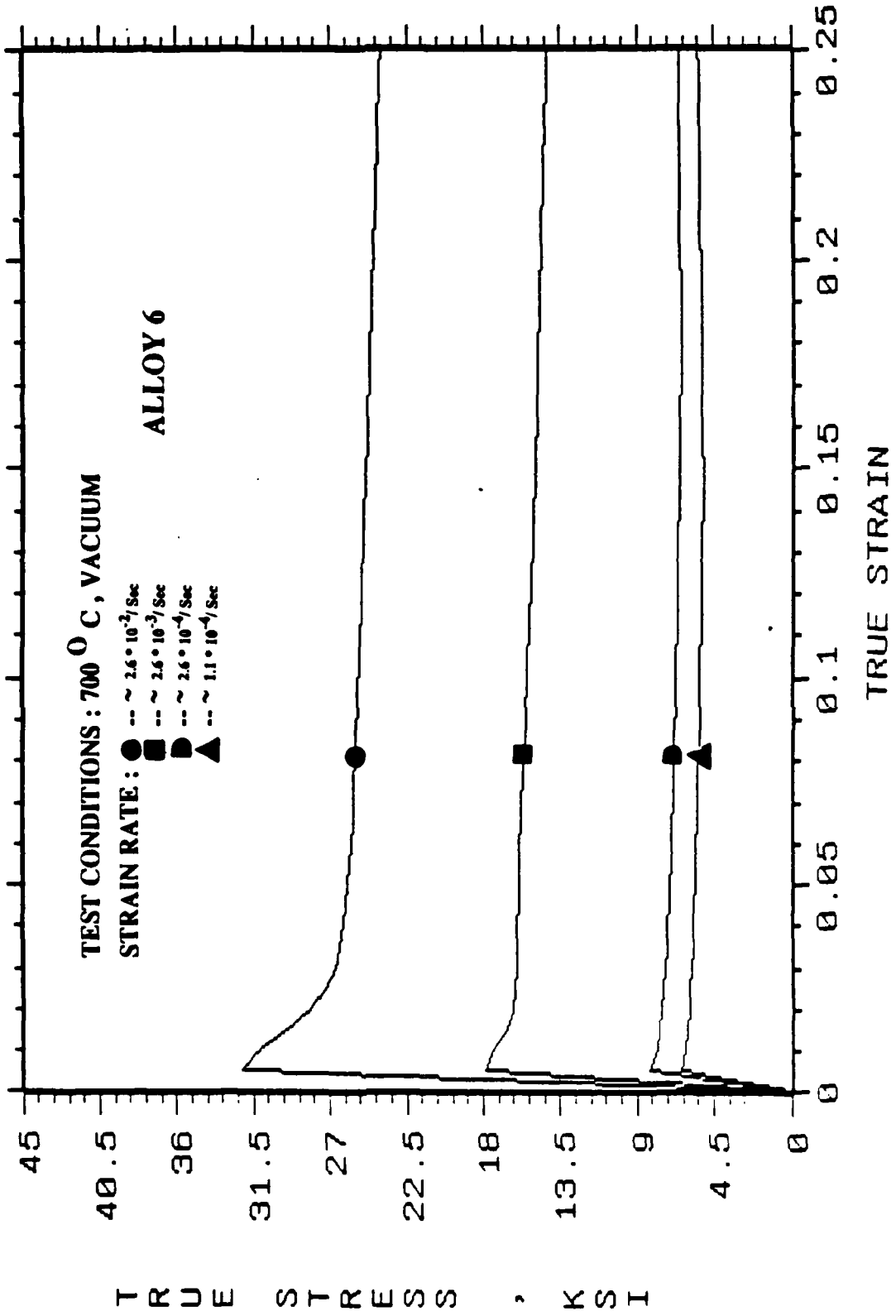
FIG 8 : FLOW STRESS Vs BETA VOLUME PERCENT FOR DIFFERENT ALPHA-BETA Ti-Mn ALLOYS
THE FLOW STRESS CORRESPONDS TO 0.2 % PLASTIC STRAIN
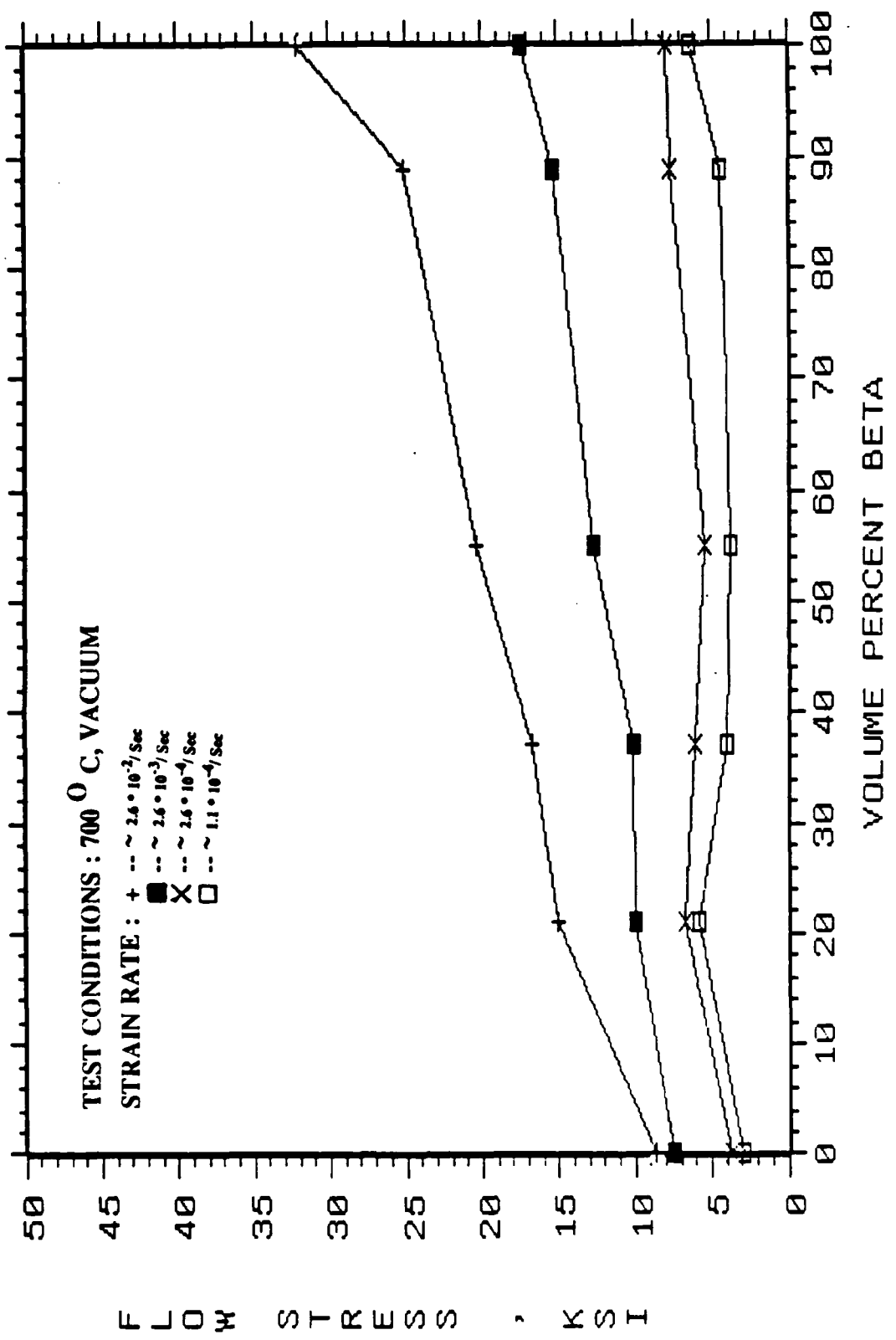
FIG 9 : FLOW STRESS Vs BETA VOLUME PERCENT FOR DIFFERENT ALPHA-BETA Ti-Mn ALLOYS
THE FLOW STRESS CORRESPONDS TO 0.5 % PLASTIC STRAIN

TEST CONDITIONS : 700 $^0$ C, VACUUM

STRAIN RATE :  +  -- ~ 2.6 $\cdot$ 10$^{-2}$/Sec
            ■  -- ~ 2.6 $\cdot$ 10$^{-3}$/Sec
            X  -- ~ 2.6 $\cdot$ 10$^{-4}$/Sec
            □  -- ~ 1.1 $\cdot$ 10$^{-4}$/Sec

FLOW STRESS , KSI

VOLUME PERCENT BETA

**FIG 10 : FLOW STRESS Vs BETA VOLUME PERCENT FOR DIFFERENT ALPHA-BETA Ti-Mn ALLOYS THE FLOW STRESS CORRESPONDS TO 5 % PLASTIC STRAIN**

TEST CONDITIONS : 700 $^{O}$ C, VACUUM

STRAIN RATE :
+ -- ~ $2.6 \cdot 10^{-2}$/Sec
■ -- ~ $2.6 \cdot 10^{-3}$/Sec
X -- ~ $2.6 \cdot 10^{-4}$/Sec
□ -- ~ $1.1 \cdot 10^{-4}$/Sec
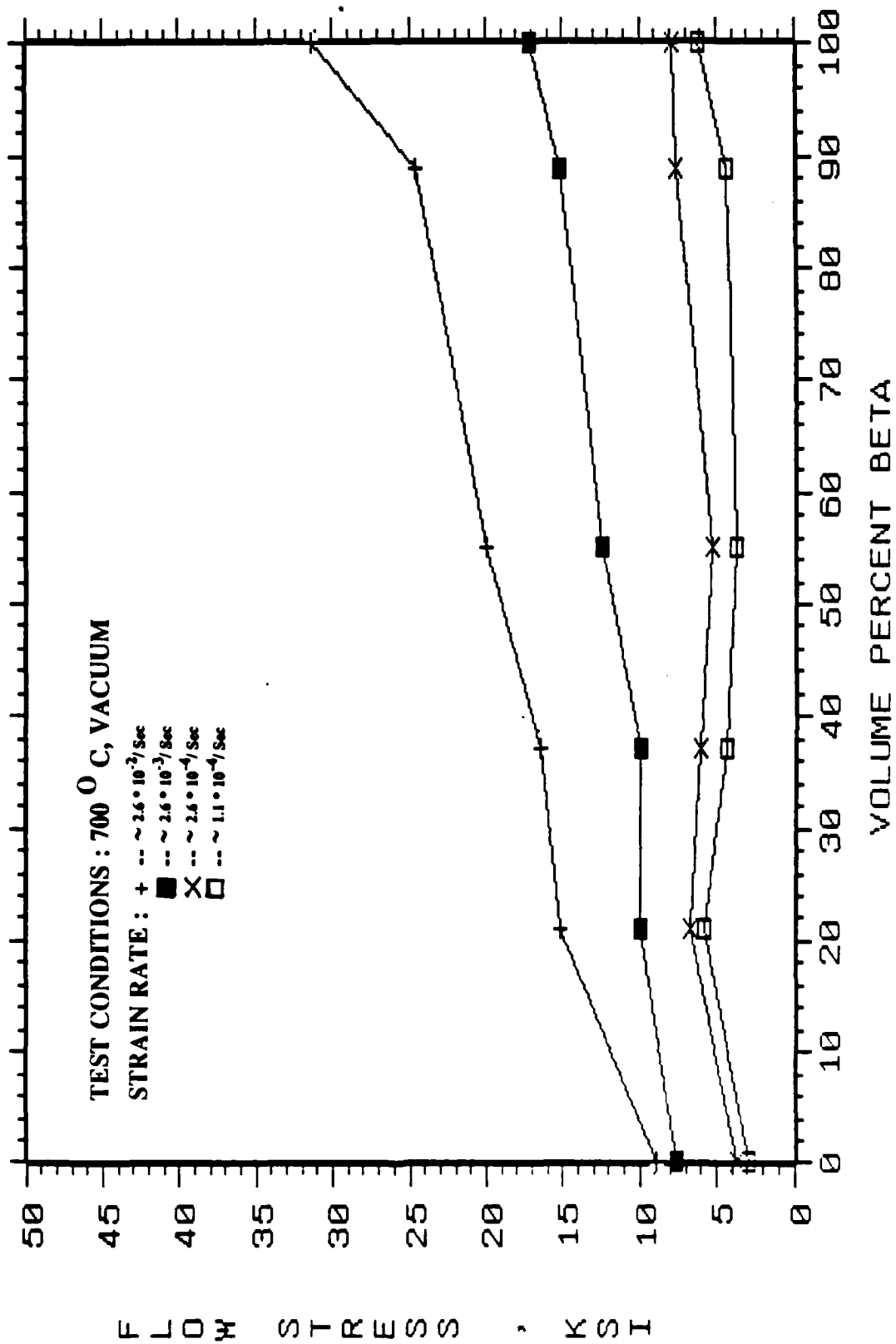
FLOW STRESS , KSI

VOLUME PERCENT BETA
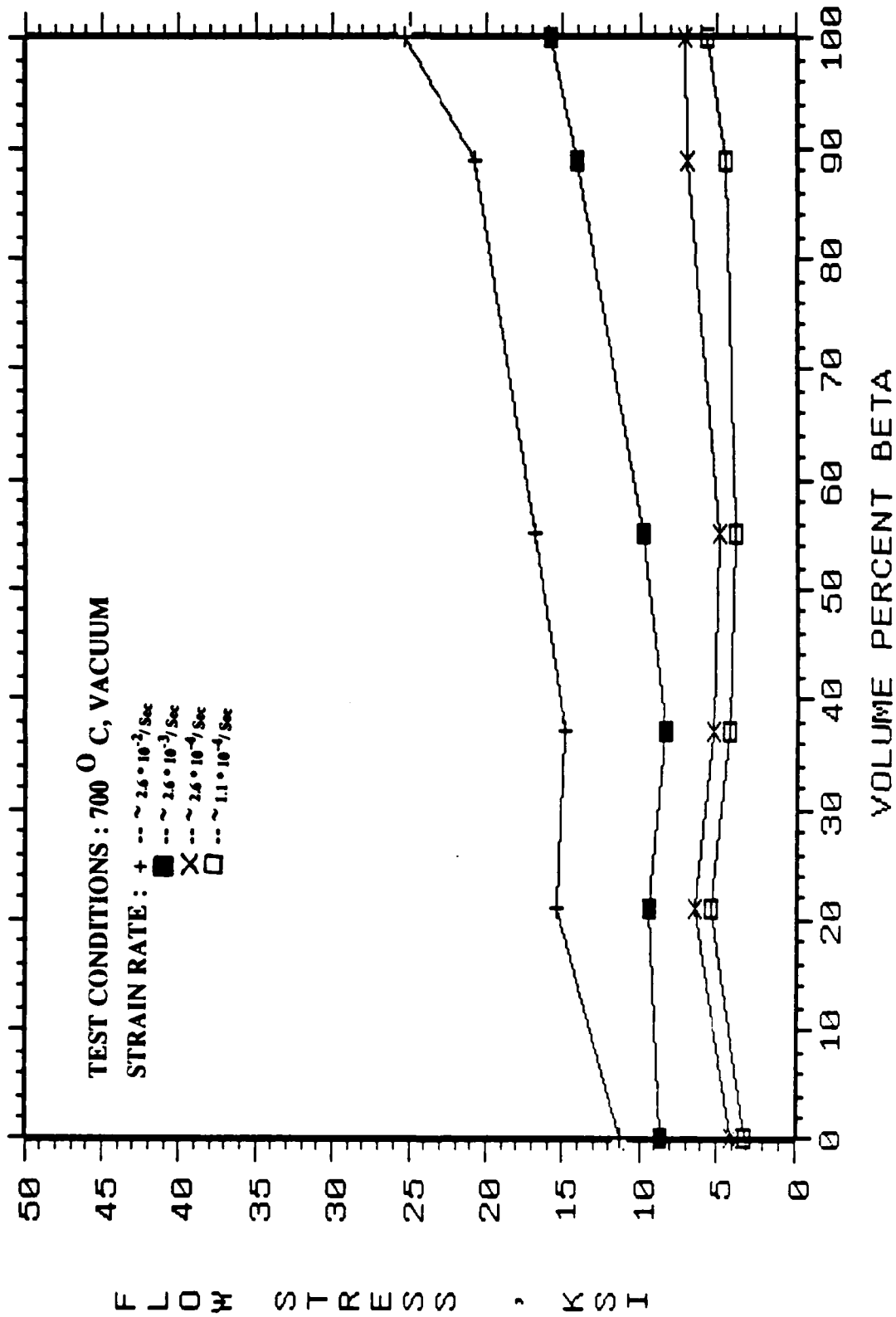
**FIG 11 : FLOW STRESS Vs BETA VOLUME PERCENT FOR DIFFERENT ALPHA-BETA Ti-Mn ALLOYS FLOW STRESS CORRESPONDS TO 10 % PLASTIC STRAIN**
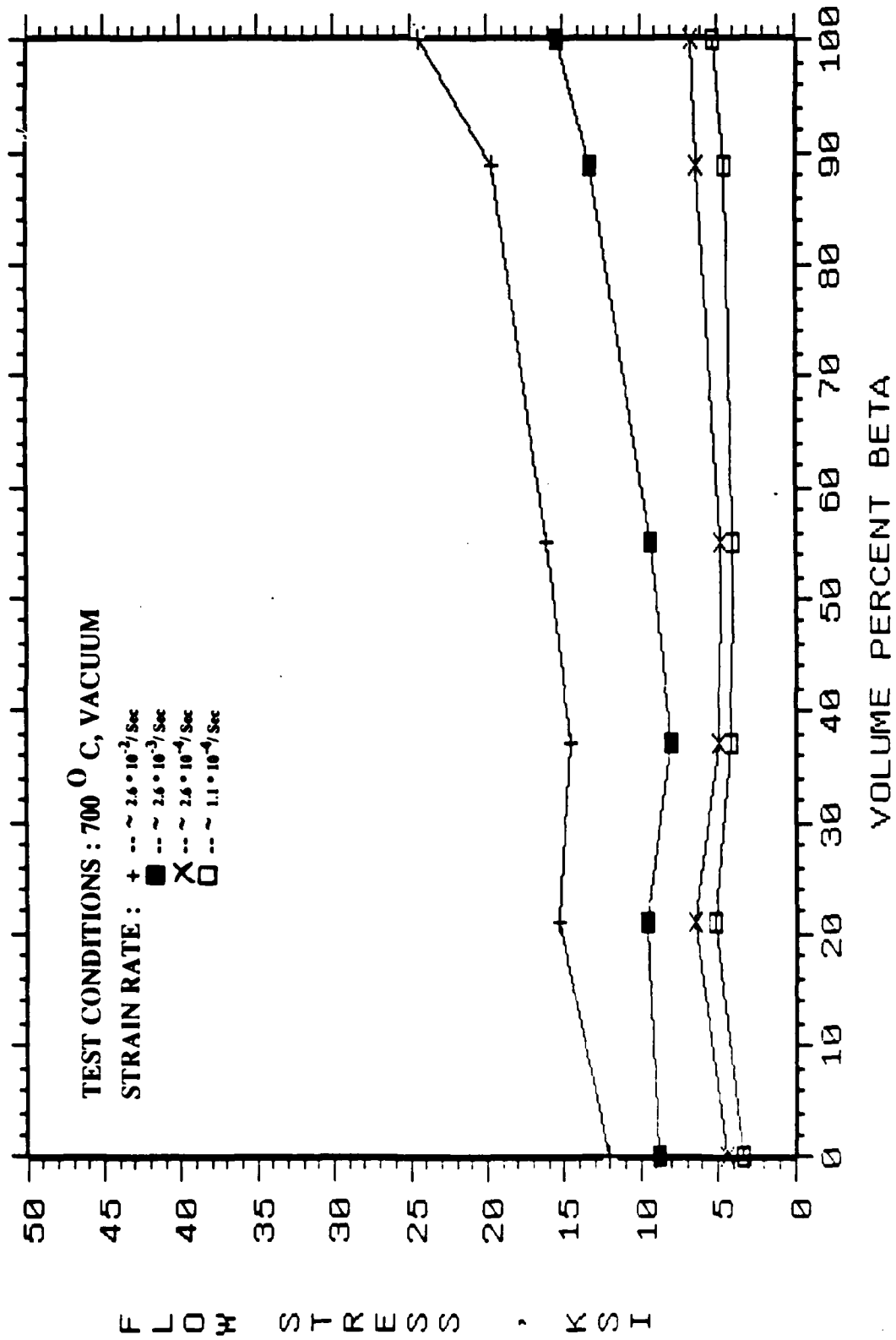
FIG 12 : FLOW STRESS Vs BETA VOLUME PERCENT FOR DIFFERENT ALPHA-BETA Ti-Mn ALLOYS
THE FLOW STRESS CORRESPONDS TO 20 % PLASTIC STRAIN

113

FIG 13 : STRAIN RATE SENSITIVITY (m ) Vs BETA VOLUME PERCENT FOR DIFFERENT ALPHA-BETA Ti-Mn ALLOYS DETERMINED FROM LOG σ Vs LOG ε PLOT. THE SLOPE OF THE PLOT IS THE STRAIN RATE SENSITIVITY (m).

TEST CONDITIONS : 700 °C, VACUUM

σ WAS DETERMINED FOR A TRUE STRAIN CORRESPONDING TO 0.001 FOR FOUR DIFFERENT STRAIN RATES.
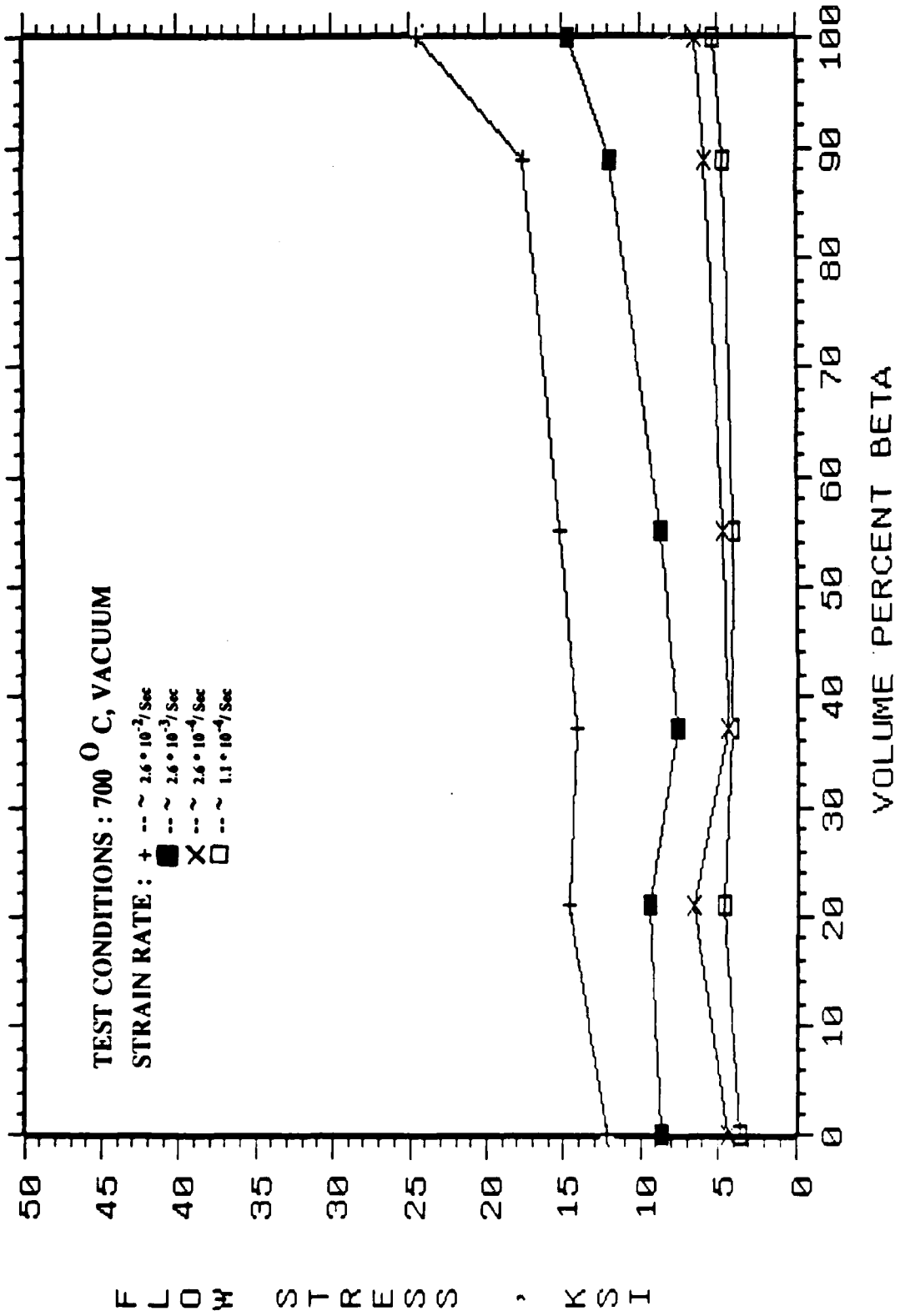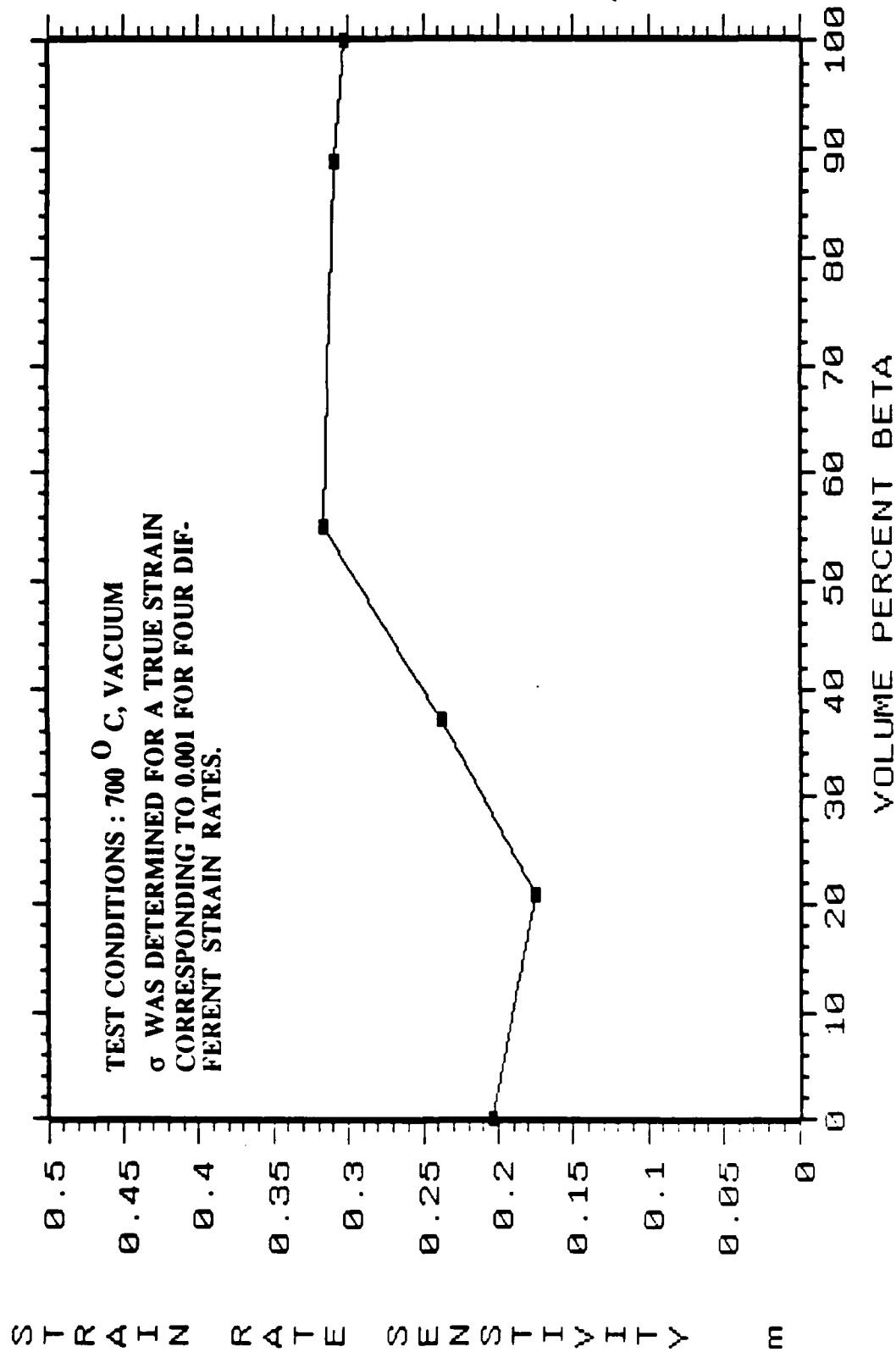
FIG 14 : TRUE STRESS - TRUE STRAIN CURVES OF ALLOY 1 (100 % α, Ti-Mn ALLOY) TESTED IN VACUUM AT 923 °C AT DIFFERENT STRAIN RATES.

115
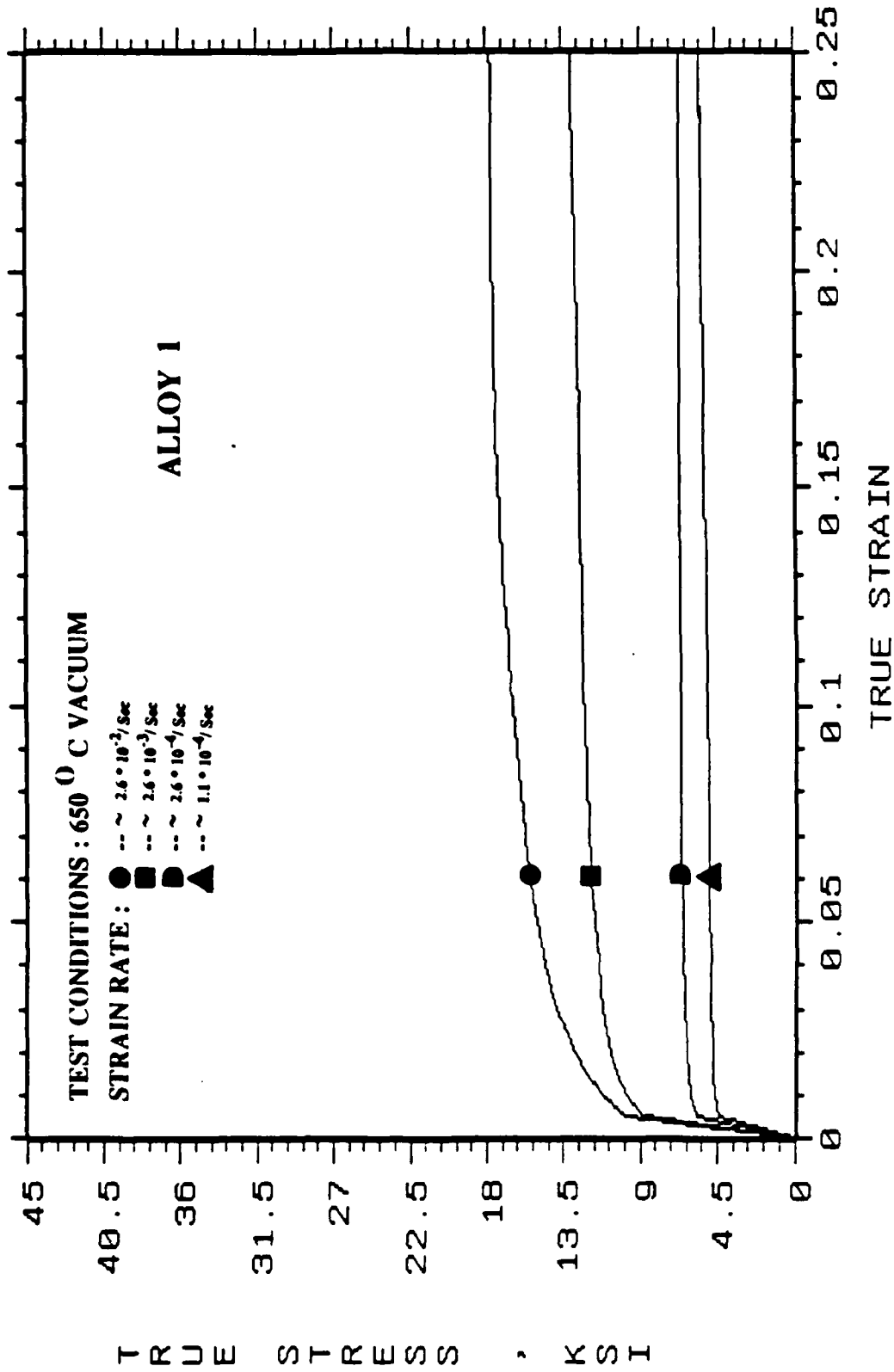
FIG 15 : TRUE STRESS - TRUE STRAIN CURVES OF ALLOY 2 ( 95.6 %α - 6.4 % β , Ti-Mn ALLOY)
TESTED IN VACUUM AT 923 °K AT DIFFERENT STRAIN RATES.
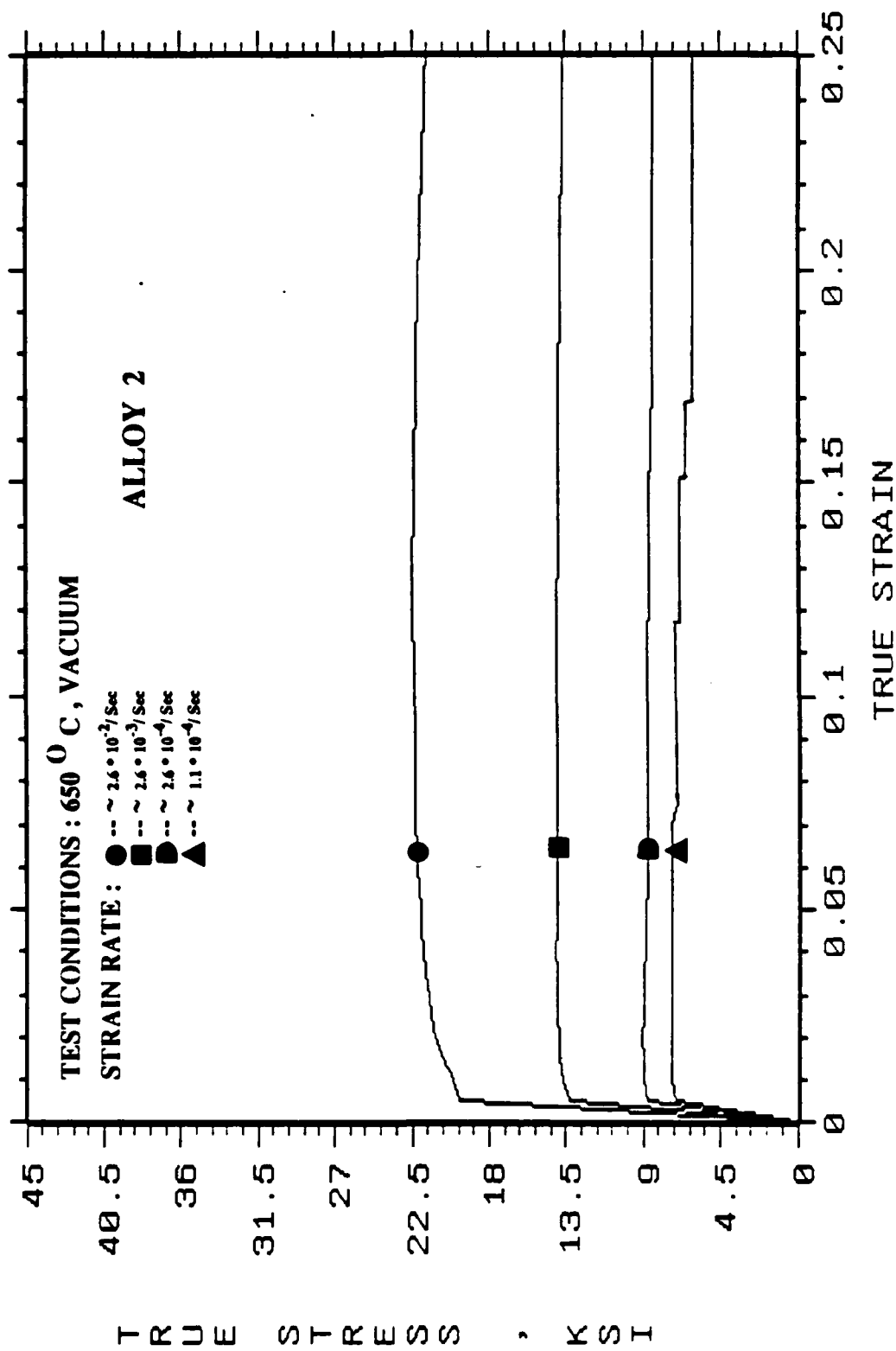
FIG 16 : TRUE STRESS - TRUE STRAIN CURVES OF ALLOY3( 68.4 %α - 21.6 % β , Ti-Mn ALLOY)
TESTED IN VACUUM AT 923 $^O$K AT DIFFERENT STRAIN RATES.
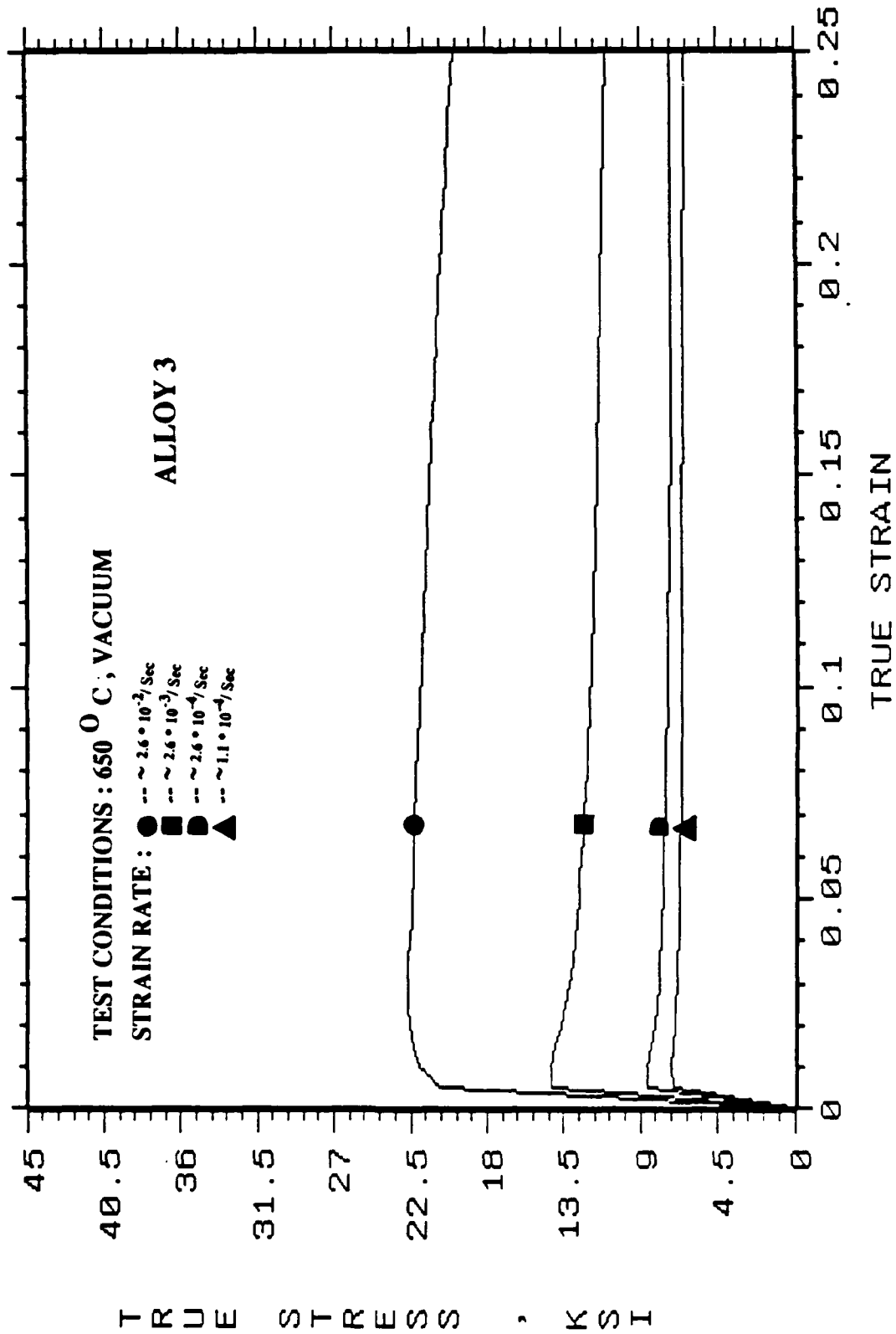
**FIG 17 : TRUE STRESS - TRUE STRAIN CURVES OF ALLOY 4( 56.7 %α - 43.3 % β , Ti-Mn ALLOY) TESTED IN VACUUM AT 923 $^O$K AT DIFFERENT STRAIN RATES.**
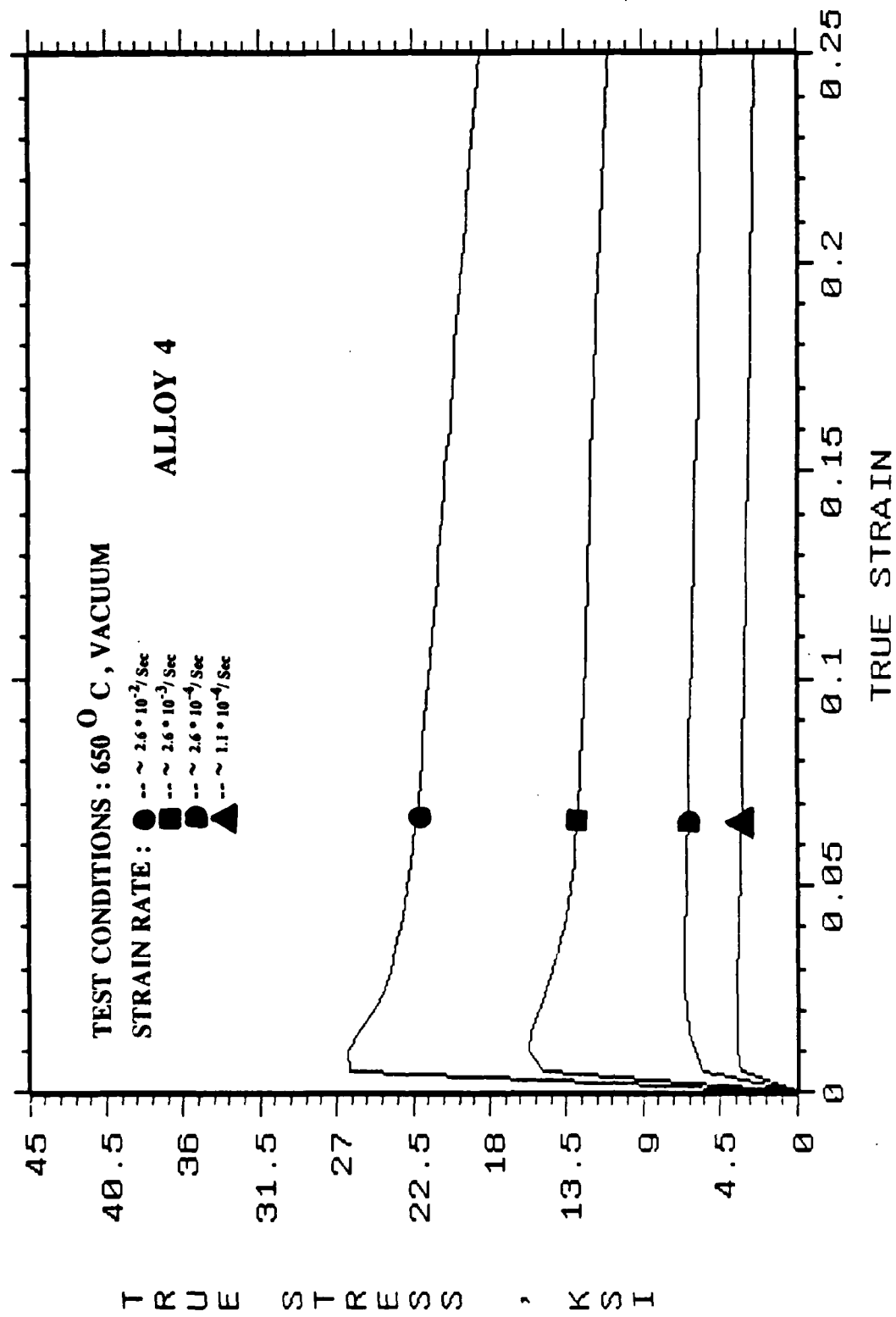
FIG 18 : TRUE STRESS - TRUE STRAIN CURVES OF ALLOY 5( 24.4 %α - 75.6 % β , Ti-Mn ALLOY) TESTED IN VACUUM AT 923 °K AT DIFFERENT STRAIN RATES.

119
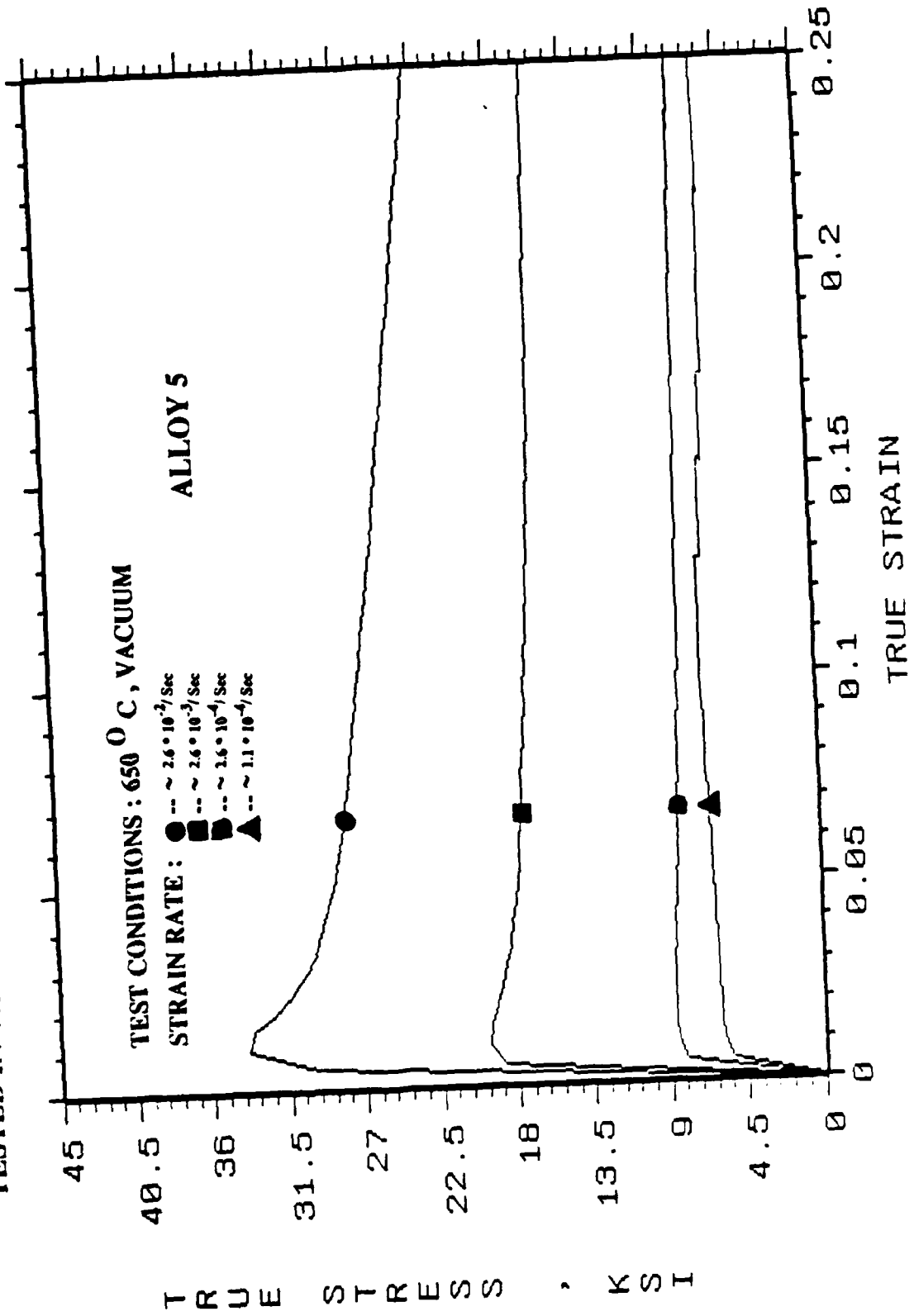
FIG 19 : TRUE STRESS - TRUE STRAIN CURVES OF ALLOY 6( 12.1 %α - 87.9 % β, Ti-Mn ALLOY) TESTED IN VACUUM AT 923 °K AT DIFFERENT STRAIN RATES.

120
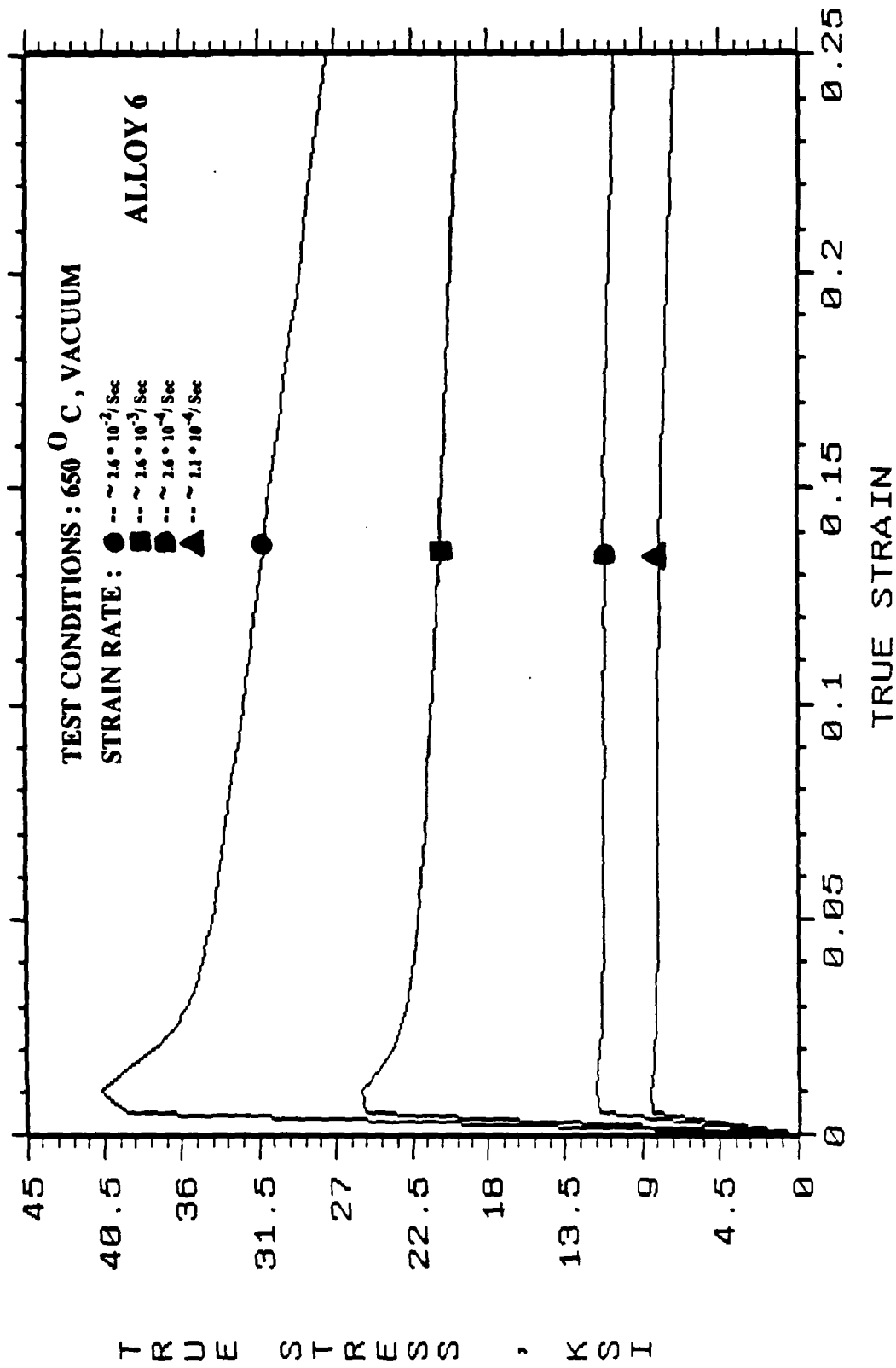
FIG 20 : FLOW STRESS Vs BETA VOLUME PERCENT FOR DIFFERENT ALPHA-BETA Ti-Mn ALLOYS
THE FLOW STRESS CORRESPONDS TO 0.2 % PLASTIC OFFSET

121
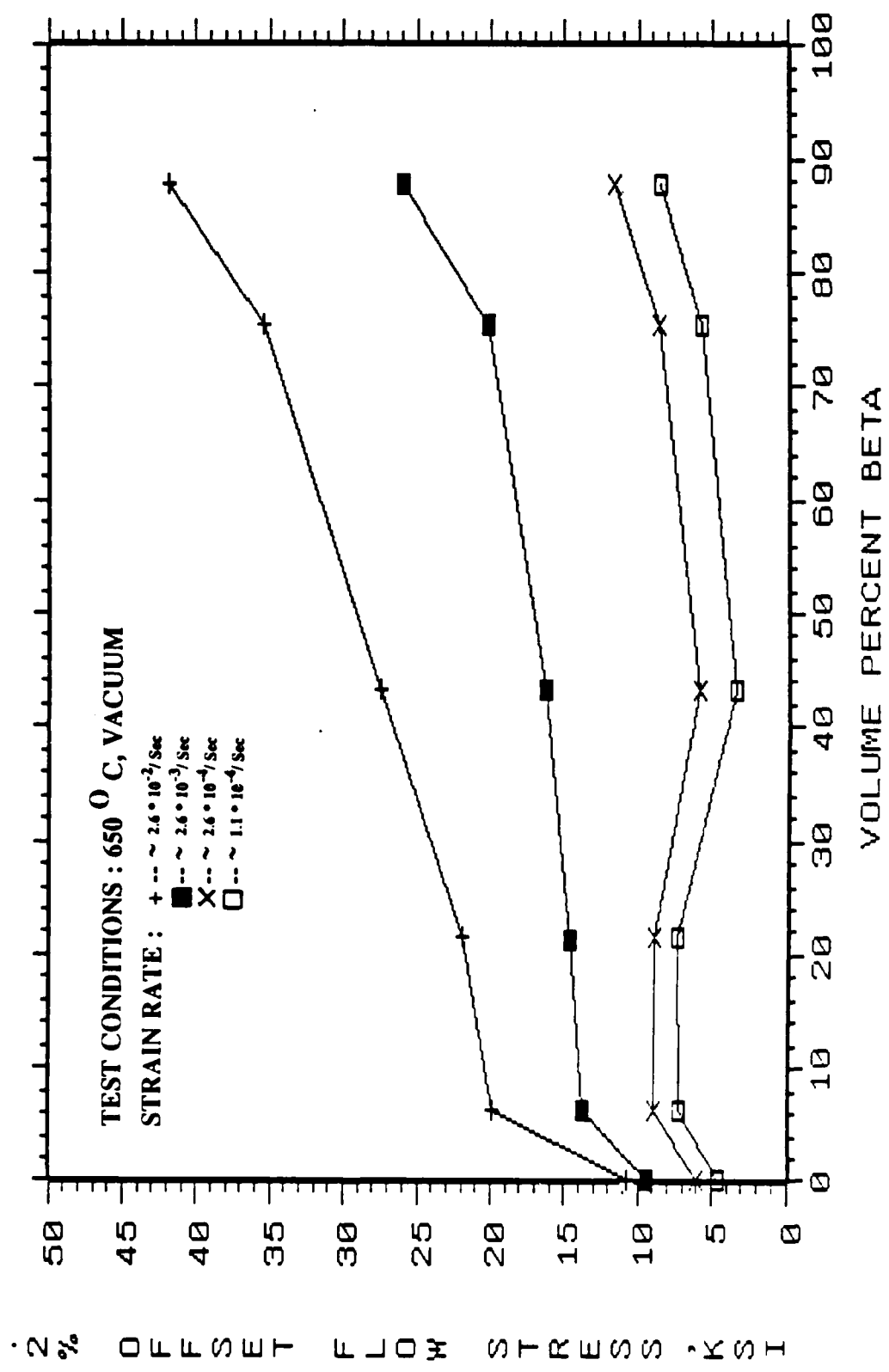
FIG 21 : FLOW STRESS Vs BETA VOLUME PERCENT FOR DIFFERENT ALPHA-BETA Ti-Mn ALLOYS
THE FLOW STRESS CORRESPONDS TO 5 % PLASTIC STRAIN

122
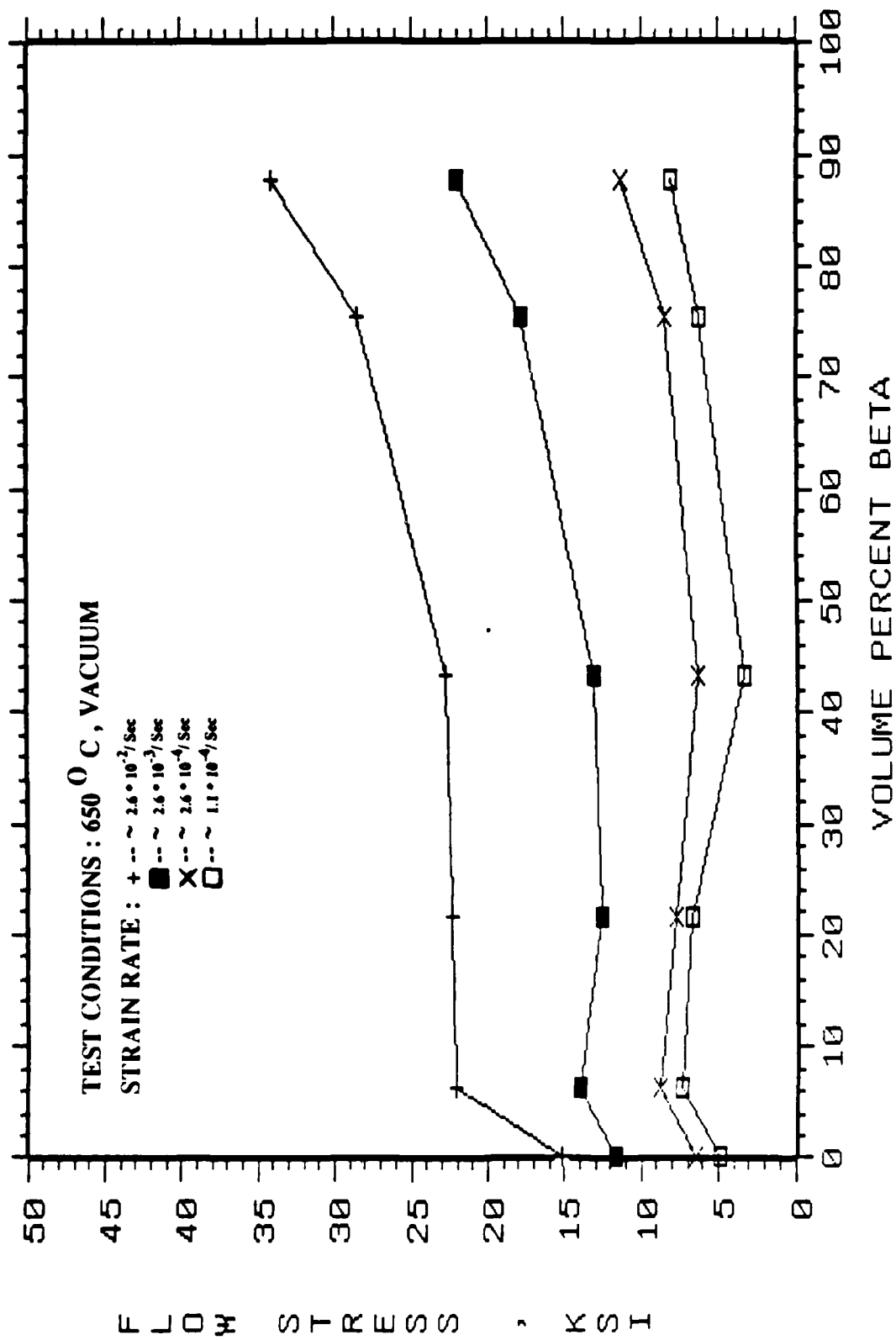
FIG 22 : FLOW STRESS Vs BETA VOLUME PERCENT FOR DIFFERENT ALPHA-BETA Ti-Mn ALLOYS
THE FLOW STRESS CORRESPONDS TO 0.5 % PLASTIC STRAIN

123
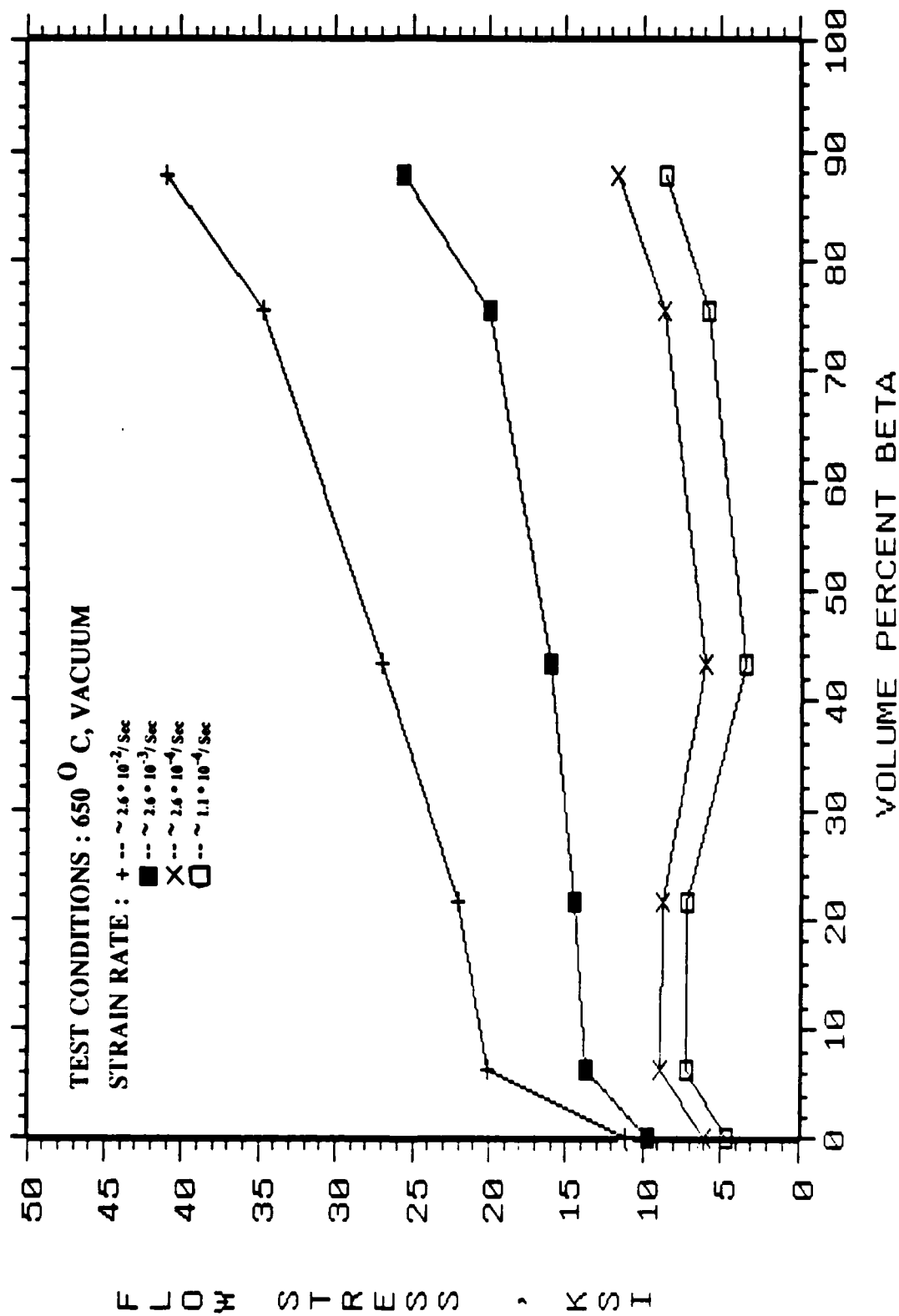
# FIG 23 : FLOW STRESS Vs BETA VOLUME PERCENT FOR DIFFERENT ALPHA-BETA Ti-Mn ALLOYS THE FLOW STRESS CORRESPONDS TO 10 % PLASTIC STRAIN
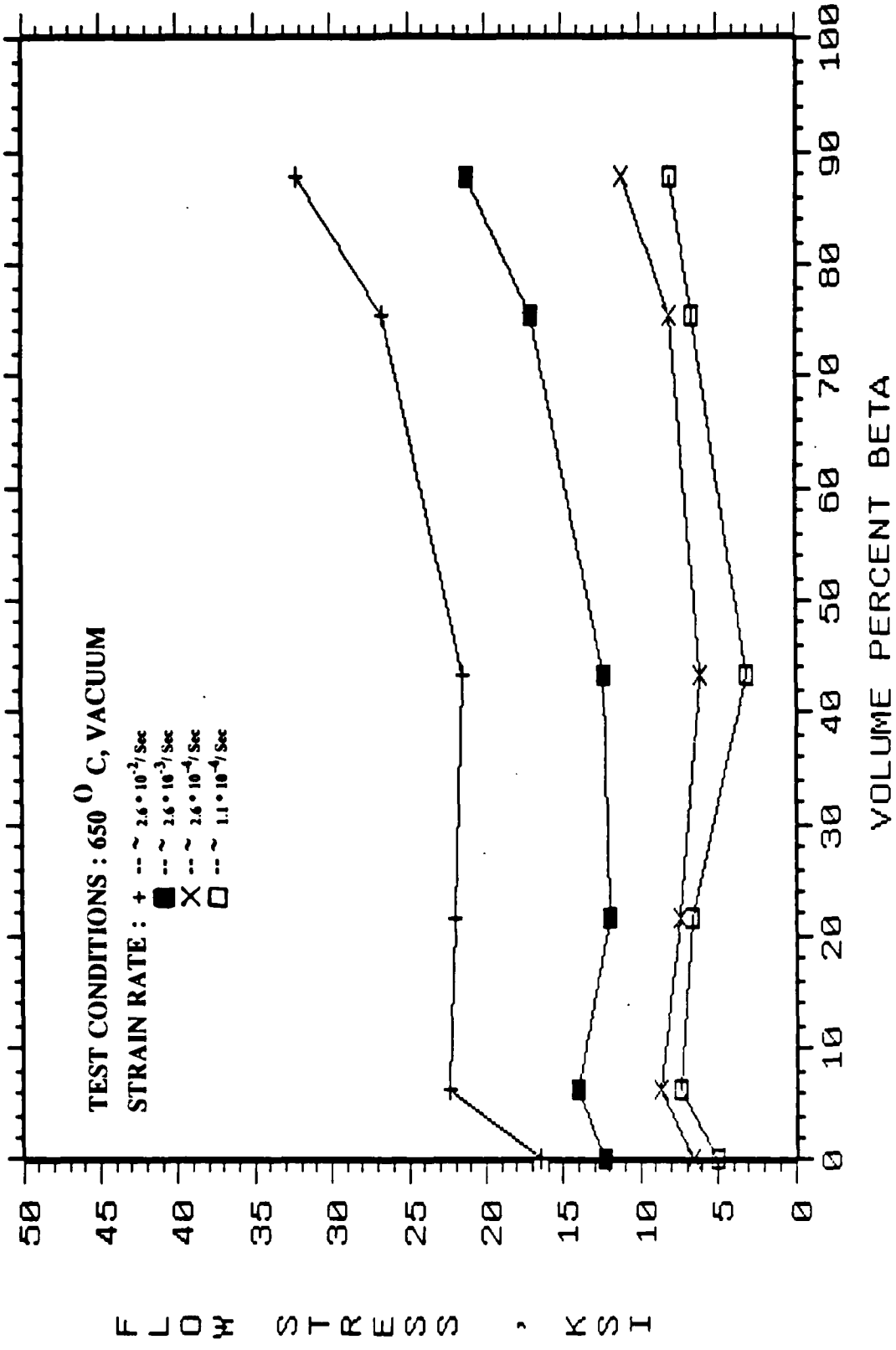
FIG 24 : FLOW STRESS Vs BETA VOLUME PERCENT FOR DIFFERENT ALPHA-BETA Ti-Mn ALLOYS
THE FLOW STRESS CORRESPONDS TO 20 % PLASTIC STRAIN

125

FIG 25 : STRAIN RATE SENSITIVITY (m ) Vs BETA VOLUME PERCENT FOR DIFFERENT ALPHA-BETA Ti-Mn ALLOYS DETERMINED FROM LOG σ Vs LOG ε PLOT.THE SLOPE OF THE PLOT IS THE STRAIN RATE SENSITIVITY (m).



TEST CONDITIONS : 650 °C, VACUUM

σ WAS DETERMINED FOR A TRUE STRAIN CORRESPONDING TO 0.001 FOR FOUR DIFFERENT STRAIN RATES.
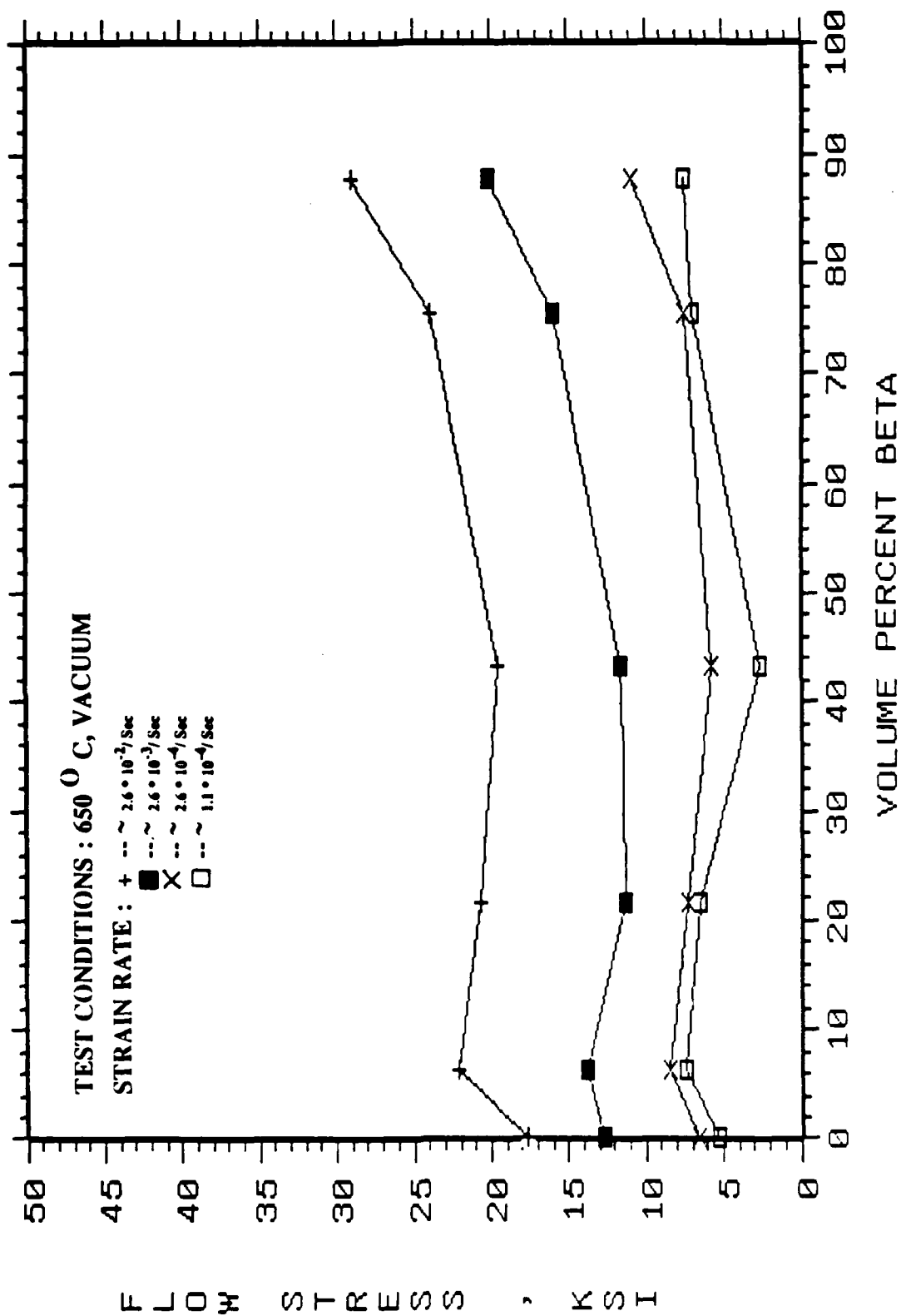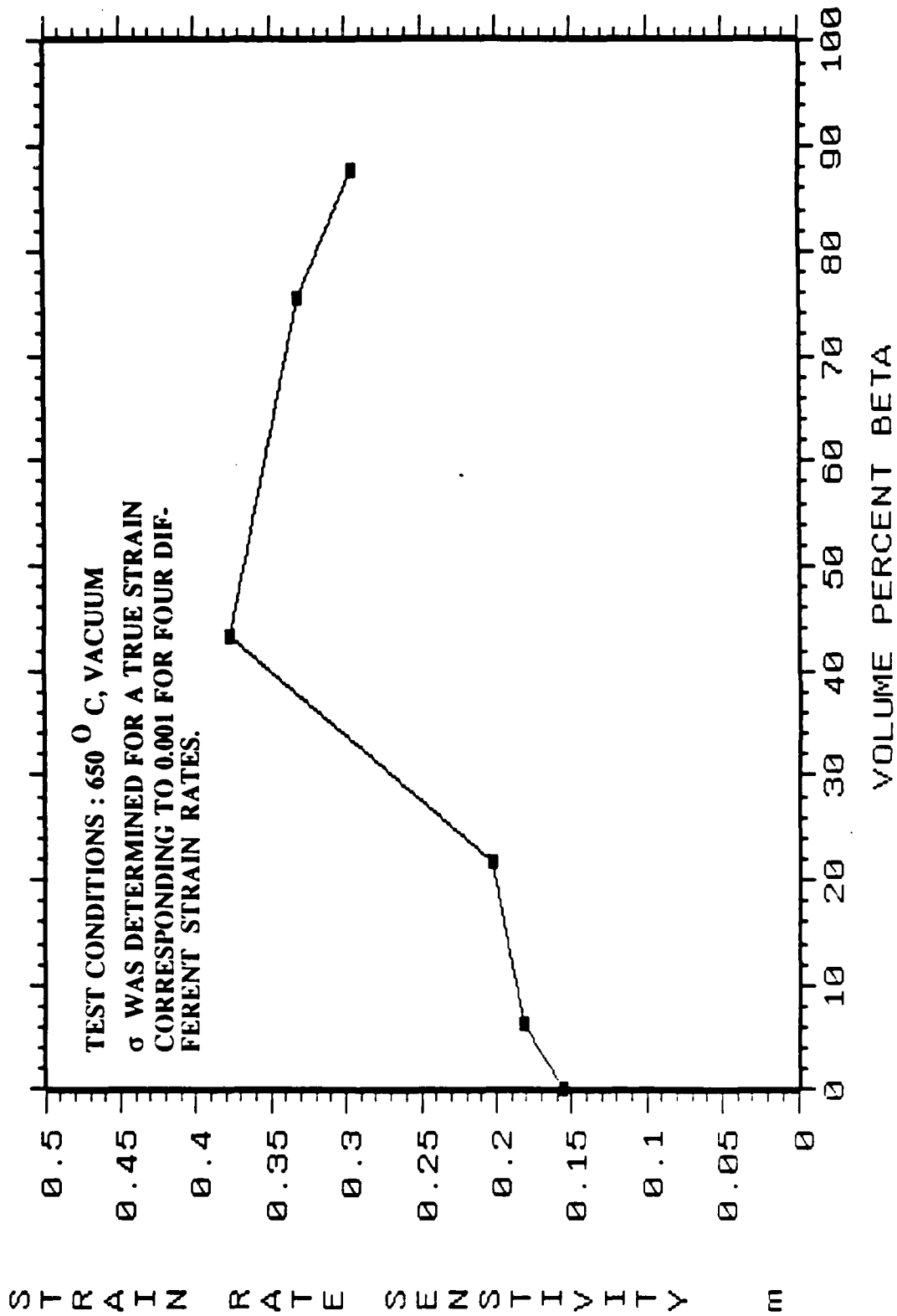
# 4. TECHNICAL PRESENTATIONS AND PUBLICATIONS

## PRESENTATIONS

1. "The Effect of Microstructure On High Temperature Tensile Properties Of Two Phase Titanium Alloys" - J.G.Shyue,S.Ankem and R.J.Arsenault - TMS - AIME Annual Meeting, Denver, Colorado, Feb. 1987.

2. "Grain Growth In Two Phase Titanium Alloys" - G.Grewal and S.Ankem - Third International Conference On Progress In Microstructure, Aachen, West Germany, May 1987.

3. "The Effect Of Temperature On The Particle Growth Of Two Phase Materials" - G.Grewal and S.Ankem ; Presented at The TMS - AIME Fall Meeting, Cincinnati, Ohio, Oct. 1987.

4. "FEM Modeling Of The Stress-Strain Behavior Of Two Phase Materials" - M.N.Vijayshankar and S.Ankem ; Presented at the TMS - AIME Fall Meeting, Cincinnati, Ohio, Oct. 1987.

## PUBLICATIONS

1. "Isothermal Particle Growth In Two Phase Titanium Alloys" - G.Grewal and S.Ankem; Prepared, being submitted for publication in " Metallurgical Transactions ".

2. "Effect Of Volume Percent Of Phases On The High Temperature Tensile Deformation Of Two Phase Ti-Mn Alloys" - S.Ankem, J.G.Shyue, R.J.Arsenault and M.N.Vijayshankar; Being prepared, will be submitted for publication in " Materials Science and Engineering ".

## 5. KEY PERSONNEL FOR THE SECOND PERIOD

Dr. S.Ankem - Principal Investigator

G.Grewal - Ph.D. Candidate

M.N.Vijayshankar - Ph.D. Candidate

END
DATE
FILMED

4-88

DTIC